VTRC
Virginia Transportation Research Council

We Bring Innovation to Transportation

Refinement of the Inverted T-Beam System for Virginia

http://www.virginiadot.org/vtrc/main/online_reports/pdf/20-r25.pdf

EZRA BIN ARIF EDWIN
Design Engineer
Simpson Gumpertz and Heger

BECKY GILBERTSON
Engineering Associate
Wiss, Janney, Elstner Associates Inc.

VIJAYKANTH PULUMATI
Design Engineer
Blue Ridge Design

C.L. ROBERTS-WOLLMANN, Ph.D., P.E.
Professor
Via Department of Civil and Environmental Engineering
Virginia Tech

Final Report VTRC 20-R25

VIRGINIA TRANSPORTATION RESEARCH COUNCIL
530 Edgemont Road, Charlottesville, VA 22903-2454
vtrc.virginiadot.org

Standard Title Page - Report on Federally Funded Project

1. Report No.: FHWA/VTRC 20-R25	2. Government Accession No.:	3. Recipient's Catalog No.:
4. Title and Subtitle: Refinement of the Inverted T-Beam System for Virginia		5. Report Date: April 2020 6. Performing Organization Code:
7. Author(s): Ezra Bin Arif Edwin, Becky Gilbertson, Vijaykanth Pulumati, and C.L. Roberts-Wollmann, Ph.D., P.E.		8. Performing Organization Report No.: VTRC 20-R25
9. Performing Organization and Address: The Charles E. Via, Jr. Department of Civil and Environmental Engineering Virginia Polytechnic Institute and State University Blacksburg, VA		10. Work Unit No. (TRAIS): 11. Contract or Grant No.: 109584
12. Sponsoring Agencies' Name and Address: Virginia Department of Transportation 1401 E. Broad Street Richmond, VA 23219 Federal Highway Administration 400 North 8th Street, Room 750 Richmond, VA 23219-4825		13. Type of Report and Period Covered: Final Contract 14. Sponsoring Agency Code:
15. Supplementary Notes: This is an SPR-B report.		

16. Abstract:

The inverted T-beam system is well suited for short to medium spans, and can be built quickly and efficiently. The system was developed for Virginia, based on a similar system used in Minnesota, and has been used in two structures in the commonwealth. Previous research helped to develop the original details, but additional research was recommended to continue to refine the system. This report presents the results of the research performed to refine the system.

Analysis was performed to develop preliminary design tables for three sizes of the inverted T-beam, utilizing normal weight and lightweight concrete, debonding strands, and specialized construction techniques to extend the usable span length. It was found that with typical construction methods, the 18-in deep section with a 7½-in topping over the webs can span 50 ft, regardless of concrete unit weight. Span lengths of up to 70 ft can be achieved with special construction methods, such as staged deck placement or temporary shoring.

Push-off tests were performed to determine the optimum surface roughening technique to ensure full composite action between the precast beams and the cast-in-place topping. Formed patterns with angular edges and approximately the same area of positive and negative elevation resulted in the highest bond strengths.

Three sub-assemblage specimens, each having different connection and surface roughening details, were tested to investigate the performance of transverse connections under cyclic loads. The specimens were subjected to 3.65 million cycles of load, representing about 50 years of service loads on an actual bridge. Two connection details were deemed adequate for bridges with a high traffic volume. A non-contact lap splice detail with poor surface roughening did not exhibit an adequate factor of safety against a bond failure.

Work was performed to optimize the cast-in-place topping concrete mixture to minimize the possibility of cracking due to differential shrinkage between the precast beam and the cast-in-place topping. Performance criteria and prescriptive mixture proportions were developed, which along with fully saturating the beam surfaces before placing the topping and providing a full seven-day moist cure for the topping, should result in a relatively crack-free deck.

Finally, analysis was performed to determine the best orientation of transverse reinforcement in the topping concrete for skewed bridges. It was found that the stresses in the transverse reinforcement remain very low, even if cracking does occur above the flange-to-flange connection, so orientation is not critical. However, orienting the reinforcement perpendicular to the axis of the beams is recommended for the non-contact lap splice (no-connection) detail, so the bars in the topping and in the beam are oriented in the same direction.

17 Key Words: Inverted T-beam, longitudinal connection, surface roughening, cast-in-place topping	18. Distribution Statement: No restrictions. This document is available to the public through NTIS, Springfield, VA 22161.		
19. Security Classif. (of this report): Unclassified	20. Security Classif. (of this page): Unclassified	21. No. of Pages: 73	22. Price:

Form DOT F 1700.7 (8-72) Reproduction of completed page authorized

FINAL REPORT

REFINEMENT OF THE INVERTED T-BEAM SYSTEM FOR VIRGINIA

Ezra Bin Arif Edwin
Design Engineer
Simpson Gumpertz and Heger

Becky Gilbertson
Engineering Associate
Wiss, Janney, Elstner Associates Inc.

Vijaykanth Pulumati
Design Engineer
Blue Ridge Design

C.L. Roberts-Wollmann, Ph.D., P.E.
Professor
Via Department of Civil and Environmental Engineering
Virginia Tech

Project Manager
Bernard L Kassner, Ph.D., P.E., Virginia Transportation Research Council

In Cooperation with the U.S. Department of Transportation
Federal Highway Administration

Virginia Transportation Research Council
(A partnership of the Virginia Department of Transportation
and the University of Virginia since 1948)

Charlottesville, Virginia

April 2020
VTRC 20-R25

DISCLAIMER

The project that is the subject of this report was done under contract for the Virginia Department of Transportation, Virginia Transportation Research Council. The contents of this report reflect the views of the author(s), who is responsible for the facts and the accuracy of the data presented herein. The contents do not necessarily reflect the official views or policies of the Virginia Department of Transportation, the Commonwealth Transportation Board, or the Federal Highway Administration. This report does not constitute a standard, specification, or regulation. Any inclusion of manufacturer names, trade names, or trademarks is for identification purposes only and is not to be considered an endorsement.

Each contract report is peer reviewed and accepted for publication by staff of Virginia Transportation Research Council with expertise in related technical areas. Final editing and proofreading of the report are performed by the contractor.

ABSTRACT

The inverted T-beam system is well suited for short to medium spans, and can be built quickly and efficiently. The system was developed for Virginia, based on a similar system used in Minnesota, and has been used in two structures in the commonwealth. Previous research helped to develop the original details, but additional research was recommended to continue to refine the system. This report presents the results of the research performed to refine the system.

Analysis was performed to develop preliminary design tables for three sizes of the inverted T-beam, utilizing normal weight and lightweight concrete, debonding strands, and specialized construction techniques to extend the usable span length. It was found that with typical construction methods, the 18-in deep section with a 7½-in topping over the webs can span 50 ft, regardless of concrete unit weight. Span lengths of up to 70 ft can be achieved with special construction methods, such as staged deck placement or temporary shoring.

Push-off tests were performed to determine the optimum surface roughening technique to ensure full composite action between the precast beams and the cast-in-place topping. Formed patterns with angular edges and approximately the same area of positive and negative elevation resulted in the highest bond strengths.

Three sub-assemblage specimens, each having different connection and surface roughening details, were tested to investigate the performance of transverse connections under cyclic loads. The specimens were subjected to 3.65 million cycles of load, representing about 50 years of service loads on an actual bridge. Two connection details were deemed adequate for bridges with a high traffic volume. A non-contact lap splice detail with poor surface roughening did not exhibit an adequate factor of safety against a bond failure.

Work was performed to optimize the cast-in-place topping concrete mixture to minimize the possibility of cracking due to differential shrinkage between the precast beam and the cast-in-place topping. Performance criteria and prescriptive mixture proportions were developed, which along with fully saturating the beam surfaces before placing the topping and providing a full seven-day moist cure for the topping, should result in a relatively crack-free deck.

Finally, analysis was performed to determine the best orientation of transverse reinforcement in the topping concrete for skewed bridges. It was found that the stresses in the transverse reinforcement remain very low, even if cracking does occur above the flange-to-flange connection, so orientation is not critical. However, orienting the reinforcement perpendicular to the axis of the beams is recommended for the non-contact lap splice (no-connection) detail, so the bars in the topping and in the beam are oriented in the same direction.

FINAL CONTRACT REPORT

REFINEMENT OF THE INVERTED T-BEAM SYSTEM FOR VIRGINIA

Ezra Bin Arif Edwin
Design Engineer
Simpson Gumpertz and Heger

Becky Gilbertson
Engineering Associate
Wiss, Janney, Elstner Associates Inc.

Vijaykanth Pulumati
Design Engineer
Blue Ridge Design

C.L. Roberts-Wollmann, Ph.D., P.E.
Professor
Via Department of Civil and Environmental Engineering
Virginia Tech

INTRODUCTION

Background and Motivation

Due to continually increasing demands on the transportation network, there is a need for new construction, replacement, and rehabilitation of bridge infrastructure. Shutting down road networks for extended periods of time is costly, giving rise to Accelerated Bridge Construction (ABC) practices. ABC relies on the ability to prefabricate as many bridge elements as possible, minimize on-site formwork, and thereby speed up the construction process. Current examples of ABC systems used in the United States include adjacent box-beam and voided-slab systems.

In April 2004, the Federal Highway Administration (FHWA) and the American Association of State Highway and Transportation Officials (AASHTO) sent representatives to Europe and Japan to observe bridge construction practices that could be adapted to ABC in the United States. One such design in France was the Poutre-Dalle (meaning beam-slab) system, which consisted of precast, prestressed inverted T-beam units placed side-by-side, connected by a transverse connection. A cast-in-place topping was subsequently applied over the entire system (Ralls et al., 2005) Minnesota was the first state in the United States to adopt a similar system, and between 2005 and 2011, the University of Minnesota conducted a number of studies on the inverted T-beams. Also during this period, twelve bridges were constructed in Minnesota using their own modifications to the Poutre-Dalle system (Menkulasi, 2014). Figure 1 shows the original and Minnesota inverted T-beams.

Figure 1. Development of the Inverted T-Beam System, Original Poutre-Dalle System left (reprinted with permission from Matiere, from their website at https://www.matiere-tp.com/beam-slab), MnDOT System right (Hagen et al., 2005, reprinted with permission)

The inverted T-beam system offers advantages over traditional ABC systems such as adjacent box-beams and voided slabs, because of the improved connection of the adjacent members. In traditional systems, these joints are formed by a shear key filled with a non-shrink grout. The grout must resist shear and tensile stresses generated by the transverse distribution of loads when vehicles cross the bridge; those stresses eventually lead to cracking in the joint and in the topping concrete above the joint, which is termed "reflective cracking." Reflective cracking allows for the ingress of water and chlorides into the joint, which leads to deterioration of reinforcement in the superstructure. Inverted T-beams provide a solution to this issue by using a thicker cast-in-place topping over the longitudinal joints between members, and by providing reinforcement in the joint region capable of resisting transverse bending stresses. These design improvements reduce the development and propagation of cracks to the surface of the deck, thereby reducing deterioration of the superstructure.

Previous Research on the Virginia Inverted T-Beam

During 2014-2015, two bridges were constructed in Virginia using an inverted T-Beam system with modifications to the Minnesota concept (see Figure 2). One structure was completed on a high volume bridge – U.S. Rte. 360 over the Chickahominy River near Richmond, Virginia – and another was constructed on a low volume road – Towlston Road over Rocky Run in Fairfax, Virginia. Prior to construction, researchers at Virginia Tech tested some modified inverted T-beam systems. The objectives of the research were to: 1) compare the different geometries and joint types (Mercer, 2012), 2) identify a topping mixture that would result in low amounts of restrained shrinkage cracking, 3) investigate stresses in the pretensioned anchorage zones for these uniquely shaped sections, 4) investigate the capability of the section to develop composite action, and 5) determine suitable live load distribution factors to be used when designing a bridge using this system (Menkulasi, 2014).

Mercer and Menkulasi conducted monotonic testing on five sub-assemblage specimens and finite element modeling to investigate the transverse connection between adjacent beams and to address constructability issues faced when using the Minnesota Department of Transportation

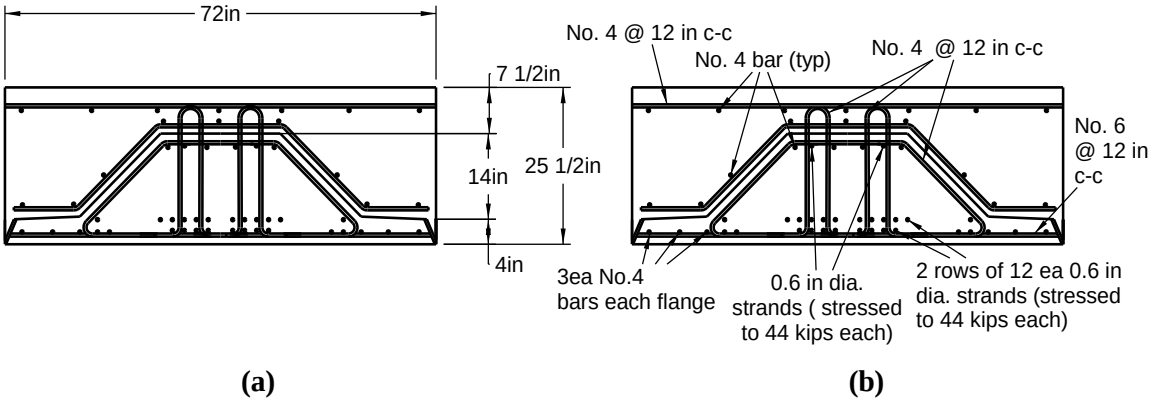

Figure 2. Virginia inverted T-beam with Welded Connection, a) Dimensions and b) Reinforcing

(MnDOT) detail. The sub-assemblages differed in combinations of tapered or vertical web geometry along with three different connection details: a welded connection, an overlapping bar connection, and a connection that depended on bond – named the "no-connection" detail. During the testing, the researchers increased the monotonic loading on each specimen in 10-kip increments until the first crack; afterwards, the increment was 5 kips. When a crack appeared (or appeared to propagate), the specimen was cycled at that increment until the crack stabilized (stopped propagating), at which point the load was taken to the next increment until failure.

The results of the testing showed all systems to perform well under testing conditions. Overall, the tapered web systems were found to perform better than vertical webs due to the increased interface resistance. The no-connection detail was found to be the most efficient to construct due to the elimination of the mechanical tie between adjacent beams and the ease of creating forms for these beams. However, this detail was recommended for use only on bridges with low traffic counts. The flexural strengths of the welded connection and extended bar details were certainly higher than the no-connection detail, but the welded connection was deemed more suitable for construction of bridges with high daily traffic.

Both options for the Virginia system eased fabrication through modification of the connection between adjacent beams. Furthermore, both designs eliminated the need for horizontal reinforcement penetrating the sides of the beams, which was present in the Poutre Dalle and Minnesota design. Additionally, the profile of Virginia's inverted T-beam allowed for the transfer of transverse bending stresses through a combination of tensile bond and shear stresses developed at the interface of the precast and cast-in-place components. This profile also provided a more gradual change in shape at top corners of the web, reducing stress concentrations at these locations. The development of the inverted T-beam system in Virginia is further described in Roberts-Wollmann et al. (2016).

The conclusions from these investigations led to recommendations to: 1) determine if the bridge system could accommodate spans longer than 65 ft [the current system is intended for use in bridges with spans ranging from 20 to 45 ft], 2) further investigate the behavior of the transverse connections under cyclic loading, 3) optimize the topping concrete to minimize cracking, and 4) determine the best orientation for transverse reinforcement in skewed bridges.

PURPOSE AND SCOPE

The purpose of this study was to enhance the design of the Virginia inverted T-beam system initially developed in the previous study, and thus increase the application of this system. Therefore, the scope of this research was limited to the refinement of the system, following the recommendations from the previous study. The primary objectives of this research were to:

- Develop a standard set of design tables for the inverted T-beam system that could be used by bridge designers in preliminary design.
- Perform push-off tests on a variety of surface roughening techniques to develop recommendations for the best treatments of the interfaces between the precast and cast-in-place concretes to ensure composite action, particularly for the no-connection detail.
- Perform cyclic tests of the welded connection and the no-connection details to determine their efficacy on high volume roads.
- Perform additional material tests to refine recommendations for the topping concrete mixture.
- Perform analysis to determine the best details for transverse reinforcement in the topping concrete for skewed bridges.

METHODS

Development of Preliminary Design Tables

This section presents the development of the preliminary design tables. Designs were developed analytically using design requirements from the AASHTO LRFD Bridge Design Specifications (2017). The specific aspects of design considered during the development are discussed first, followed by presentation of several iterations of design calculations that were required to arrive at the final tables.

Design Aspects Considered for the Preliminary Design Tables

The strand arrangements for each span length were selected based on design considerations including flexural strength, deflections and camber, and allowable stresses at the ends and midspan of the member. It is important to note that partial debonding of strands at the ends of the member was included to meet allowable stress limits at these locations. Numbers of partially debonded strands adhered to the limits set out in the AASHTO LRFD Bridge Design Specifications Section 5.11.4.3 (AASHTO 2014).

Flexural strength of the member was calculated per the AASHTO LRFD Bridge Design Specifications (AASHTO 2014) Section 5.7 for prestressed concrete members assuming rectangular section behavior. Required flexural strength was calculated at midspan, which was assumed to be the location of critical flexural demand for the preliminary design of a simply supported beam. Applied loads consisted of combinations of permanent loads and live loads in accordance with the Strength I Limit State in AASHTO Table 3.4.1-1. Permanent loads included self-weights of the beams and topping concrete, prestressing forces (including allowances for loss of prestress), and allowances for the weights of barriers, medians and future wearing

surfaces. Live loads were applied per AASHTO Section 3.6 and consisted of the design lane load and the design truck or tandem. Live load distribution factors were determined per AASHTO Section 4.6.2.2 for a bridge of cross-section type "f" (precast beam with shear keys with a cast-in-place concrete overlay). This cross-section type was determined to be appropriate based on a previous study carried out by Menkulasi (2014). The distribution factors were used to determine the fraction of the total bridge live load that would be carried by a single beam in the system. The worst-case beam was the one having the highest distribution factor, and was used conservatively for all design calculations.

The calculation of deflections included the effects of self-weight of the precast and cast-in-place components, as well as the effects of service level live loads acting on a single girder, calculated using the distribution factor method. The cambers were calculated as the upward deflections of the girder due to the effects of prestressing. The difference between the upward deflections and downward deflections was taken to be the final deflection, and was compared to a limit of L/800, provided by AASHTO Section 2.5.2.6 (AASHTO 2014). Long-term deflections due to creep and shrinkage were not included in these calculations.

Allowable stresses were checked in accordance with the limits set out in AASHTO Section 5.9.4 (AASHTO 2014). The stress at the extreme tensile and compressive fibers of the section were calculated assuming linearly elastic behavior. Stresses were checked against these limits at three stages during the lifetime of the structure, first at transfer of the prestressing force into the concrete, then at the time of deck placement, and finally during service life once all long-term prestress losses had occurred. In the first stage, prestress forces, and the self-weight of the beam section were considered to act on the beam section alone since the cast-in-place topping had not been constructed at this time. During the second stage, prestress forces, the self-weight of the beams, and the weight of the wet cast-in-place topping concrete were assumed to act on the beam section alone as composite action could not yet be assumed to have been achieved. In the final stage, it was assumed that the stresses resulting from the first two stages of the structure's life were locked-in. Additional stresses due to the self-weight of overlays, barriers, medians, and stresses resulting from live loads were assumed to act on the composite section, and the final stress state was calculated as the sum of the locked-in stresses and these additional stresses acting on the composite section.

Iteration 1 – Based on Previous Research Recommendations

Menkulasi (2014) recommended that the Inverted T-beam system be extended to spans longer than 40 ft. He suggested two additional cross-sections, one for shorter spans from 20 ft to 35 ft, and a larger one for spans longer than 40 ft. Figures 3 through 5 show the three cross-sections, named small, medium and large. The medium cross-section was the original shape tested in the previous research study. The first iteration of the preliminary design tables was developed based on these cross-sections and the following design considerations: flexural strength, deflection and camber, and allowable stress checks at three critical stages – at transfer of prestressing force into the concrete, at deck placement, and at final service after all prestress losses have occurred. This iteration did not include the effects of strand debonding, or shear strength.

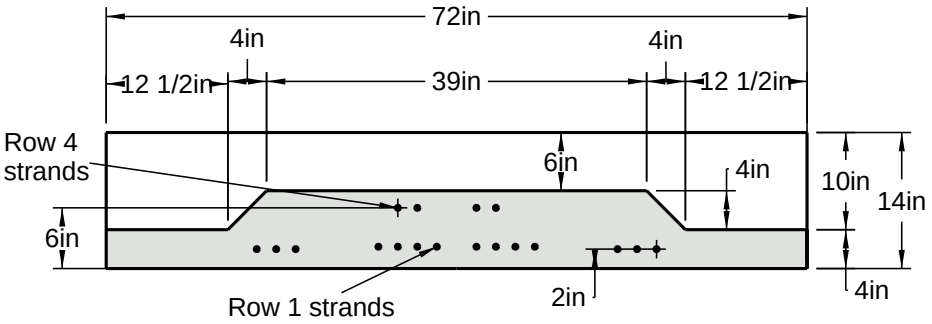

Figure 3. Inverted T-beam System - Small Cross-Section

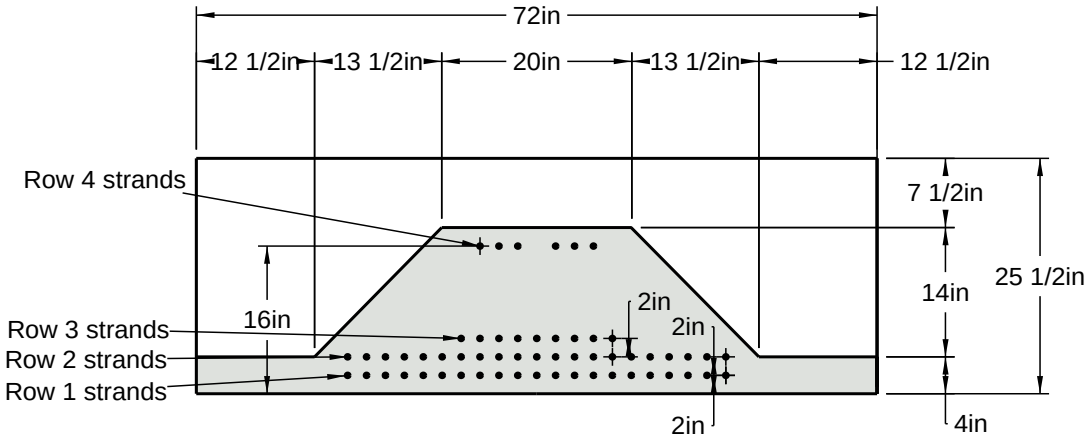

Figure 4. Inverted T-beam System - Medium Cross-Section

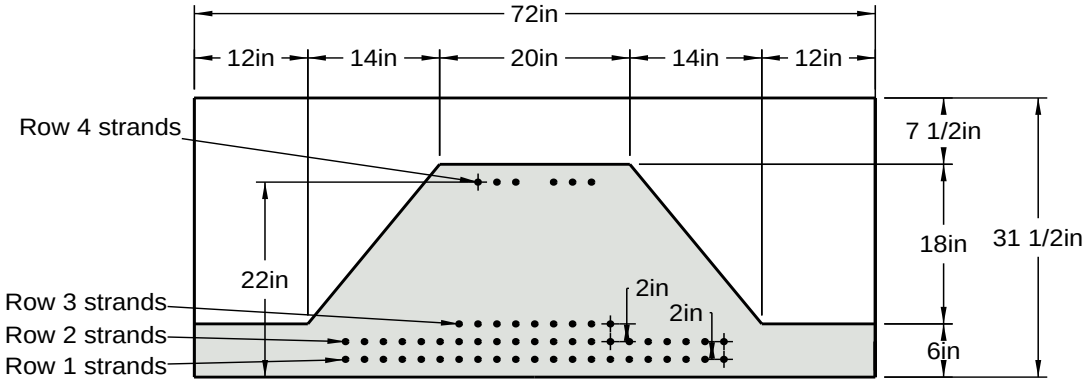

Figure 5. Inverted T-beam System - Large Cross-Section

Iteration 2 – Including the Effects of Strand Debonding and Strand Layout Optimization

Once span lengths reached a limit caused by exceeding tensile and compressive allowable stresses, the beneficial effect of debonding strands was investigated. The maximum limits set by AASHTO Section 5.11.4.3 (AASHTO, 2014) were adhered to. Additionally, altering the geometric layout of the strands in the precast section could change the location of the centroid of prestressing, which in turn could potentially reduce the overall stresses in the section. Both the strand debonding and alternative strand layouts were analyzed using a MATLAB algorithm (see Edwin, 2017).

Iteration 3 – Using Lightweight Concrete

To reduce the midspan stresses at service, the possibility of using lightweight concrete was investigated. Two options were considered; lightweight concrete cast-in-place topping with a normal weight precast girder (LW Option 1) and a lightweight concrete topping with a lightweight concrete girder (LW Option 2). The unit weight of the lightweight concrete was 125 pcf.

Iteration 4 – Based on Conclusions from Meeting with VDOT Representatives

Following Iteration 3, the inverted T-beam project team met VDOT personnel to discuss the preliminary findings. The geometry of the precast sections was discussed, along with ideal outcomes for the beams regarding span lengths and possible methods of achieving these outcomes. Based on the final standard details of the inverted T-beam the maximum number of strands in the bottom two rows was limited to 20. Further investigations carried out during this design iteration were based on those discussions.

Based on the conclusions drawn from the meeting, it was decided to discontinue the investigation of the small and large cross-sections and focus on the medium cross-section. The ideal situation was considered to be getting the medium cross-section to span around 75 ft. Possible methods of achieving this mentioned during the meeting included the addition of mild reinforcement to the section, using higher strength concrete, or debonding the top strands during the construction operation. The idea of cutting the top strands prior to placing the deck was also suggested. These ideas formed the basis of the investigation carried out during this design iteration.

The calculations revealed that the limiting design considerations were the midspan stresses under the final in-service load configuration. As a result, no method which altered the stressing sequence would affect the final condition enough. Increasing the concrete compressive strength to 10 ksi was attempted, and was found to be effective to allow span lengths over 55 ft.

Two additional options were then proposed by the researchers and investigated. Because the largest components of stresses on the beam were due to the prestressing and concrete self-weights acting on the bare beam section alone, it followed that, by achieving some composite action at the midspan of the beam prior to application of all of these loads, the stresses would be lower. Therefore, the possibility of a staged deck placement was investigated, where part of the midspan section was placed first, allowed to harden sufficiently to achieve composite action, followed by placement of the remainder of the deck. In addition to this, the idea of using temporary shoring at midspan was studied.

Horizontal Shear Push-off Specimens

The objective of this part of the research project was to perform push-off tests on a variety of surface roughening techniques to develop recommendations for the best treatments of the interfaces between the precast and cast-in-place concretes to ensure composite action,

particularly for the no-connection detail. The tops of the bottom flanges, sides of the web, and the top surface of the web need to be roughened to ensure good bond with the cast-in-place topping concrete. A variety of surface treatments were selected and their horizontal shear strengths were compared using push-off tests.

Surface Roughening Techniques

Ten surface treatments were selected for investigation. The treatments were selected based on expected ease of construction and shear strength. A total of 30 specimens were constructed with three specimens for each of the ten treatments examined. Roughening type, spacing, and other characteristics were varied amongst the treatments. Table 1 summarizes the selected surface treatments, also referred to as textures, and their corresponding characteristics. The last column lists the specimen names that are associated with each surface texture and spacing. The specimen names were created so that the information pertinent to each specimen would be easily discernable from the name. Figure 6 shows an example specimen name with each of the components labeled.

Table 1. Summary of Selected Surface Texture Attributes and Specimen Names

Texture Name	Amplitude, in	Spacing, in	Debonding	Specimen Names
Raked	0.25	1	---	RK-1-01, RK-1-02, RK-1-03
		2	---	RK-2-01, RK-2-02, RK-2-03
		3	---	RK-3-01, RK-3-02, RK-3-03
Rectangular Grooves	0.25	1	TuffCoat®	RG-1-01, RG-1-02, RG-1-03
Trapezoidal Grooves	0.25	1.5	TuffCoat®	TG-1.5-01, TG-1.5-02, TG-1.5-03
		3	TuffCoat®	TG-3-01, TG-3-02, TG-3-03
Cross Hatch	0.25	3.5	TuffCoat®	CH-3.5-TC-01, CH-3.5-TC-02, CH-3.5-TC-03
			Plastic	CH-3.5-PL-01, CH-3.5-PL-02, CH-3.5-PL-03
Square Knobs	0.25	2.5	TuffCoat®	SK-2.5-01, SK-2.5-02, SK-2.5-03
Exposed Aggregate	0.25	---	---	EA-01, EA-02, EA-03

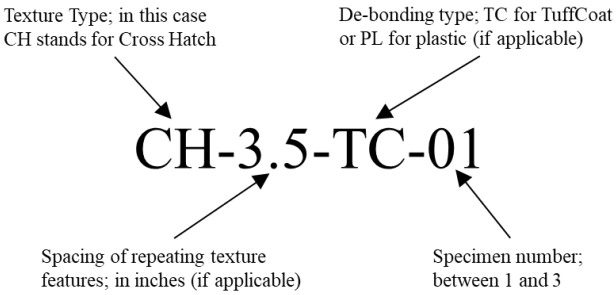

Figure 6. Specimen Naming Scheme

Diagrams of the details for each texture are shown in Figure 7. The drawings include top-down views and cross-section views of each texture. Dimensions are given for all aspects necessary to reproduce the texture. The cross-hatch, square knobs and exposed aggregate textures provide horizontal shear strength in two directions, which can be advantageous on surfaces such at the top of the bottom flange. This surface is subjected to horizontal shear due to both longitudinal and transverse bending.

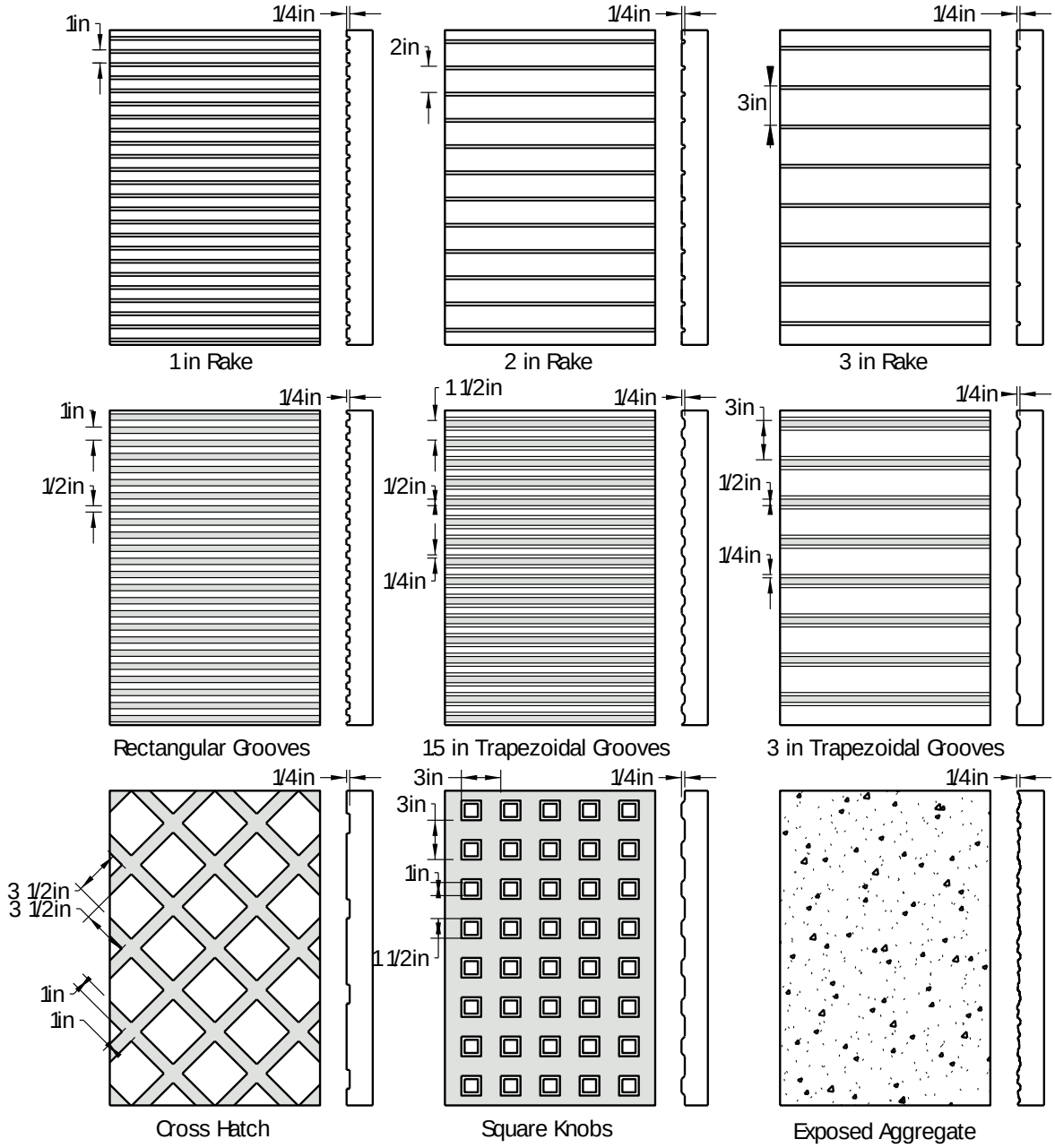

Figure 7. Details for Selected Surface Textures

Specimen Detailing

Geometry

The specimens comprised two sections: a bottom that simulated a precast section, and a top that simulated a cast-in-place slab. Both sections were 16-in wide "L" shapes with the same dimensions and reinforcement as shown in Figure 8. The top section is cast directly on top of the previously cast beam-side specimen (as shown in Figure 9). The interface between the two sections measured 16 in by 24 in for a total of 384 in^2.

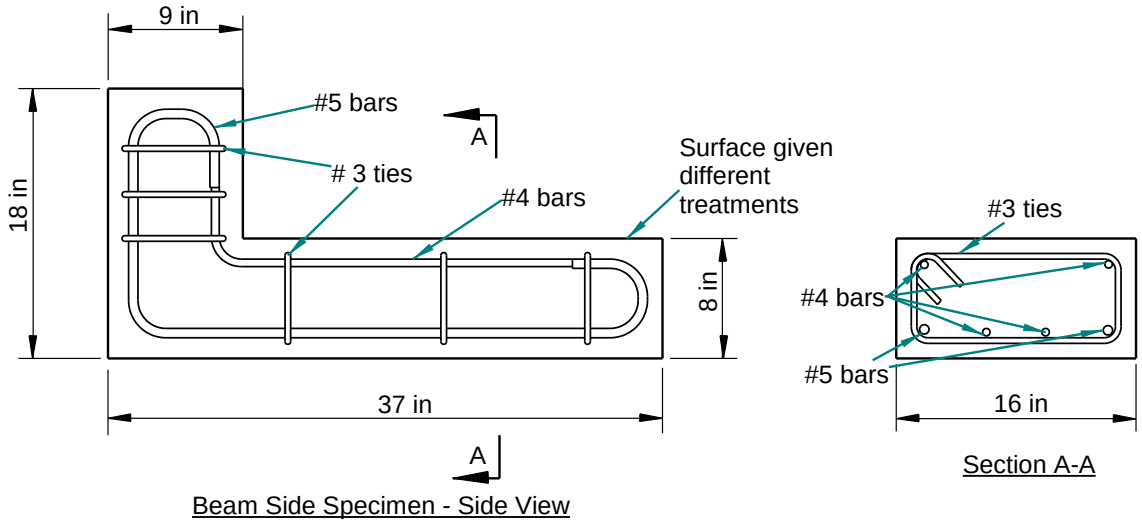

Figure 8. Dimensions of Horizontal Shear Push-off Specimen Sections

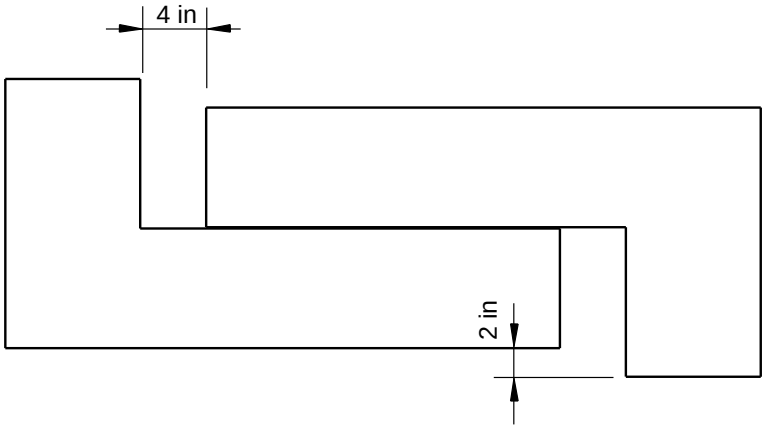

Figure 9. Dimensions of Joined Horizontal Shear Push-off Sections

Reinforcement

There was no reinforcement across the shear interface of these specimens. A minimum of 1 in of cover was provided to all bars and A615 Grade 60 reinforcing steel was used. The reinforcing steel can be seen in Figure 8, with more details found in Gilbertson (2018).

Concrete Specifications

The specimens were meant to simulate the precast concrete beams of the Virginia Inverted T-Beam bridge system, so the same concrete mixtures that were used for the precast and cast-in-place parts of the sub-assemblage tests performed by Menkulasi (2014) were used for these specimens as well as the sub-assemblage tests in this research. The bottom section was a specified 8000-psi concrete mix and the top section was a specified 4000-psi concrete mix. Both mixes were specified to have at least 5% air content and between 5 and 7 in of slump. Mix designs for both concrete mixes can be found in Gilbertson (2018).

Specimen Construction

The 30 specimens were cast in three batches, six specimens in the first batch and twelve in the second and third. Each batch of specimens required two concrete placement stages, one for the bottom section and one for the top. Figure 10 shows the formwork for the bottom section, and Figure 11 shows the formwork in place for the top section cast in the second stage.

Figure 10. Forms and Reinforcing for Push-off Specimens for Bottom Section

Figure 11. Forms and Reinforcing for Push-off Specimens for Top Section

The bottom sections were moist cured using wet burlap and plastic for 7 days after the initial placement. Afterwards, the forms were removed from the specimens and then were prepared for the concrete placement of the second section. The placement of the top sections typically occurred when the bottom sections were between 10 and 14 days old.

The placement of the concrete for the top section consisted of filling the form and consolidating. The exposed surface was troweled and then the seven-day moist curing process commenced after initial set was reached. The formwork was removed after the moist cure was finished and the specimens were stored for at least 28 days before testing.

Surface Roughening Methods

There were three categories of surface roughening that required different production methods in this research: raked surfaces, exposed aggregate, and manufactured textures. The raked surfaces were produced by handmade rakes constructed from 7-wire prestressing strand.

The individual wires of the strand served as the tines of the rake and were spread out and trimmed to achieve the required spacing. When used, the rake was placed at one edge of the finished concrete surface prior to initial set and pulled across to create 0.25-in deep grooves at the specified spacing.

The exposed aggregate surfaces were produced using a simple method utilizing a spray bottle of water and a soft brush. After the concrete surface was cast and finished, water was misted over the surface until it looked as if bleed water had collected on the surface. The surface was left to rest until there was no water sitting on the surface (concrete was still moist), and then the misting was repeated. These steps were repeated until the exposed surfaces that were not being treated had stiffened, approximately an hour. The surface was then rinsed heavily and softly brushed until the aggregate was exposed. This process increased the water-to-cement ratio of the top surface layer of concrete paste such that it was easily brushed away while the subsurface paste was unaltered. The possible amplitude of the exposed aggregate depended greatly upon the size of the aggregate, because at least 50% of each individual piece of aggregate needed to be anchored in concrete paste to create a sufficiently strong surface texture. Since the mix design used for the bottom section of the specimens in this research was a typical mix used by precast plants, the aggregate was small such that only a 3/16-in amplitude could be achieved.

The manufactured textures were produced using ¾-in plywood that was carved with the desired pattern. Plywood sheets were cut to be large enough to cover the exposed surface area plus some overhang on all sides. A router was used to carve out the patterns with a combination of mortising and v-groove router bits.

During casting, these patterned plywood boards were pressed into the exposed portion of the leg of the bottom specimen section to form the manufactured textures, but a debonding method was needed to ensure the plywood released from the concrete after setting. The carved plywood on its own has open grains that allow for the ingress of wet concrete, resulting in a significant bond between the form and concrete which leads to difficult form removal. In previous specimens constructed by Menkulasi (2014), the carved plywood surfaces were coated with form oil, but formwork was still very difficult to remove. An alternate method of closing off these open wood grains was to place plastic sheeting between the form and the concrete during placement. This method was used in the first no-connection detail sub-assemblage specimen of this research and was found to produce rounded textures that were believed to result in a low interface shear strength.

An alternative method for closing off the wood grains was devised that used TuffCoat® from Rhino Linings Corporation, a pick-up truck bed liner. This “elastomeric polyurea hybrid lining” was applied using an air sprayer and dried within minutes. A uniform coating was key to achieving the best formwork release, so a two-coat approach was taken to ensure that all the corners in each textured surface had been covered. Before concrete placement, formwork release oil was applied to each coated texture.

Testing Apparatus

To test the horizontal shear strength across the interface of the specimens, two forces were required: a lateral force and a normal force. The lateral force was applied through a 200-ton hydraulic cylinder on one end of the specimen, directly in line with the interface, while the other end was fixed against a support. To monitor the force during testing, there was a 200-kip load cell between the cylinder and specimen which was suspended from the specimen by way of a fabricated steel bracket.

To simulate normal dead and live loading on the interface and to correct any effects from eccentricity of the load, a normal force was applied orthogonally to the interface and was equal to 10 percent of the lateral force or expected shear strength. This load was created using a steel harness that was constructed with four 1-in threaded steel rods and 2-in x 1-in x 0.1875-in steel channels welded together. Each rod had a strain gauge that was calibrated to associate the strain read by the gauge with the tension force in the rod. The rods connected the top and bottom channel assemblies, with a nut at either end. These nuts were tightened to induce tension in the rods. During testing, the change in the normal force due to formation and widening of the crack that formed at the interface was tracked to ensure that large increases in force were not occurring when the interface broke.

The bottom section of the specimen rested on three 2-in rollers, which allowed for movement of the bottom relative to the top during testing. The instrumentation used for this test included four rod strain gauges, a load cell, and four linear variable differential transformers (LVDTs) to measure the relative movement between the top and bottom sections. The set-up can be seen in Figure 12.

Figure 12. Horizontal Shear Push-off Specimen Testing Apparatus

Testing Procedure

After the specimen had been placed in the apparatus and instrumentation attached, the rods were tightened to the specified normal force. The shear strength of the specimens was assumed to be 150 kips; so, the applied normal force was 15 kips, or 3.75 kips in each rod. The specimen was loaded gradually until the interface experienced shear failure, which was evident by both a loud popping noise and a sudden increase in displacement between the sections. After

the shear failure, the cylinder was re-engaged to determine the residual shear strength of the specimen after the interface crack occurred. The cylinder was then disengaged and the interface of the failed specimen was inspected

Sub-assemblage Tests

Specimen Detailing

The purpose of testing sub-assemblage specimens was to determine the behavior of the connections between adjacent beams when subjected to cyclic loads in the transverse bending direction in a real bridge. A sub-assemblage is a specimen designed to represent a portion of the overall bridge, and is described below. Three Virginia Inverted T-Beam sub-assemblage specimens were constructed, two with the no-connection detail and one with the welded configuration, both of which had been tested previously by Menkulasi (2014). The reason for a specimen with the welded connection was to serve as a control specimen against which the performance of the no-connection details could be compared, when subjected to the same laboratory loading conditions. Additionally, the sub-assemblage specimens were designed to test the connection between the precast beam's sloped sides and flanges and the cast-in-place slab. The first no-connection detail specimen used a cross-hatched surface roughening with plastic sheet as the debonding technique. The failure of this specimen was caused by poor interface bond, so a second no-connection detail specimen was tested, using a surface roughening technique selected based on the push off test results.

Geometry

A section, selected from a cross-section of a full-scale bridge, included two precast beams and the cast-in-place topping. Each beam directly supported a single wheel load corresponding to a design vehicle, as seen in Figure 13. Each specimen was 12 ft wide by 4 ft long by 25.5 in tall. The 4-ft length in the longitudinal direction of the bridge was chosen because this was a multiple of the welded connection spacing, and a multiple of the spacing of the original MnDOT extended bar connection.

The cross-sectional geometry of each of the test specimens is shown in Figures 14 and 15. The specimens have the same dimensions, with the only difference being at the location between the tips of the flanges of the precast sections. Comparing the geometry of the test specimens in Figure 15 and Figure 16 to the geometry of the inverted T-beam that was used in the Rte. 360 Bridge shown in Figure 4, it can be seen that the outside flange of each of the specimens was replaced by an extended web. This extension created a better bearing condition at the supports, reducing the chance of any unforeseen failure mode near the supports during testing.

Connections

Two specimens used the no-connection detail shown in Figure 14. The no-connection detail was used on the Towlston Road Bridge. The third specimen used the welded connection

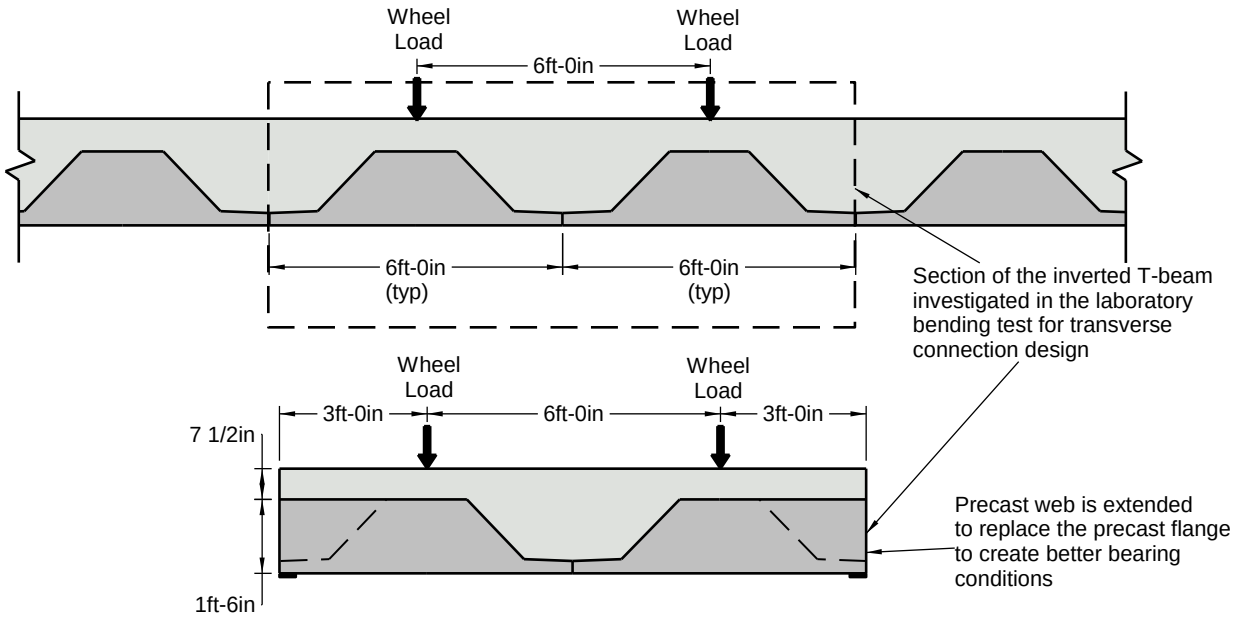

Figure 13. Virginia Inverted T-Beam Sub-assemblage Specimen as Section of a Larger Bridge Assembly

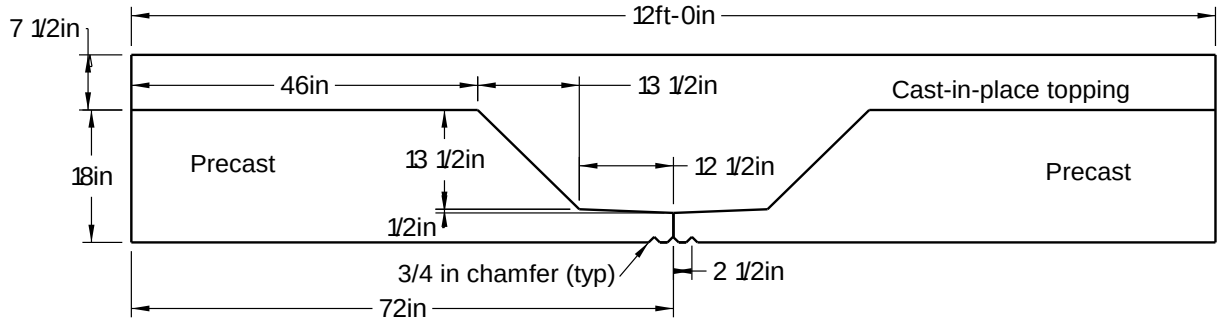

Figure 14. Cross-sectional Geometry of No-Connection Detail Test Specimens

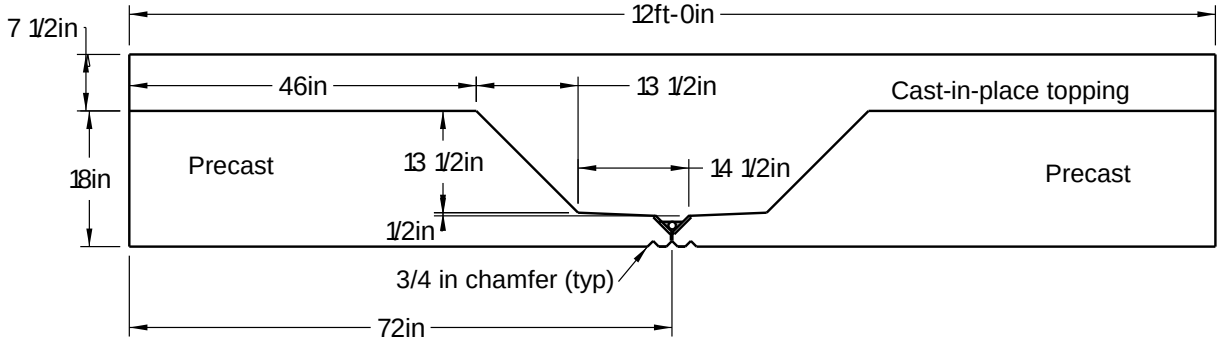

Figure 15. Cross-sectional Geometry of Welded Connection Test Specimen

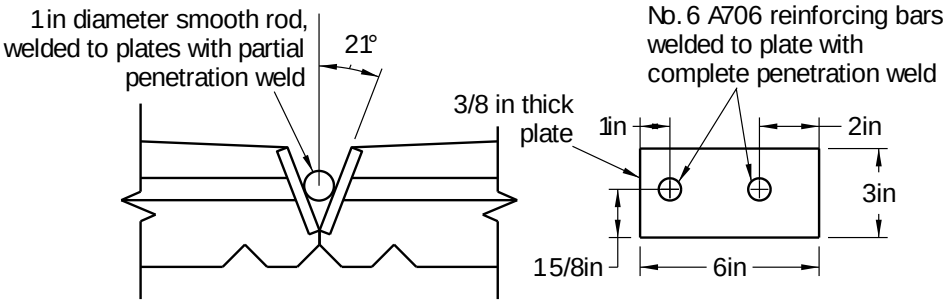

Figure 16. Welded Connection Details

shown in Figure 15, with details of the connection in Figure 16. This connection was deemed suitable for high volume bridges, and was used on the U.S. Rte. 360 Bridge over the Chickahominy River.

The two connections transfer transverse bending forces between adjacent members through different mechanisms. The no-connection detail relies on a perfect bond between the precast concrete and the cast-in-place concrete to develop a non-contact lap splice between the reinforcement in the bottom of the flanges and the reinforcement following the shape of the cast-in-place topping. In other words, the tension carried in the bottom reinforcement due to transverse bending is transferred from the bottom bars in the precast beam to the bottom bars in the cast-in-place topping through the overlapping of the bars, which are not in contact. The tension must be transferred through the concrete and across the interface. Cohesion between the precast beam and the cast-in-place topping, aided by roughening of the surface of the precast components, allows the system to act as a monolithic beam. In the welded connection, the reinforcement in the flange of the section is in tension, under positive bending conditions. The tension force is transferred through the reinforcement, into the embedded plate via a complete joint penetration weld, and then into the smooth rod that is field welded to the plate with a partial joint penetration weld (see Figure 16).

Reinforcing Steel

The reinforcement layout is shown in Figure 17 and Figure 18. The No. 6 bars in the flange of the welded connection were A706 Grade 60 weldable reinforcement so that the reinforcement could be welded to the plates. All other reinforcement was A615 Grade 60.

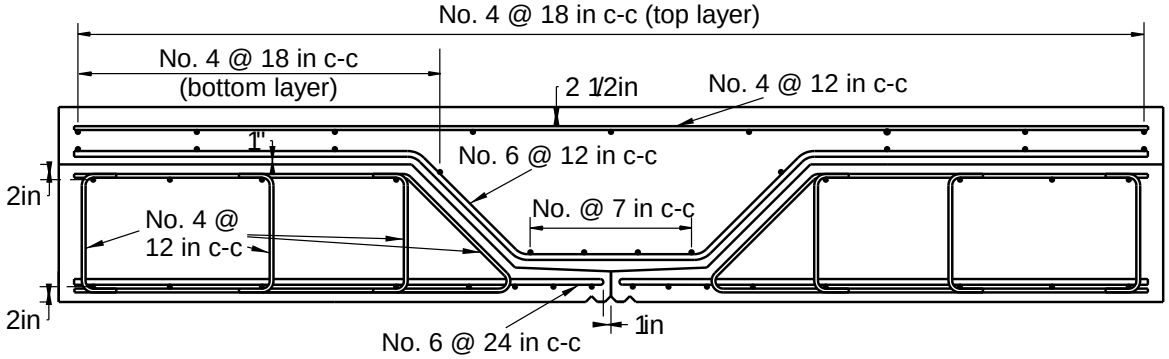

Figure 17. No-Connection Detail Reinforcement Layout

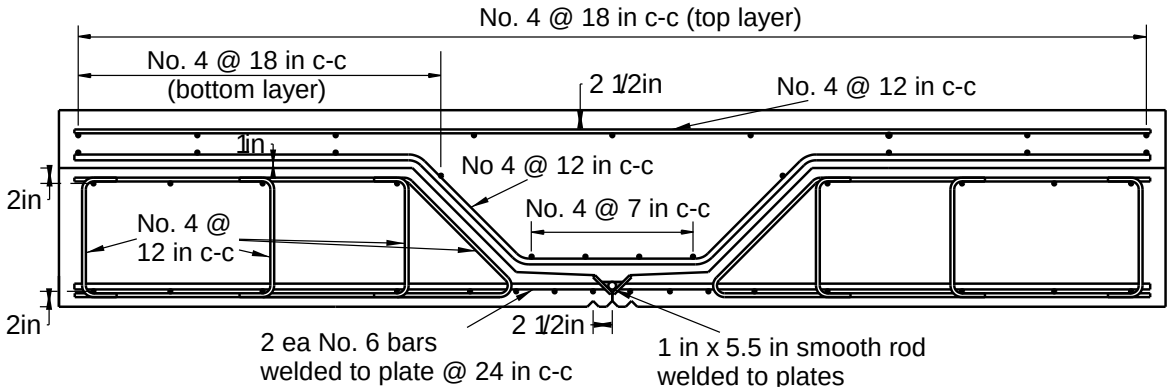

Figure 18. Welded Connection Reinforcement Layout

The design of the reinforcement in the test specimens was based on work carried out by Menkulasi (2014). Menkulasi used his analytical models to quantify the transverse bending moments resulting from the two-way plate bending behavior of the real bridge, and he sized the transverse reinforcement based on an allowable stress of 30 ksi. This analysis resulted in the No. 6 weldable bars in the precast flange. The reinforcement in the cast-in-place topping (Figure 18) was designed as shrinkage and temperature reinforcement and was not relied on for flexural strength. For the no-connection detail, the reinforcement in the flanges was initially designed by Menkulasi (2014) to resist the weight of the wet concrete topping and was No. 3 bars at 18 in center-to-center spacing. After Menkulasi's the first test, this reinforcement was increased to No. 6 bars because the initial design created a weak link in the system that resulted in a reduced flexural capacity. The No. 6 bars in the bottom flange are bent in a U-shape with the short leg of the U at the flange tip in order to improve the development of the bars. The bent No. 6 bars at 12 in spacing in the bottom of the cast-in-place topping for this specimen were sized based on the transverse live load moments at service, similar to the welded connection bottom flange steel. The remainder of the steel in the specimen was designed as shrinkage and temperature reinforcement.

Specimen Construction

Surface Roughening

To ensure monolithic action would be achieved between the two concretes cast at different times, the surfaces of the concrete in contact were required to be roughened to a ¼-in minimum amplitude, as required by AASHTO (2014). Surface roughening methods varied, depending on the locations within the specimen. Above the extended web region, the surface of the concrete was raked to a ¼-in amplitude (see Figure 19).

Surface roughening on the angled web and the flange sections of the specimen was achieved by creating a pattern of indentations on the formwork that was used on these surfaces. Various methods for creating these indentations were investigated. For the first specimen, after casting small trials, it was decided to create the surface roughening by indenting the forms and covering them with a thin sheet of painter's plastic. This was considered to be the most efficient for construction, and it was thought to provide a sufficiently roughened surface while being easy to remove and reuse the forms. Figure 20 shows the surface roughness that was used for the first

Figure 19. Raked Surface Finish above Extended Web Region

Figure 20. Cross-hatched Surface Roughness with Plastic Sheet as Bond Breaker

no-connection specimen and the welded connection specimen. For the second no-connection specimen, a trapezoidal groove with a 1.5 in spacing was selected for the surface treatment, based on the results of the push-off tests. Figure 21 shows the flanges after form removal.

Figure 21. Trapezoidal Surface Roughness

Formwork and Casting

Figure 22 presents the formwork used for the sub-assemblage specimens. Casting of the concrete for each specimen was carried out in two stages. The first stage was to cast the precast beam, and the second involved placing the cast-in-place (CIP) topping. The precast beam concrete had a specified 28-day compressive strength of 8000 psi, while the cast-in-place topping had a specified 28-day compressive strength of 4000 psi. Details of the mix proportions can be found in Edwin (2017) and Gilbertson (2018).

Figure 22. Sub-Assembly Formwork for Inverted T-beam (left) and CIP Topping (right)

Welded Connection

The embedded plate welded connection was constructed by creating a block-out in the tip of the flange of the formwork and placing the steel plate in this block-out. This allowed the concrete to be placed around the cutout at the flange, with the plate protruding. This can be seen in Figure 23.

Figure 23. Welded Connection after Welding Was Completed

After this, the two precast beams were placed adjacent to each other with the flanges, and embedded plates, making contact with each other. A piece of 1 in diameter smooth A36 steel rod was then dropped into the gap between the two embedded steel plates, and the gap was filled with weld material.

Analytical Methods to Determine Loading Protocol

Prior to testing, finite element analysis was carried out using ABAQUS software. The intention of carrying out this analysis was to determine the loads that needed to be applied to the test specimen to result in a stress state in the longitudinal joint representative of that which would occur in a real bridge. Two analytical models were created; the first was a full-scale model of the U.S. Rte. 360 over Chickahominy River Bridge, which was the first in Virginia to be constructed using the inverted T-beam system. The second model was the sub-assemblage specimen.

Model of the U.S. Rte. 360 Bridge over the Chickahominy River

The finite element analysis model representing the full-sized U.S. Rte. 360 Bridge over the Chickahominy River, which can be seen in Figure 24, comprised three-dimensional solid elements. The cross-section of the bridge model consisted of two parts, the precast inverted T-beams and the cast-in-place topping. In the longitudinal direction, the model consisted of two simply supported spans. Span lengths were 40.75 ft from the center of the abutment to the center of the bearing pad at the pier bent. At the pier bent, there was a 1.33-ft wide continuity pour along the full width of the bridge. In the transverse direction, the model was 112.33 ft wide. This width was made up of eighteen 6-ft wide precast inverted T-beams and two rectangular precast edge beams, which were 2.17 ft wide.

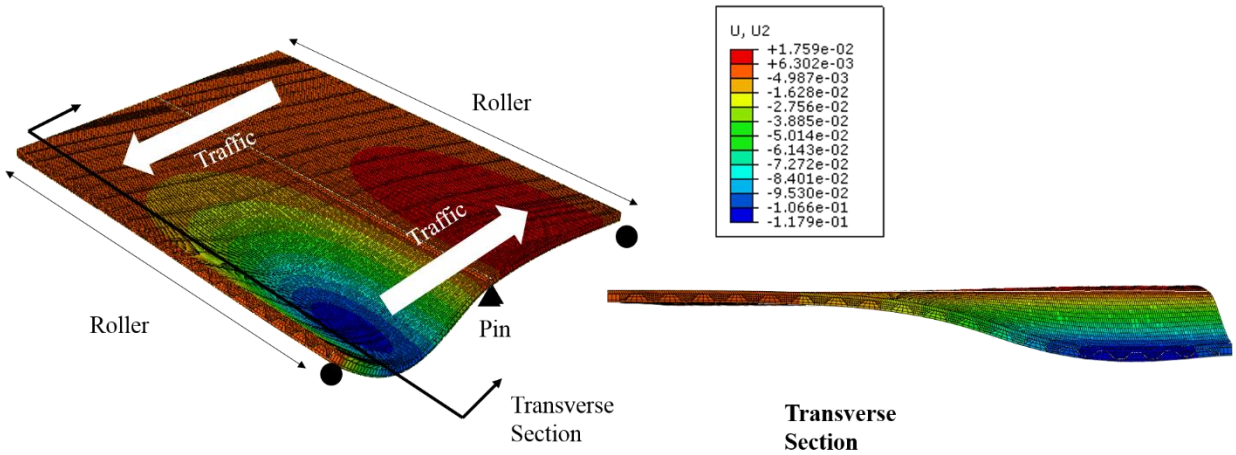

Figure 24. ABAQUS Model of the Full U.S. Rte. 360 Bridge over the Chickahominy River, Deflections in inches

Both the precast beam and the CIP topping were defined as elastic, isotropic materials. The Young's Modulus and Poisson's Ratio for the precast beam were defined as 5420 ksi and 0.2 respectively – for a concrete with a specified 28-day strength of 8000 psi. For the CIP topping with a specified 28-day strength of 4000 psi, these respective values were specified as 3830 ksi, and 0.2. The expected maximum stresses during the testing were expected to remain within the linear-elastic range of concrete behavior, therefore simplification of the model using elastic material properties was deemed to be sufficient.

The support conditions for the model were specified as a roller along the bottom edge of the end of the beams located at an abutment, and a pinned support along the bottom edge of each beam at the central bent. The bottom face of the CIP topping was constrained to deform with the top faces of the precast beams, assuming perfect bond between the precast beam and the CIP topping.

Loads were applied in accordance with the HL-93 design loading described in AASHTO (2014). This consisted of a design lane load uniformly distributed across the width of the 12-ft wide design lane, and the design truck or tandem. The loads were applied to give the worst-case transverse stress at the location of the joint between the girders. For the U.S. Rte. 360 Bridge, the design tandem created the worst-case bending stresses in the joint region as compared to the design truck.

Self-weights were not included in the analysis of the full bridge because in an actual bridge construction, the beam units would be precast, and then the CIP topping would subsequently be placed on top. The transverse bending stresses would not develop until after composite action has been achieved. Therefore, the only dead loads contributing to the transverse bending stresses at the joints would be the superimposed dead loads (that is, the future wearing surfaces and barriers). The weight of the future wearing surface (0.025 ksf) and barrier weight (0.3 k/ft) were distributed across the full lane width along with the design lane load to get the distributed load applied in the model.

Sub-assemblage Model

A finite element model representing the specimen that was to be tested in the laboratory at Virginia Tech can be seen in Figure 25. The cross-sectional geometry of the test specimen is in Figure 14.

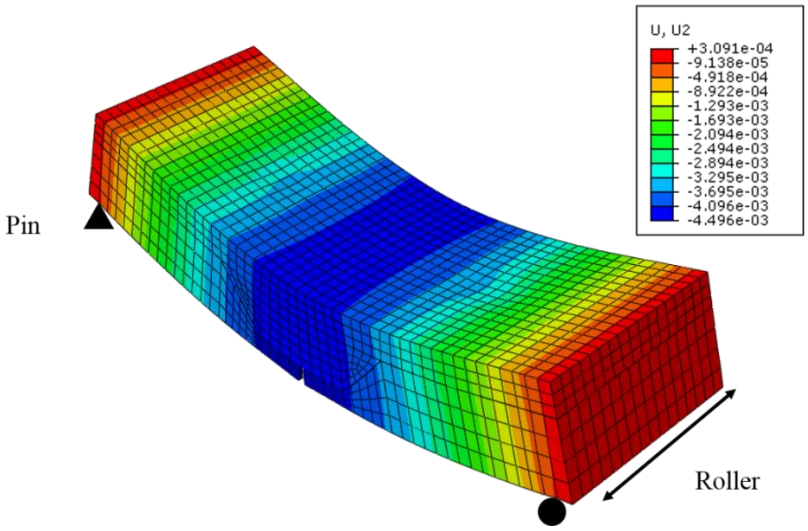

Figure 25. ABAQUS Model of the Sub-assemblage Specimen. Deflections in inches

The material properties used in the sub-assemblage were identical to the material properties in the full bridge model. Boundary conditions for the sub-assemblage model consisted of a pin type connection along the bottom edge of one end of the beam, and a roller type connection at the opposite end. The surfaces of the beam and CIP topping concretes that were in contact with one-another were constrained to move together with the assumption of perfect bond between the two concretes.

The loading configuration for the sub-assemblage model represented the test setup in the laboratory, including the self-weight of the specimen. The reason is because, under laboratory conditions, the CIP topping is cast on top of the precast beam and composite action is gained prior to the specimen being lifted into position for loading. Therefore, transverse bending stresses develop due to its own self-weight and prior to loading, unlike an actual bridge. The specimen was loaded via two 9-in by 18-in uniformly distributed loads, centered over its quarter points. The two point loads represented the wheel loads applied by the design truck or tandem in the real bridge. The magnitude of the loads applied in the model was altered until the magnitude of stresses in the cast-in-place topping at the location of the longitudinal joint between the precast beams was similar to the stresses in the same location in the full bridge model. These results dictated the loading that was applied to the test specimen in the lab setup.

Determination of Required Load on Sub-assemblage

The results of the analysis showed that the stresses in the full bridge model occurring in the vicinity of the joint, summed to around 0.17 ksi from superimposed dead loads and the HL-93 design loading. The results of the sub-assemblage model showed that under a 27 kip load, the stress at the critical location near the joint also attained a value of 0.17 ksi. The test load was increased to 30 kips to be slightly more conservative.

Testing Apparatus

Test Frame and Load Application

Two types of loading were performed on the sub-assemblage specimens: cyclic loading and monotonic loading to failure. For the cyclic loading, a 55-kip MTS hydraulic actuator applied the compressive load. For the ultimate failure test, the same set-up was used, but the actuator was switched for a 200-ton hydraulic cylinder and 250-kip load cell. Monotonic load testing for the welded connection specimen was carried out over the course of two days due to the equipment setup required to fail this specimen. With the setup used for the cyclic testing, the MTS actuator could apply a maximum load of only 130 kips. It was decided to load the specimen to the 130 kips using the setup already in place in order to get initial results, and then to switch to a 200 ton static ram to complete the failure testing.

Figure 26 shows the test set-up. The specimen was supported on two beams that were spaced 12 ft, center-to-center, and were bolted to the strong floor. A ¼-in rubber bearing pad was placed between the specimen and support beams to decrease any stress concentrations that could occur if the specimen were to bear on just the edge of the beams. Two 9-in by 18-in by 2.5-in bearing pads were placed on top of the specimen, centered along the short side, 3 ft from

the end and spaced 6 ft, center-to-center. The bearing pads simulated the tires of a loaded semi-truck. A spreader beam was centered on top of the bearing pads to spread the load from the actuator. The actuator was suspended from the cross beams of the reaction frame, and braced by angles bolted to the columns.

Figure 26. Test Set-up for Virginia Inverted T-Beam Bridge System Sub-assemblage Specimen

Instrumentation

A total of 18 instruments were used for the sub-assemblage tests: six wire potentiometers (wire pots), six LVDTs, and six strain gauges to measure the deflection, cracking along the beam-CIP topping interface, and strain in the steel reinforcement for both the precast beam and the CIP topping, respectively. A diagram of the wire pot and LVDT locations can be seen in Figures 27 and 28. The strain gauges are shown in Figures 29 and 30.

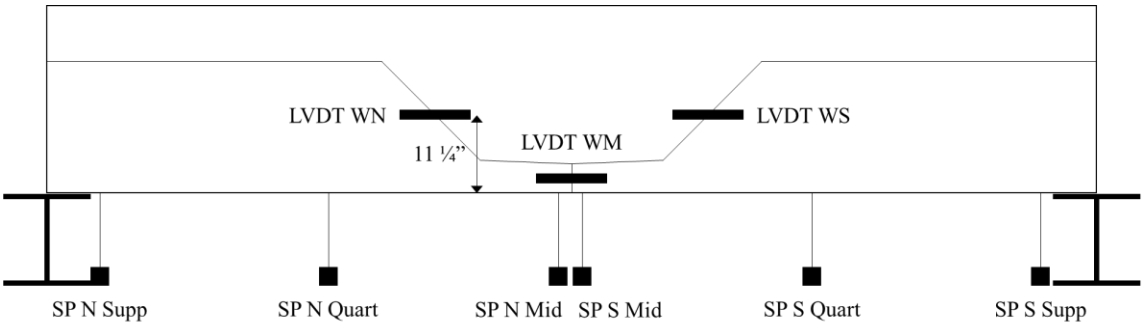

Figure 27. Elevation View of Wire Pots and LVDT on Sub-assemblage Specimen

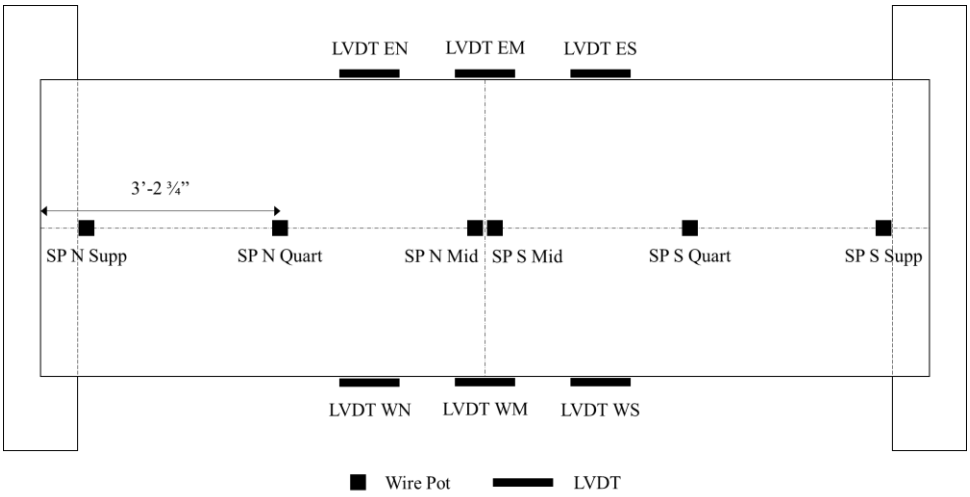

Figure 28. Plan View of Wire Pot and LVDT Locations on Sub-assemblage Specimens. LVDT = linearly variable displacement transducer.

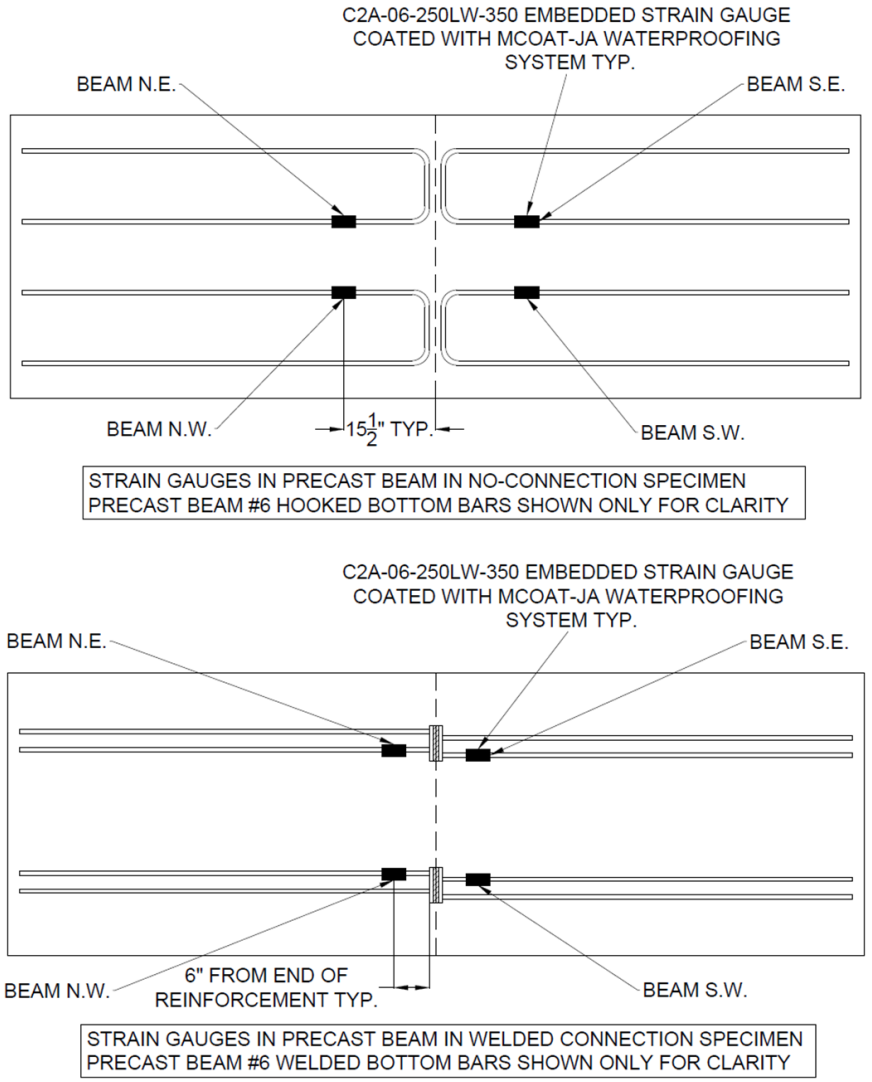

Figure 29. Plan Views of Precast Beam Portion of Sub-assemblage, with Embedded Strain Gauge Locations

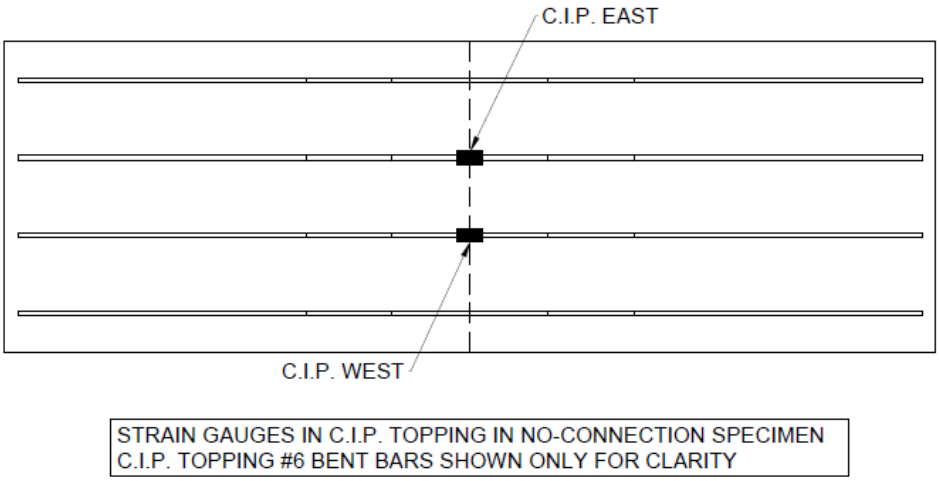

Figure 30. Plan View of CIP Topping Portion of Sub-assemblage, with location of Embedded Strain Gauges

Testing Sequence

Cyclic Loading

The sub-assemblage specimen underwent 3,650,000 cycles of 30 kips. This represents an Average Daily Truck Traffic (ADTT) of 200 for 50 years. The cycles were performed at 2.75 Hz and the minimum load during the cycles was set to 3 kips in order to prevent uplift of the actuator from the spreader beam. The cycling was paused at 0, 10, 100, 1000, 10,000, 100,000, 300,000, and every 200,000 cycles until 3,650,000 cycles in order to perform manual monotonic tests. Readings were recorded at 1 sec intervals during the monotonic tests.

Ultimate Strength Load Testing

After completion of the cyclic test, the specimen was tested to failure. Before loading began, the specimen was inspected for any visible cracking. The test then began and the load was raised to 30 kips, where the load was held and the specimen was again inspected for cracks. The test proceeded in 10-kip intervals, pausing to look for cracking each time, until the specimen was no longer able to hold additional load. Readings from the instrumentation were taken continuously throughout the loading process.

Topping Mixture Optimization Study

Mixture Designs

The topping mixture optimization study was carried out in two phases, with a total of ten mixtures designed for Phase I: five normal weight aggregate mixtures and five lightweight aggregate mixtures. The mixtures and their abbreviations are shown in Table 2. The total cementitious content and replacement levels for supplementary cementitious materials were chosen based on VDOT practice and previous research. Slag cement and fly ash were used to

replace Portland cement on a 30% and 20% ratio, by weight, respectively. The water-cement ratio was 0.45. The air content was targeted at 6.5% ± 1.5%. The targeted slump was 6 in ± 1.5 in. The targeted compressive strength was 4000 psi. All the batches had chemical admixtures in the quantities shown in Table 3. Mixture proportions are shown in Table 4 and Table 5. VDOT Class A4—General Bridge Deck Concrete using Portland cement only (Mokarem, 2008) was used as base mix with 600 lb/yd^3 as a limit to total cementitious content. The total cementitious content in lightweight aggregate mixes was limited to 650 lb/yd^3. The amount of fine aggregate replacement with saturated lightweight fine aggregate was limited to 12% based on previous studies (Henkensiefken, 2009). Details of the constituent materials can be found in Pulumati (2018).

Table 2. Design Mixtures' Abbreviations

Design Mix	Explanation
LWCA+SLAG	Lightweight coarse aggregate with 30% slag
LWCA+SLAG+SLWF	Lightweight coarse aggregate with 30% slag and saturated lightweight fines
LWCA+FA	Lightweight(LW) coarse aggregate with 20% fly ash
LWCA+SLAG+SRA	Lightweight coarse aggregate with 30% slag and shrinkage reducing admixture
Control mix LWCA	Lightweight coarse aggregate with ordinary Portland cement
NWCA+SLAG	Normal weight coarse aggregate with 30% slag
NWCA+SLAG+SLWF	Normal weight(NW) coarse aggregate with 30% slag and saturated lightweight fines
NWCA+FA	Normal weight coarse aggregate with 20% fly ash
NWCA+SLAG+SRA	Normal weight coarse aggregate with 30% slag and shrinkage reducing admixture
Control mix NWCA	Normal weight coarse aggregate with ordinary Portland cement

Table 3. Quantities of Admixtures Used

Admixture	Quantities, oz/100 lb cementitious
High range water reducer	10
Air entraining admixture	0.75
Shrinkage reducing admixture	15

Table 4. Normal Weight Aggregate Mixtures (in lb/yd^3)

Ingredients	NWCA+ SLAG	NWCA+ SLAG+ SLWF	NWCA+ FA	NWCA+ SLAG + SRA	Control mix NWCA
Portland cement	420	420	480	420	600
Slag cement	180	180	0	180	0
Fly ash	0	0	120	0	0
NW coarse aggregate	1703	1700	1637	1703	1644
NW fine aggregate	1282	1028	1328	1283	1353
LW fine aggregate	0	142	0	0	0
Water	270	270	270	270	270
Total	3855	3740	3835	3856	3867
Unit weight	143	138	142	143	143

Table 5. Lightweight Aggregate Mixtures (in lb/yd^3)

Ingredients	LWCA+ SLAG	LWCA+ SLAG+ SLWF	LWCA+ FA	LWCA+ SLAG + SRA	Control mix LWCA
Portland cement	455	455	520	455	650
Slag cement	195	195	0	195	0
Fly ash	0	0	130	0	0
LW coarse aggregate	841	900	816	841	875
NW fine aggregate	1378	1100	1400	1377	1333
LW fine aggregate	0	150	0	0	0
Water	295	295	295	295	295
Total	3164	3095	3161	3163	3153
Unit weight	117	115	117	117	117

In Phase II, the four best performing mixtures from Phase I were selected for additional study. Two mixtures with normal weight course aggregate and two mixtures with lightweight course aggregate were selected.

Mixing

All batches were mixed using a 2.5-ft^3 capacity pan mixer. The batch size for all of the batches was 1.5 ft^3. The lightweight course aggregates were allowed to soak in water for a minimum of 24 hours and batched in the saturated surface-dry condition. Moisture content and absorption of all the aggregates was determined and required corrections were made in the amount of water added into the mixer. The mixing procedure was the same for each batch to minimize variation due to batching.

Material Testing

Test Specimens

For every batch of concrete that was cast in Phase I, sixteen 4-in x 8-in cylinders and three 11.25-in x 3-in x 3-in prisms were cast in accordance with ASTM C192/C192M, Section 7. After casting the concrete, the specimens were covered with a plastic tarp to prevent loss of water and then demolded after 24 hours. The demolded specimens were moist cured for seven days using wet burlap. Testing for compressive strength, tensile strength and modulus of elasticity was done at 7, 14, 28, 56 days. Data from unrestrained shrinkage bars was collected on 1, 7, 14, 28 days and every month thereafter. In Phase II, along with the test specimens above, four 6-in x 12-in cylinders were also cast for compressive creep tests.

Fresh Concrete Properties

Slump, air content and unit weight were the fresh properties tested for each batch of concrete cast. Slump was tested according to ASTM C143 – Standard Test Method for Slump of Hydraulic-Cement Concrete. Air content and unit weight were tested according to ASTM C231 – Standard Test Method for Air Content of Freshly Mixed Concrete by the pressure method.

Compressive Strength

Compressive strength testing was done in accordance with ASTM C39 – Standard Test Method for Compressive Strength of Cylindrical Concrete Specimens. Every mix was tested for compressive strength using 4-in x 8-in cylinders at 7, 14, 28 and 56 days, and the data obtained was an average of two cylinders for every reading, except at 28 days when three cylinders were tested.

Splitting Tensile Strength

Splitting tensile strength testing was done in accordance with ASTM C496 – Standard Test Method for Splitting Tensile Strength of Cylindrical Concrete Specimens. Every mix was tested for splitting tensile strength using 4-in x 8-in cylinders at 7, 14, 28 and 56 days, and the data obtained was an average of two cylinders for every reading.

Modulus of Elasticity

Tests to determine the modulus of elasticity of the concrete specimen were done in accordance with ASTM C469 – Standard Test Method for Static Modulus of Elasticity and Poisson's Ratio of Concrete in Compression. Modulus of elasticity of every mix was determined using 4-in x 8-in cylinders at 7, 14, 28 and 56 days, and the data obtained was an average of two cylinders for every reading.

Unrestrained Shrinkage Tests

The unrestrained shrinkage test was performed in accordance with ASTM C157 – Standard Test Method for Length Change of Hardened Hydraulic-Cement Mortar and Concrete. The specimens used to test unrestrained shrinkage were 11.25-in x 3-in x 3-in prism specimens. These specimens were stored in an environmental chamber that was maintained at a humidity of 35%. The unrestrained shrinkage data was collected just after demolding; these initial readings were the basis for determining the length change of the specimens, recorded at 7, 14, and 28 days after casting, and once a month thereafter. Phase I readings were taken for 56 days, and Phase II for 10 to 11 months.

Compressive Creep Tests

In addition to the tests performed in Phase I, compressive creep tests were also performed for each concrete mix in Phase II in accordance with ASTM C512 – Standard Test Method for Creep of Concrete in Compression. Four 6-in x 12-in concrete cylinders were cast for each mix. Specimens were demolded twenty-four hours after placement and placed under moist cure for seven days. Two sets of DEMEC mechanical strain gauge locating discs were installed on each cylinder to determine length change over time. Data from compressive strength testing was collected and used to calculate the appropriate load for creep testing, which was 40% of the compressive strength.

Three cylinders were stacked under a hydraulic load cell in a controlled environmental chamber. An initial reading was taken to determine a reference. Cylinders were then loaded to the calculated compressive load and monitored for length change over time. Readings were taken every 24 hours for 7 days, then weekly for 30 days, then monthly thereafter. The fourth cylinder was not loaded, but was placed adjacent to the creep test and monitored for length change due to shrinkage strain. Elastic strain is the strain measured immediately after the creep specimens are loaded. Creep strain is the increase in strain over time as a result of the applied load. The total strain was calculated as the summation of elastic strain, shrinkage strain, and creep strain. Creep strain divided by the initial elastic strain gives the value of the creep coefficient.

Prediction Models

The AASHTO LRFD Bridge Design Specifications (2014) allow the use of three creep and shrinkage models: the AASHTO LRFD, ACI 209.2R-08 and CEB MC 90-99 models, which are briefly explained below. Details of the all three models can be found in Pulumati (2017). The results of the creep and shrinkage tests in Phase II were compared to the three models to determine the best model to predict the time-dependent properties of the CIP topping mixtures, both at an early age and later.

AASHTO LRFD Model

The AASHTO LRFD model accounts for effects of relative humidity, volume-to-surface ratio, and compressive strength at time of loading. The time development factor varies with the compressive strength at time of loading. Detailed calculations for shrinkage and creep are given in section 5.4.2.3 of AASHTO LRFD Bridge Design Specifications (2014).

ACI 209.2R – 08 Model

The ACI 209.2R model is recommended by the ACI Committee 209 (2008). This model is applicable to all normal weight and lightweight concrete with Type I and Type III cement. The ACI model accounts for humidity and volume-to-surface ratio, but not the compressive strength of the concrete. With a known mix design, the ACI model also includes factors for slump, aggregate proportions, air content and cement content.

CEB MC 90-99 model

The CEB MC90-99 model also accounts for relative humidity and strength, cement type, age at loading, and duration of loading. It is a somewhat more complicated model than the other two. One interesting aspect of the CEB MC90-99 model is that the volume-to-surface ratio effects both the ultimate creep and shrinkage coefficients and also the function describing development with time. Additional details of the model can be found in CEB (1999).

Age Adjusted Effective Modulus (AAEM) Method

The best of the three creep and shrinkage models analyzed above was used along with an AAEM approach to determine if the creep and shrinkage exhibited by the topping mixtures were

sufficient to prevent reflective cracking from developing in the topping. Previous work by Menkulasi (2014) determined that the worst-case tensile stresses, which developed due to differential shrinkage, occurred in the transverse direction where the CIP topping was thin and the beam section was thick. As shown in Figure 31, this is where the CIP topping is 7 in thick and the beam is 18 in thick. The section is slightly different from the Route 360 Bridge, but it is the same section used previously by Menkulasi. The reinforcement details shown in the figure are from the design plans of the Route 360 Bridge for a 6-ft length of the bridge in the direction of traffic.

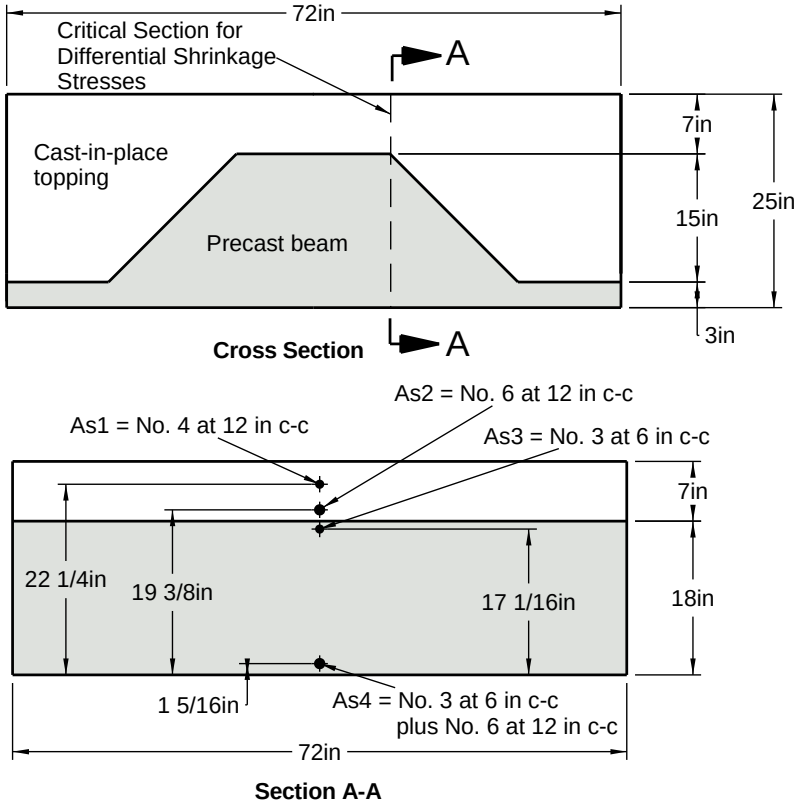

Figure 31. Transverse Section of the Inverted T-Beam System

Because the deck and the girder are cast at different times, there will be differences in their shrinkage and creep characteristics (and consequently, their behavior) once the two components begin to act compositely. This difference in shrinkage and creep will create forces in the deck and girder. These forces increase in magnitude with increasing differences in the age of the two components. When placed on top of the girder, the topping will try to shrink, but will be restrained by the girder, which will have already undergone most of its shrinkage. This restraint provided by the girder on the deck creates tensile forces in the deck. These forces can sometimes be greater than the tensile strength of concrete and thus cause cracking in the deck. These internal forces act as a constant stress applied to the deck and result in creep of concrete. Figure 32 shows the forces and moments acting on the composite section due to differential shrinkage and creep.

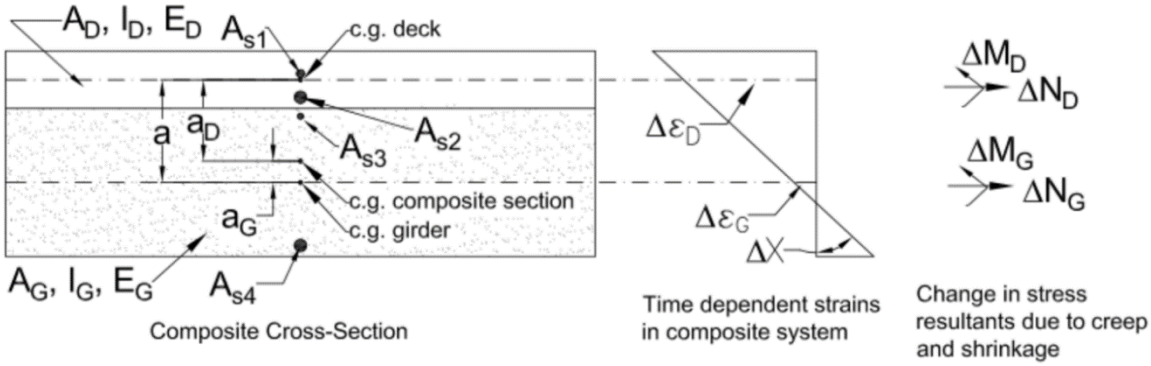

Figure 32. Forces in the cross section due to differential shrinkage and creep (from Menkulasi (2014)

The stresses and strains in the system can be quantified using equilibrium principles, material constitutive relationships and compatibility relationships, as dictated by the AAEM method. Equations 1 through 9 are used to find the unknowns. Equations 1 and 2 can determine the change in strains of the deck and girder by calculating the change in elastic strains and creep strains due to both the change in forces in that particular section and the shrinkage strains. The change in strain in any steel layer can be determined by calculating the elastic strain due to the change in axial force in that corresponding layer (Equation 3). Similarly, the change in curvature can be determined by calculating the elastic and creep curvatures due to the change in moment, as shown in Equation 4 and Equation 5. Moreover, because there are no additional external forces and moments acting, the sum of change in axial forces and moments has to be zero, as shown in Equation 6 and Equation 7. The principle of compatibility, as shown in Equations 8 and 9, can be used by assuming perfect bond between the steel reinforcement and concrete deck and girder. A set of equations can be formed to solve for the unknowns using any mathematical solving tool. Once the unknowns are evaluated, the stress in any layer of the composite section can be found.

$$\Delta\varepsilon_d = \frac{\Delta \mathrm{N_d}}{E_d * A_d}(1 + \mu * \varphi_d) + \varepsilon_{shd} \qquad \text{Equation 1}$$

$$\Delta\varepsilon_g = \frac{\Delta \mathrm{N_g}}{E_g * A_g}\left(1 + \mu * \varphi_g\right) + \varepsilon_{shg} \qquad \text{Equation 2}$$

$$\Delta\varepsilon_s = \frac{\Delta \mathrm{N_s}}{E_s * A_s} \qquad \text{Equation 3}$$

$$\Delta X_d = \frac{\Delta \mathrm{M_d}}{E_d * I_d}(1 + \mu * \varphi_d) \qquad \text{Equation 4}$$

$$\Delta X_g = \frac{\Delta \mathrm{M_g}}{E_g * I_g}(1 + \mu * \varphi_g) \qquad \text{Equation 5}$$

$$\Delta N_d + \Delta N_g + \sum_{i=1}^{n} \Delta N_{s-i} = 0 \qquad \text{Equation 6}$$

$$\Delta M_d + \Delta M_g + \sum_{i=1}^{n} (\Delta N_{s-i} * a_{s-i}) = 0 \qquad \text{Equation 7}$$

$$\Delta\varepsilon_d = \Delta\varepsilon_g - \Delta X * y_{cg} \quad \text{Equation 8}$$

$$\Delta\varepsilon_s = \Delta\varepsilon_g \pm \Delta X * y_{cg} \quad \text{Equation 9}$$

where:

A_d = area of cast-in-place deck

A_g = area of precast girder

A_s = area of steel layer considered

$a_{s\text{-}i}$ = distance between centroids of the steel layer considered and the point of interest

E_d = modulus of elasticity of the cast-in-place deck

E_g = modulus of elasticity of the precast girder

E_s = modulus of elasticity of mild steel

I_d = moment of inertia of the cast-in-place deck

I_g = moment of inertia of the precast girder

y_{cg} = distance between centroids of layers considered

ε_{shd} = Shrinkage strain of the deck

ε_{shg} = Shrinkage strain of the girder

$\Delta\varepsilon_d$ = Change in strain in the deck due to shrinkage and creep

$\Delta\varepsilon_g$ = Change in strain in the girder due to shrinkage and creep

$\Delta\varepsilon_s$ = Change in strain in the any steel layer due to shrinkage and creep

ΔX_d = Change in curvature of the deck due to shrinkage and creep

ΔX_g = Change in curvature of the girder due to shrinkage and creep

ΔN_d = Change in axial force in deck due to shrinkage and creep

ΔN_g = Change in axial force in girder due to shrinkage and creep

ΔN_s = Change in axial force in any steel layer due to shrinkage and creep

ΔM_d = Change in moment in deck due to shrinkage and creep

ΔM_g = Change in moment in girder due to shrinkage and creep

$\Sigma\Delta N_{s\text{-}i}$ = Sum of change in axial forces in all the steel layers

μ = aging coefficient

φ_d = Creep coefficient of the deck

φ_g = Creep coefficient of the girder

As described above, the AAEM method was used to quantify stresses and strains in the transverse direction of the deck at 20 years. The aging coefficient used in this project was 0.85. The shrinkage strain and creep coefficient for the deck were obtained by using ACI 209 prediction model, which was observed to be the best model compared to the data measured in this project. The time dependent properties of the girder were predicted using the AASHTO model, which is widely accepted for high strength concrete. The baseline investigation used the concrete properties from the studies, including the measured slump, and the volume-to-surface (V/S) ratios were based on the full volume and perimeter of each section.

A parametric study was undertaken to investigate the effect of the condition of the surface of the girder before placing the deck. If the top surface of the girder is saturated with water prior to placement of the deck concrete, free water in the deck concrete would not be absorbed by the girder. This means that moisture trying to escape the system must travel to the top of the deck in order to evaporate, or 7 inches in the case of the section considered. On the other hand, a dry girder surface would allow the movement of water from the deck into the girder, thus reducing the distance travelled by water in the deck.

The effect of the ease with which water can leave the concrete is accounted for in creep and shrinkage models using the Volume-to-Surface ratio (V/S). A thin concrete element has a small V/S and shrinks more than a thicker element with a large V/S. Therefore, a sensitivity analysis was performed to investigate the stresses in the deck for different V/S ratios of deck and girder. The V/S ratio used for deck were 2, 3.5, and 7 in. The 3.5 in V/S represents the case with water escaping from both sides of the deck, where the 7 in V/S represents the case with water only escaping at the top surface. The V/S ratio for the girder were 4, 9, and 18 in. As with the deck, the small value modeled moisture escaping in both directions, while the large value modeled moisture escaping on only one surface.

The slumps of the concrete mixes in Phase II were measured after the addition of water reducing admixtures. To better understand the effect of slump, which is directly affected by water content, a sensitivity analysis was performed using the V/S ratio for the deck and girder as 3.5 in and 9 in, respectively, and by varying the slump of the deck concrete. The slump values used were 3 in, 4.5 in, 6 in, and 7.5 in, but were assumed prior to the addition of plasticizers.

For each study, the inputs were used in Equations 1 through 9 to form a set of 15 equations and solve for 15 unknowns, including four layers of reinforcement. The unknowns were: ΔN_d, ΔN_g, ΔN_{s1}, ΔN_{s2}, ΔN_{s3}, ΔN_{s4}, ΔM_d, ΔM_g, $\Delta\varepsilon_d$, $\Delta\varepsilon_g$, $\Delta\varepsilon_{s1}$, $\Delta\varepsilon_{s2}$, $\Delta\varepsilon_{s3}$, $\Delta\varepsilon_{s4}$, and ΔX. Since plane sections must remain plane, the curvature in the deck and the curvature in the girder are equal ($\Delta X = \Delta X_d = \Delta X_g$)

Investigation of Transverse Reinforcement for Skewed Bridges

This part of the project investigated the optimum layout for the transverse reinforcement in the topping concrete for skewed bridges. The two possibilities are to arrange the transverse reinforcement perpendicular to the longitudinal axes of the beams, or parallel to the skew. These two options are presented in Figure 33. The perpendicular options presented challenges in detailing the reinforcement near the ends of the bridge, while the skew option allowed one type of bar to be used along the full length of the bridge.

A parametric study was undertaken using finite element models to determine the stresses over the joint between the flanges of adjacent beams. Solid elements were used to model the precast beam and the cast-in-place topping, and the two were constrained to deform together. Bridge models with six simply-supported beams with a 42-ft span length were created with 30 degrees of skew for both of the two transverse reinforcement arrangements. An elastic analysis was performed because previous studies had shown that the transverse stresses remained lower

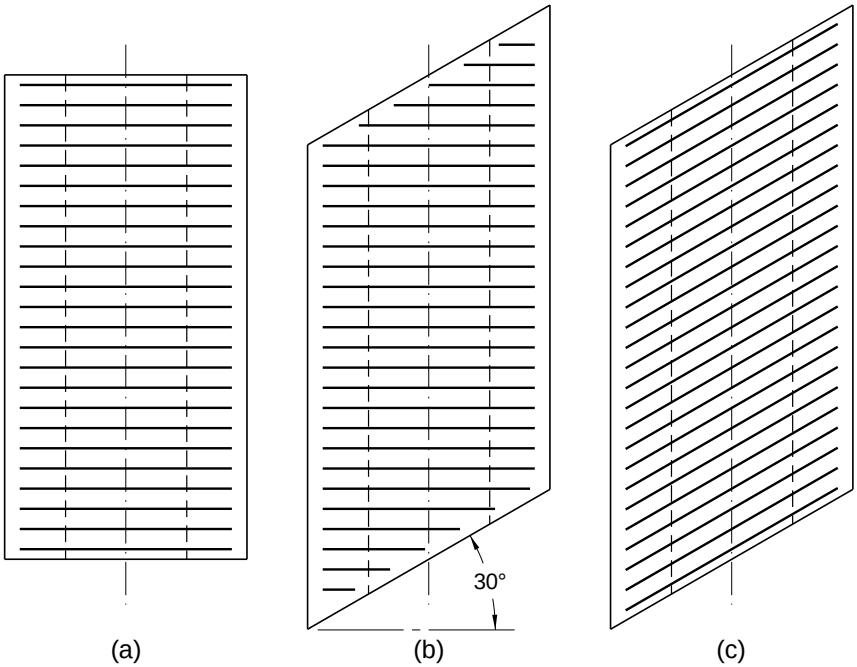

Figure 33. Options for Transverse Reinforcement in Skewed Inverted T-Beam Bridges: a) Square Bridge, b) Perpendicular to Longitudinal Axis, c) Parallel to Skew.

than the cracking stress. The location of comparison was in the topping concrete directly above the location where the flanges of adjacent beams touched. In addition, the model included an intentional crack as well as a reinforcing bar in the topping concrete above the location where the adjacent flanges touch.

RESULTS AND DISCUSSION

Development of Preliminary Design Tables

Iteration 1

Table 6 shows the results of the first iteration of design tables developed for the three cross-sections with normal weight concrete and no debonding. Figures 3 through 5 define the locations of the rows of strands. The span lengths were limited by the number of strands that could be accommodated without exceeding allowable stresses in the end regions of the beams.

Iteration 2

Debonding strands and varying the number of strands in each layer resulted in the maximum span lengths for the Small and Large sections increasing by 5 ft each, as shown in Table 7. For all sections, the limiting design consideration became the midspan service stress check.

Table 6. Iteration 1 - Inverted T-beam Preliminary Design Tables – Number of 0.6-in Diameter Strands per Row for the Three Cross-Sections of the Inverted T-Beam System

Small				
Length, ft	**Row 1**	**Row 2**	**Row 3**	**Row 4**
10	10	0	0	1
15	10	0	0	1
20	10	0	0	1
25	11	0	0	1
Medium				
Length, ft	**Row 1**	**Row 2**	**Row 3**	**Row 4**
30	10	0	0	2
35	11	0	0	2
40	17	0	0	4
45	23	0	0	5
Large				
Length, ft	**Row 1**	**Row 2**	**Row 3**	**Row 4**
50	23	1	0	6
55	23	8	0	7

Table 7. Iteration 2 - Inverted T-beam Preliminary Design Tables – Number of 0.6-in Diameter Strands per Row for the Three Cross-Sections of the Inverted T-Beam System

Small										
Length ft	**Debonding**					**Debonding & Strand Geometry Optimized**				
	Row 1	**Row 2**	**Row 3**	**Row 4**	**Number Debonded**	**Row 1**	**Row 2**	**Row 3**	**Row 4**	**Number Debonded**
15	10	0	0	2	0	10	0	0	2	0
20	10	0	0	2	0	10	0	0	2	0
25	11	0	0	2	0	12	1	0	0	2
30	19	0	0	2	2	17	2	0	0	2
Medium										
Length ft	**Debonding**					**Debonding & Strand Geometry Optimized**				
	Row 1	**Row 2**	**Row 3**	**Row 4**	**Number Debonded**	**Row 1**	**Row 2**	**Row 3**	**Row 4**	**Number Debonded**
30	10	0	0	2	0	10	0	0	2	0
35	11	0	0	2	0	8	4	2	2	0
40	20	0	0	4	2	10	6	6	2	0
45	23	5	0	4	6	13	9	9	2	2
Large										
Length ft	**Debonding**					**Debonding & Strand Geometry Optimized**				
	Row 1	**Row 2**	**Row 3**	**Row 4**	**Number Debonded**	**Row 1**	**Row 2**	**Row 3**	**Row 4**	**Number Debonded**
50	23	6	0	5	6	12	8	6	2	6
55	23	14	0	5	10	15	12	12	3	8
60	23	23	2	6	12	21	17	15	4	14

Iteration 3

From Tables 8 and 9, it can be seen that LW Option 1, with lightweight topping and normal weight beams, did not reduce stresses significantly enough to increase the span lengths. However, the amount of prestressing required for each cross-section could be reduced in most instances. Using LW Option 2, with lightweight topping and beam, the span lengths for the largest section could be increased, but the other sections remained at the same span length with less prestressing required.

Table 8. Iteration 3 - Inverted T-beam LW Option 1 Preliminary Design Tables - Number of 0.6 in Diameter Strands per Row for the Three Cross-Sections of the Inverted T-Beam System

Small - NW Beam, LW Deck										
Length ft	Debonding					Debonding & Strand Geometry Optimized				
	Row 1	Row 2	Row 3	Row 4	Number Debonded	Row 1	Row 2	Row 3	Row 4	Number Debonded
15	10	0	0	2	0	10	0	0	2	0
20	10	0	0	2	0	10	0	0	2	0
25	10	0	0	2	0	11	1	0	0	2
30	18	0	0	2	2	16	2	0	0	2
Medium - NW Beam, LW Deck										
Length ft	Debonding					Debonding & Strand Geometry Optimized				
	Row 1	Row 2	Row 3	Row 4	Number Debonded	Row 1	Row 2	Row 3	Row 4	Number Debonded
35	11	0	0	2	0	7	4	2	2	0
40	15	0	0	2	4	8	6	4	2	0
45	23	4	0	4	6	11	8	8	2	0
50	23	14	0	4	8	15	11	11	2	6
Large - NW Beam, LW Deck										
Length ft	Debonding					Debonding & Strand Geometry Optimized				
	Row 1	Row 2	Row 3	Row 4	Number Debonded	Row 1	Row 2	Row 3	Row 4	Number Debonded
50	23	4	0	5	4	11	7	7	2	6
55	23	13	0	5	10	15	11	11	3	8
60	23	23	0	6	12	19	16	16	4	12

Table 9. Iteration 3 - Inverted T-beams LW Option 2 Preliminary Design Tables - Number of 0.6 in Diameter Strands per Row for the Three Cross-Sections of the Inverted T-Beam System

Small - LW Beam, LW Deck										
Length ft	Debonding					Debonding & Strand Geometry Optimized				
	Row 1	Row 2	Row 3	Row 4	Number Debonded	Row 1	Row 2	Row 3	Row 4	Number Debonded
15	10	0	0	2	0	10	0	0	2	0
20	10	0	0	2	0	10	0	0	2	0
25	10	0	0	2	0	11	0	0	2	0
30	17	0	0	2	0	15	2	0	0	0
Medium - LW Beam, LW Deck										
Length ft	Debonding					Debonding & Strand Geometry Optimized				
	Row 1	Row 2	Row 3	Row 4	Number Debonded	Row 1	Row 2	Row 3	Row 4	Number Debonded
35	10	0	0	2	0	10	0	0	2	0
40	16	0	0	3	2	9	4	4	2	0
45	23	2	0	4	4	10	8	6	2	0
50	23	12	0	4	8	15	11	9	2	4
Large - LW Beam, LW Deck										
Length ft	Debonding					Debonding & Strand Geometry Optimized				
	Row 1	Row 2	Row 3	Row 4	Number Debonded	Row 1	Row 2	Row 3	Row 4	Number Debonded
50	23	1	0	4	6	9	8	6	2	4
55	23	10	0	5	8	15	11	9	3	8
60	23	21	0	6	10	18	15	13	4	10
65	23	23	9	7	14	23	23	9	7	14

In this case, the limiting design considerations were either the service limit state compressive stress limits at the midspan of the beam due to effective prestress and permanent loads or the midspan tensile stresses at the service limit state. It was found that removing strands from the top of the beam reduced these stresses; however, removing too many top strands reduced the total number of strands that could be debonded, which shifted the issue back to the end zones.

Final Iteration

The preliminary design tables in the final iteration performed in this study can be seen in Table 10. The tables are intended to be used as an initial design aid for bridge engineers. Knowing the required span lengths of a bridge, designers are able to look at the table for the inverted T-beams and pick out a strand arrangement for their beam. In this sense, the preliminary design tables can also be used during conceptual design phases for cost comparisons with other adjacent bridge beam systems such as box beams and voided slabs.

Horizontal Shear Push-off Specimens

Concrete Strengths

The horizontal shear push-off specimens were cast in three batches and each had a bottom section and top section that were placed at separate times, meaning that concrete was ordered six separate times to complete construction. Three of the deliveries were for 8000-psi concrete and the other three were 4000-psi concrete. Table 11 shows the compressive strength of the top and bottom sections in each batch at the time of testing. All three of the cast-in-place concrete mixes reached a compressive strength of over 4000-psi, but only one of the precast mixes ended up with a compressive strength over 8000-psi. Further information about the mix proportions and graphs of the strength over time can be found in Gilbertson (2017).

Using the staged deck placement option, the maximum span length of the beam increased to 60 ft and by providing temporary shoring at mid-span, the maximum span length of the beam could be increased to 68 ft for the normal weight concrete and for LW Option 1, and 70 ft for LW Option 2. The limiting stresses in both of these situations are the midspan in-service stresses, with compressive stresses governing the staged deck pour option, and tensile stresses governing the temporary shoring option. Note that for spans 55 ft and above, the precast concrete compressive strength must be 7 ksi at release and 10 ksi at service, and the deck concrete strength must be 4.5 ksi. For shorter span lengths, 5 ksi release strength and 8 ksi 28-day strength for the precast, along with 4 ksi deck concrete are sufficient.

Surface Roughness Quality

There was an issue with the creation of the manufactured rectangular groove texture, which had been known to be very difficult to produce because of the amount of time required to chisel out the plywood form from the grooves in the formed concrete. The hope was that the addition of a TuffCoat® surface was enough to create a clean removal; however, that was not the

Table 10. Final Preliminary Design Tables
Number of 0.6 in Diameter Strands per Row for the Medium Cross-Section of the Inverted T-Beam System

Normal Weight Concrete					
Span Length, ft	Prestressing arrangement				
	Row 1	Row 2	Row 3	Row 4	Debonded
30	10	0	0	2	0
35	11	0	0	2	0
40	20	0	0	4	0
45	20	6	0	4	0
50	20	8	6	2	8
55[a]	20	16	4	2	14
60[a]	20	20	6	2	16
65[b]	20	20	8	2	8
68[b]	20	20	18	2	8
Light Weight Deck					
Span Length, ft	Prestressing arrangement				
	Row 1	Row 2	Row 3	Row 4	Debonded
30	10	0	0	2	0
35	11	0	0	2	0
40	16	0	0	2	4
45	18	4	0	2	6
50	18	6	4	2	2
55[a]	20	8	4	2	6
60[a]	20	20	6	2	10
65[b]	20	20	8	2	8
68[b]	20	20	18	2	8
Light Weight Deck & Beam					
Span Length, ft	Prestressing arrangement				
	Row 1	Row 2	Row 3	Row 4	Debonded
30	10	0	0	2	0
35	10	0	0	2	0
40	16	0	0	2	0
45	20	2	0	2	8
50	20	6	0	2	10
55	20	14	0	4	8
60[a]	20	20	0	4	8
65[b]	20	18	4	2	8
70[b]	20	20	14	2	8

a. This span can be reached by staging construction - pouring a third of the deck located near midspan prior to completing the deck pour, and two top strands must be cut before deck placement.
b. This span can be reached using temporary shoring at mid span - shore for approximately 10 days for topping to reach about 75% of 28-day $f`_c$ for composite action to be achieved

case. Figure 34 shows the bottom section of a specimen during removal of the textured plywood. About half of each rectangular groove was torn off with the form, and the plywood was left behind in the other half. This occurrence was consistent with the other two specimens with this pattern. Although these specimens with about 50 percent of the texture still intact were not discarded, this texture was ruled out as a possible method for this research.

Table 11. Horizontal Shear Push-off Specimens Concrete Compressive Strengths

Batch	Included Specimens (three of each designation)	Theoretical Strength	Strength at 28-days	Strength at Time of Testing
1	CH-3.5-TC RK-1	8000 psi (Precast)	8140 psi	8750 psi
		4000 psi (Cast-in-place)	5530 psi	5950 psi
2	RG-1 TG-1.5 RK-2 RK-3	8000 psi (Precast)	6290 psi	6760 psi
		4000 psi (Cast-in-place)	4100 psi	4400 psi
3	TG-3 SK-2.5 CH-3.5-PL EA	8000 psi (Precast)	7220 psi	7800 psi
		4000 psi (Cast-in-place)	4440 psi	4520-psi

Figure 34. Result of Removal of Textured Plywood Form for Rectangular Grooves

Push-off Strength Results

This section provides an analysis of typical data from one horizontal shear push-off test, summarizes the results of all tests, and compares the outcomes to AASHTO design values. A more in-depth report on the testing of each specimen can be found in Gilbertson (2017)

Typical Results

A typical plot of a load versus time during a push-off test is shown in Figure 35. This plot, created for specimen TG-1.5-02, contains data from both the horizontal applied load and the vertical clamping force in the harness. The plot shows that the test initially proceeded with the applied load increasing at a steady rate and the clamping force remaining constant. As the load reached its peak and the interface failed in shear, the clamping force in the harness increased slightly.

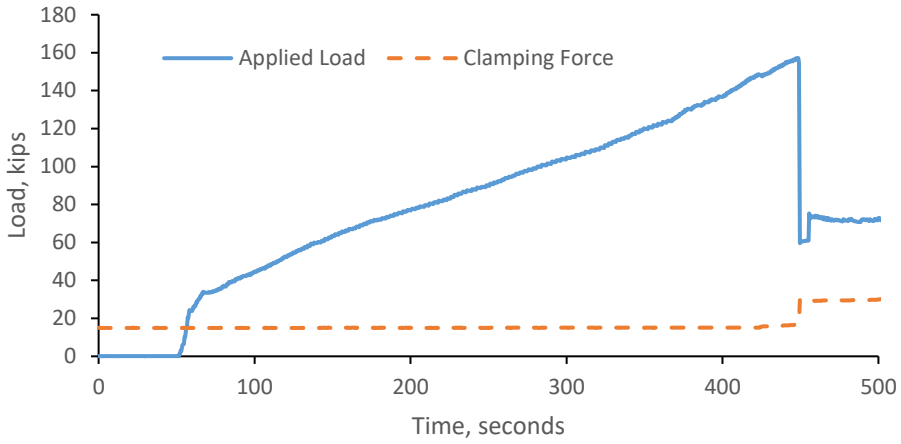

Figure 35. Plot of Load vs. Time for Horizontal Shear Push-off Specimen TG-1.5-02

Figure 36 shows a typical load versus slip plot, also from the test of TG-1.5-02. As the applied load initially increases, zero movement is induced across the shear interface, although a small amount of slip appears as the applied load nears its peak value. A corresponding slight increase in the clamping force is observed with the marginal amount of slip, caused by dilation of the interface. Once the peak load is surpassed, the load decreases by over 50% while the slip increases drastically. As the load is reengaged, the slip increases while the load remains constant, showing that the interface cannot endure further load. The clamping force increases a slight amount when the interface fractures but does not increase further after the load reengages and the slip increases, showing that the harness was designed correctly and only shows an increase in force when the interface dilates.

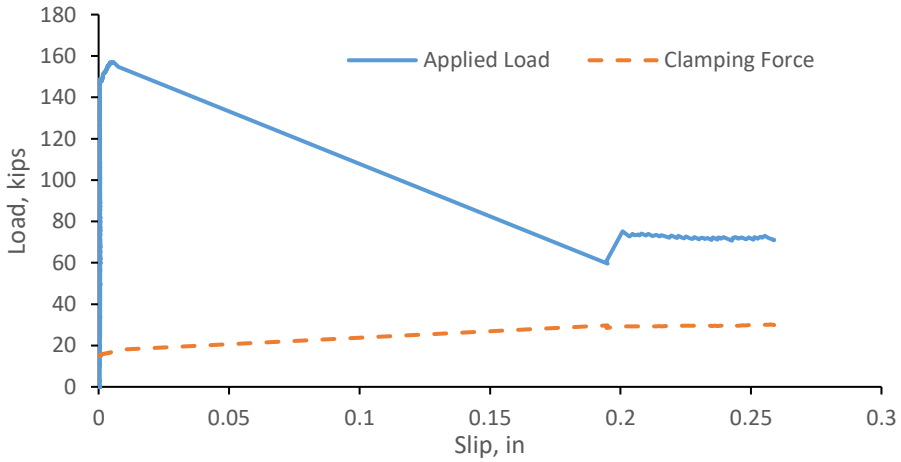

Figure 36. Plot of Load vs. Slip for Horizontal Shear Push-off Specimen TG-1.5-02

As seen in both Figures 35 and 36, the load applied to the specimen drastically decreases once the interface fractures and the small residual load is a function of the normal force applied to the specimen. This means that the interface exhibits its maximum horizontal shear strength before fracture. Table 12 shows the fracture stress for each specimen and averages for each type, while Figure 37 is a bar chart comparing the different textures.

Table 12. Horizontal Shear Push-Off Specimen Fracture Strengths

Texture Type	Specimen	Specimen Fracture Stress	Average Fracture Strength
Raked 1 in	RK-1-01	419 psi	373 psi
	RK-1-02	354 psi	
	RK-1-03	346 psi	
Raked 2 in	RK-2-01	275 psi	246 psi
	RK-2-02	258 psi	
	RK-2-03	204 psi	
Raked 3 in	RK-3-01	303 psi	321 psi
	RK-3-02	306 psi	
	RK-3-03	353 psi	
Rectangular Grooves	RG-1-01	328 psi	298 psi
	RG-1-02	287 psi	
	RG-1-03	279 psi	
Trapezoidal Grooves 1.5 in	TG-1.5-01	443 psi	393 psi
	TG-1.5-02	409 psi	
	TG-1.5-03	327 psi	
Trapezoidal Grooves 3 in	TG-3-01	341 psi	365 psi
	TG-3-02	385 psi	
	TG-3-03	370 psi	
Cross Hatch TuffCoat	CH-3.5-TC-01	473 psi	414 psi
	CH-3.5-TC-02	383 psi	
	CH-3.5-TC-03	387 psi	
Cross Hatch Plastic	CH-3.5-PL-01	Data Not Available	261 psi
	CH-3.5-PL-02	276 psi	
	CH-3.5-PL-03	245 psi	
Square Knobs	SK-2.5-01	347 psi	321 psi
	SK-2.5-02	276 psi	
	SK-2.5-03	339 psi	
Exposed Aggregate	EA-01	272 psi	302 psi
	EA-02	282 psi	
	EA-03	353 psi	

The highest average interface shear stresses were produced by the cross hatch that was debonded with TuffCoat (414 psi) and the trapezoidal grooves that were spaced 1.5 in (393 psi). Both textures include sharp angles and were designed such that the surface area of the raised portion was equal to that of the indented area. For both of these patterns, the TuffCoat material acted as a good debonding agent and helped to preserve the sharp edges unlike a plastic coating

The raked 1-in texture and the 3-in trapezoidal grooves also performed well, achieving fracture stresses over 350 psi. Even though they did not feature sharp edges, closely-spaced rakes were closer to achieving an equal surface area of raised versus lowered areas. On the other hand, the trapezoidal grooves did not feature equal surface areas of raised and lowered sections, but did have sharp edges that helped to raise the fracture strength.

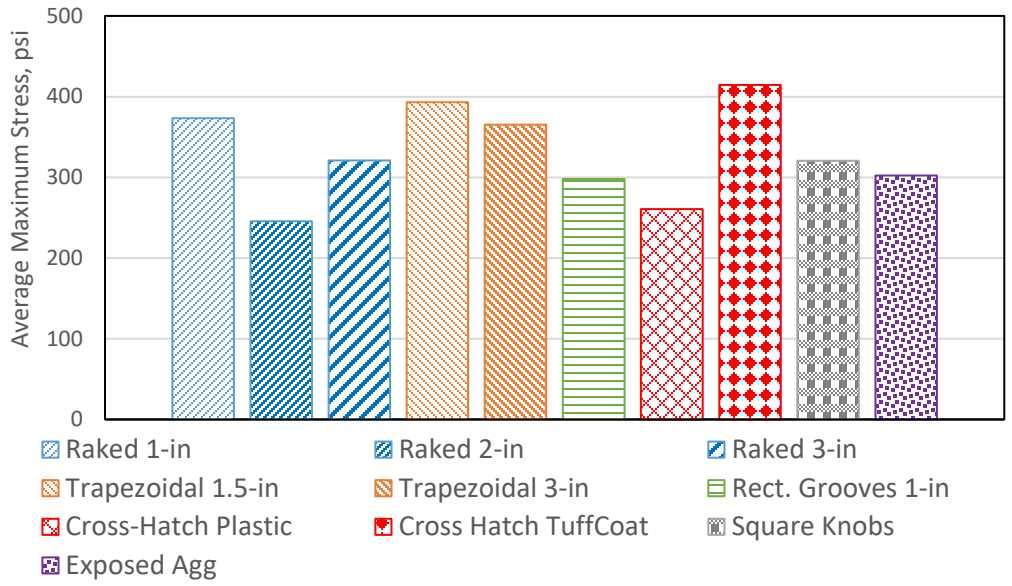

Figure 37. Interface Fracture Strength for Surface Roughening for Horizontal Shear Push-off Specimens

The rectangular grooves, square knobs, raked 3-in and exposed aggregate textures all exhibited first horizontal cracking at stresses around 300 psi. The rectangular grooves were damaged during construction, and so the stress to cause horizontal cracking of the fully intact surface is likely well above the level it obtained during these tests. Of the three specimens with square knobs, two specimens cracked at nearly 350 psi, while the third was an outlier near 280 psi. Given further testing, this texture might prove to be closer in stress to the 3-in trapezoidal grooves. The 3-in raked texture did not have close spacing or equal areas, although it did have 0.25-in grooves, which meant that it had a fracture strength that was higher than that of the exposed aggregate, which did not have any regular ridges.

The cross hatch texture with the plastic used for debonding, which was used in two of the sub-assemblage tests, produced one of the lowest interface shear stresses at fracture, with an average of only 261 psi. This value is very low, especially when compared to the 414 psi average that was achieved by the cross hatch texture with TuffCoat used for debonding. Using plastic as a debonding agent decreased the shear strength of the texture by 150 psi.

The results are inconclusive regarding the hypothesis that an increase in spacing of the grooves or rake pattern produced lower horizontal shear strength, especially when looking at the trapezoidal groove textures. The 1.5-in trapezoidal grooves achieved an average horizontal shear strength of 393 psi, but the 3-in trapezoidal grooves only reached 365 psi, which supports the hypothesis. However, the results from the raked textures do not fully support this relationship. The raked 1-in texture had an average shear stress at fracture of 373 psi, and the 3-in raked texture had an average shear stress at fracture of 321 psi, meaning that the smaller spacing between 0.25-in deep rakes produced a larger shear strength. Unfortunately, the raked 2-in did not follow the pattern, where the average shear stress at fracture was 246 psi, much lower than that of the raked 3-in. All three sets of specimens were produced in the same manner, and the 2-in raked and 3-in raked specimens were both part of Batch 2, so neither production method nor concrete composition caused this result.

Results Compared to AASHTO LRFD Bridge Design Specifications

Although the minimum interface shear reinforcement was not provided in the push-off specimens, there were two applicable cases for cohesion and friction coefficients in AASHTO LRFD, section 5.7.4.4.The first was for cast-in-place concrete slabs placed on intentionally roughened girders, where cohesion was 0.28 ksi and the friction coefficient was 1.0. In this case, the calculated strength of the push-off specimens was 320 psi. There were only four textures with an average fracture exceeding that value: 1-in raked, 1.5-in and 3-in trapezoidal grooves, and cross hatch debonded with TuffCoat. The second case assumed normal weight concrete placed on an intentionally roughened concrete surface, with a cohesion of 0.24 ksi and a friction coefficient of 1.0. The calculated strength for this scenario was 280 psi. Both the cross hatch debonded with plastic and the 2-in raked textures failed to achieve this lower design strength for interface shear.

Selected Texture for Second No-Connection Detail Sub-Assemblage Specimen

Based on the above results, the researchers specifically considered the results from the cross hatch with TuffCoat and the 1.5-in trapezoidal grooves in choosing the textured surface of the second no-connection sub-assemblage specimen. Two of the three cross hatch specimens failed at about 385 psi, with an outlier at approximately 470 psi, whereas two out of the three trapezoidal groove specimens failed above 400 psi, with the outlier at about 330 psi. Although more tests would need to be done to confirm this trend, the research team therefore reasoned that the trapezoidal grooves texture would outperform the cross hatch texture. Furthermore, the trapezoidal grooves proved easier to construct. Lastly, trapezoidal grooves have been previously utilized on a constructed Virginia Inverted T-Beam bridge. Thus, the 1.5-in trapezoidal grooved texture was chosen for use in the second no-connection detail sub-assemblage specimen.

Sub-assemblage Testing

Material Testing

Table 13 presents the concrete compressive strengths for the beam and topping concretes in each of the three sub-assemblage tests.

Table 13. Concrete Strengths for Sub-assemblage Specimens

Specimen	Compressive Strength (psi)
Welded Connection Beam	4350
Welded Connection Topping	6200
No-Connection with Poor Interface Beam	7900
No-connection with Poor Interface Topping	3800
No-Connection with Good Interface Beam	8000
No-Connection with Good Interface Topping	4560

Welded Connection Specimen

Results from Cyclic Load Test

For the welded connection specimen, there was no visually observable deterioration in performance of the specimen over the entire 3,650,000 cycles, and for each of the static load tests, the instrumentation recorded consistent values. The range of measured displacements at the 30-kip intermittent static loadings was relatively small (less than 0.012 in). This narrow range demonstrated that, between static tests, displacement results did not vary significantly. The maximum amount of displacement occurred at the south midspan and had a magnitude of 0.032 in. Similarly, the LVDTs recorded zero displacement under the 30-kip static loads, indicating no cracking or slipping of the interface during cycling. Also, all strains on the reinforcing steel in the specimen were small and consistent throughout the testing. The largest strain on the steel reinforcement was 26με, measured in the cast-in-place concrete topping. The largest measured strain on the reinforcement in the precast beam was 17με. These results further indicated that the concrete remained uncracked. The complete results of each piece of instrumentation is provided in Edwin (2017).

Results from Monotonic Test to Failure

As discussed in the Methods section, the welded connection specimen was tested using two different actuators. Thus, the results herein are presented for both of the days of loading; Day 1 is defined as loading to 130 kips using the MTS actuator, while Day 2 used the static ram to take the specimen to failure.

During the monotonic test, the first cracks appeared as hairline cracks in the precast beam section, approximately 26 in from the joint between the two adjacent beams, at 50 kips. At this load, there was no cracking in the topping, and no cracks could be observed at the interface between the precast beam and topping concrete.

The first cracks in the topping concrete appeared at an applied load of 100 kips. This crack occurred directly over the joint between the two precast beams. At this stage, cracking in the precast beams had propagated, but there were no new cracks in the precast beams. Additionally, no interface cracks had appeared.

After reaching 130 kips without failure, the actuators were switched and loading continued. Failure of the specimen occurred at a load of 194 kips, when a large crack formed in the topping directly above the joint between the two precast beams and propagated upwards through the specimen. This can be seen in Figure 38. In addition, Figure 38 shows that the cracking that had initiated in the precast beams at 50 kips had fully propagated through the beam section and had made its way into the topping. At failure, no slippage could be detected at the interface between the two components.

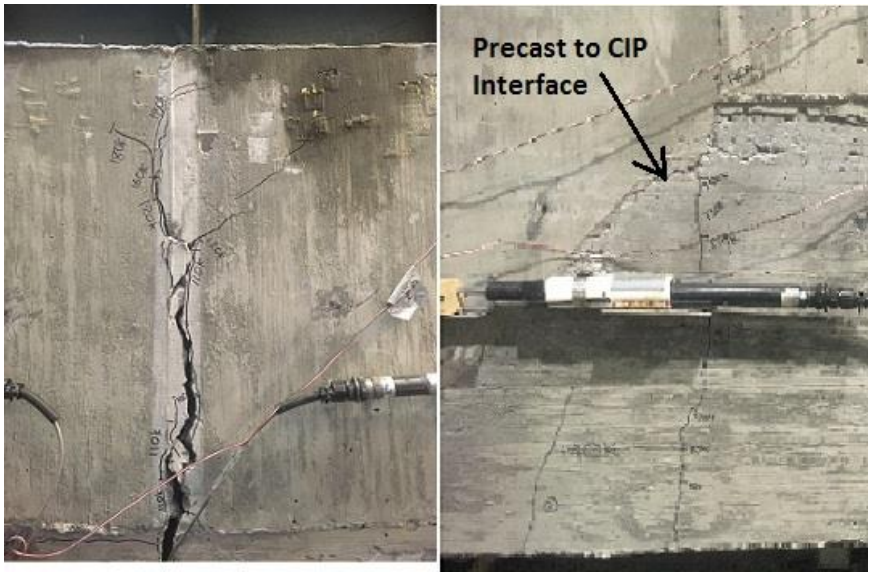

Figure 38. Welded Connection Specimen Cracking at Failure Load of 194 kips (crack at joint left and crack at interface right)

Upon further inspection of the section, it could be seen that the weld metal near the drop-in steel rod had failed. Nevertheless, the results from monotonic testing of the specimen indicated that the reinforcing welded to the plate yielded before the weld itself failed. The observed failure surface in the weld had a clean, bright appearance with no "beach marks", thus indicating a brittle fracture, albeit after ductile yielding had occurred in the bar. The weld geometry likely had a role in this failure. The root pass of the weld (at the bottom in Figure 39) contained a build-up of impurities. As the first pass was not good, that pass became the weak point of the weld, which was at the location of a high localized stress under positive bending as the joint was trying to open. Thus, the fracture initiated at this location and then propagated vertically through the weld, causing failure of the connection. Thus, the failure was caused by a weld weakness, and was not influenced by the cyclic testing.

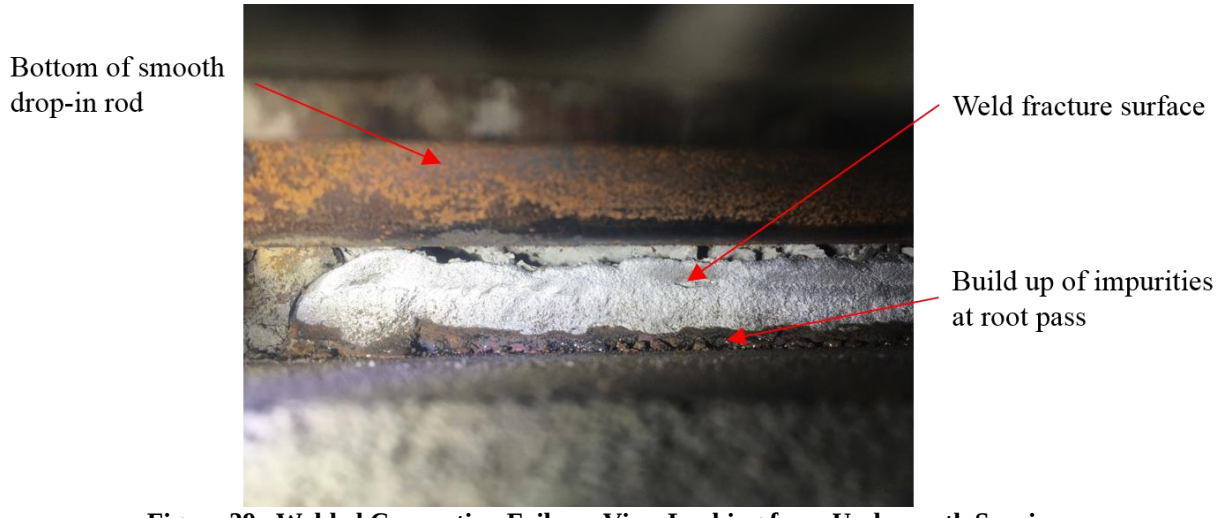

Figure 39. Welded Connection Failure, View Looking from Underneath Specimen

Figure 40 shows the applied load plotted against the midspan deflection recorded by the north midspan string pot. Since the first day of testing of the specimen caused cracking, the full plots for both days of testing are shown. Prior to cracking, the specimen showed a higher initial stiffness, as indicated by the steeper slope of the load versus deflection curve. At 110 kips, significant amounts of cracking occurred and the load-displacement behavior for the first day of testing began to exhibit a lower stiffness, at which point, the testing had to be stopped to change out testing equipment. Upon reloading the specimen on the second day of testing, the load-displacement behavior showed that the specimen exhibited a cracked stiffness, with a lower stiffness compared to the testing on Day 1. At 140 kips, inelastic behavior became apparent. Ultimately, the specimen failed at 194 kips.

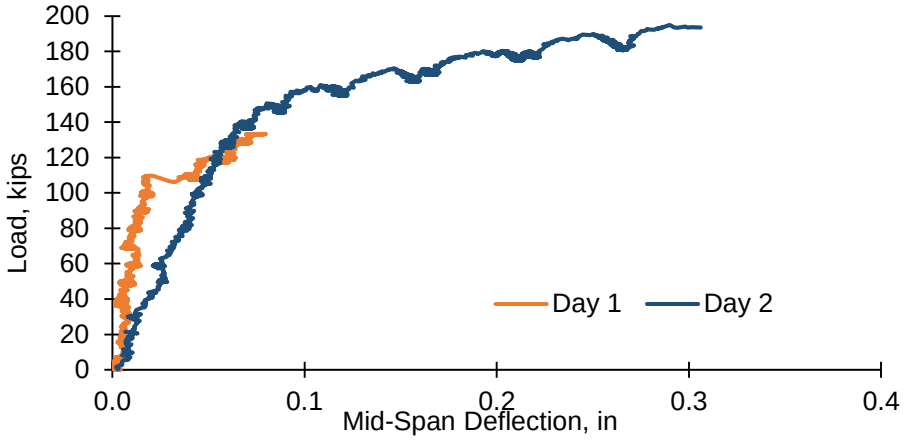

Figure 40. Welded Connection Failure Test - Load vs Midspan Deflection

Figures 41 and 42 show reinforcing steel strains vs applied load. Up until 100 kips on the first day of testing, reinforcement strains in all locations increased proportionally with load, and remained close to each other in terms of magnitudes. After that point, there was a small jump in strain of the reinforcement in the topping, possibly indicating a crack initiating. At 110 kips, all of the strain gauges experienced a jump in strain before continuing to increase linearly to 120 kips, at which point the beam reinforcement strain gauges experienced another, smaller jump in strain.

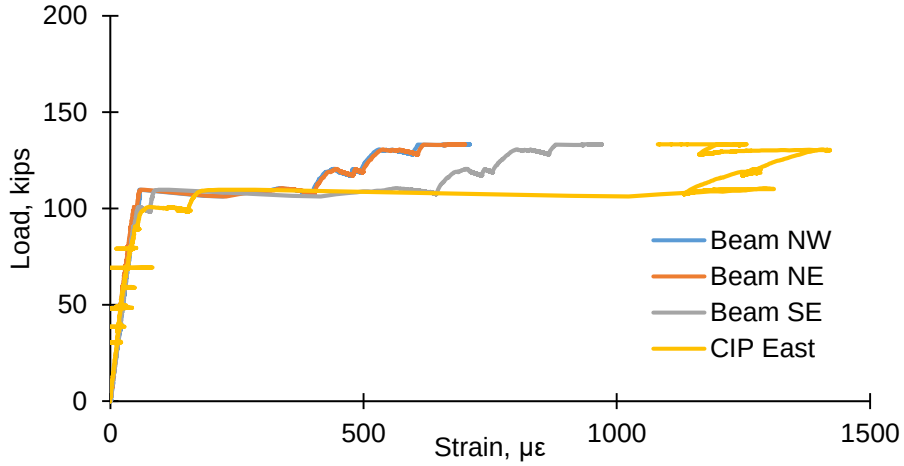

Figure 41. Welded Connection Failure Test Day 1 - Load vs Strain

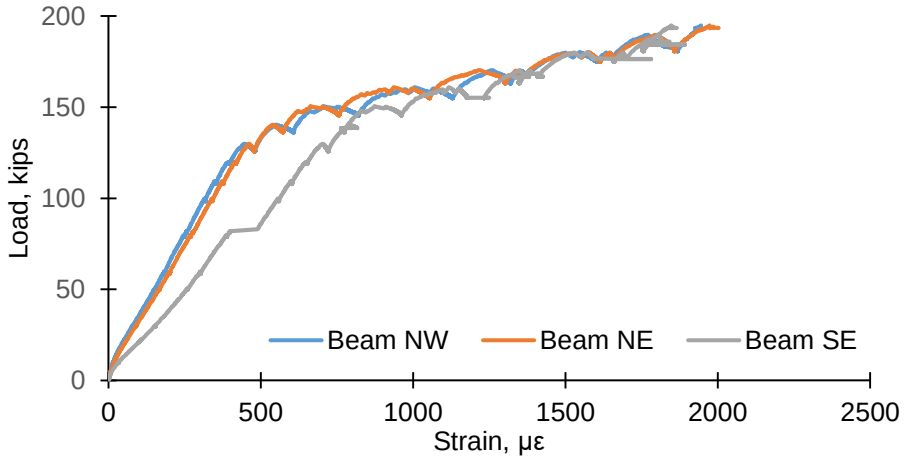

Figure 42. Welded Connection Failure Test Day 2 - Load vs Strain

On the second day of testing, as shown in Figure 42, the strains in the beam reinforcement increased at a reduced stiffness until they reached the point at which loading was stopped during the first day of testing. At this point, and upon subsequent increases in load, the strains in the reinforcement continued to increase linearly, although they increased at a lower rate, and small jumps in strain occurred. It should be noted that the maximum strains were approximately at the yield strain for Grade 60 reinforcement (2070 με).

Figure 43 shows the applied load plotted against LVDT measurements for the joint openings during the first day of testing. As can be seen, the east and west joints opened by essentially the same magnitudes. Joint opening was very small up to a load of 110 kips, which was the load at which cracking occurred in the topping above the joint. At this load, joint opening increased significantly from 0.002 in to 0.026 in. The LVDTs located higher in the cross-section showed insignificant amounts of displacements, indicating no cracking or slippage occurring at the interface surface on the tapered webs.

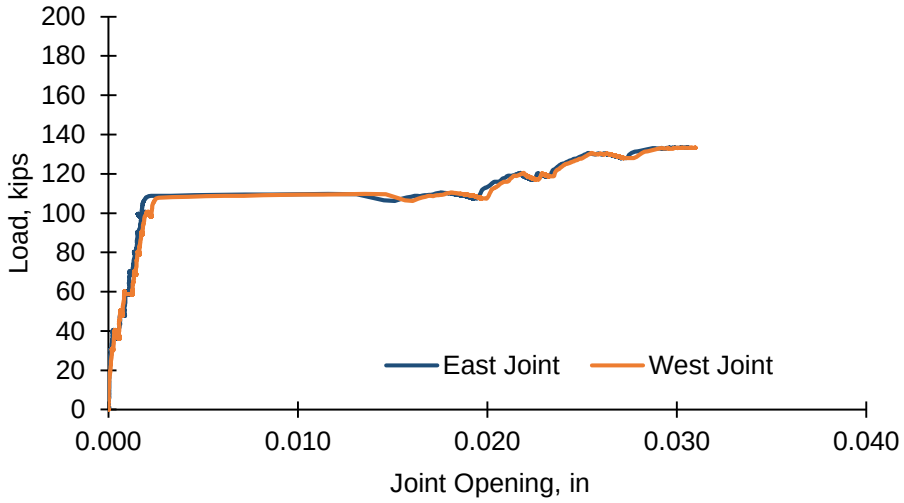

Figure 43. Welded Connection Failure Test Day 1 - Load vs Joint LVDT Measurements

Figure 44 shows the applied load plotted against the LVDT at the joint openings for the second day of testing. From 0 kips to 130 kips the behavior was linear. After 130 kips, the joints exhibited increased widening up to the failure load. The LVDTs indicated negligible slippage occurred at the interface between the precast beam and topping concrete at the tapered web locations.

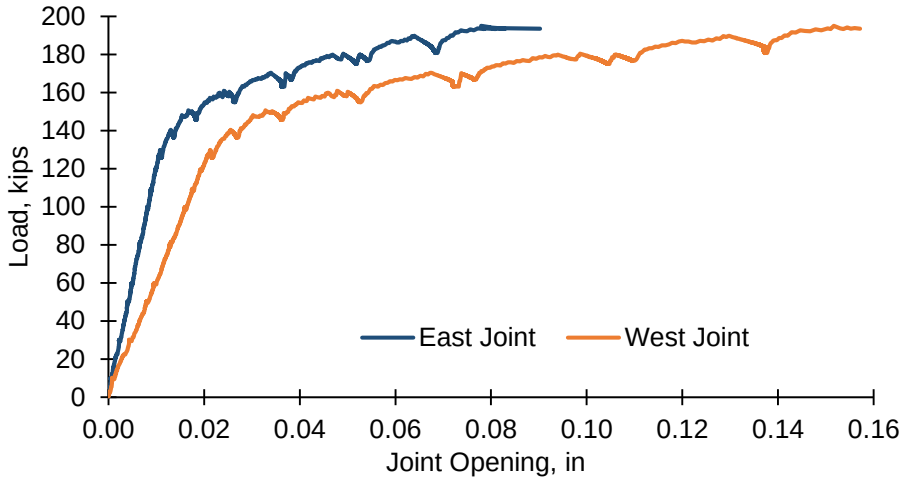

Figure 44. Welded Connection Failure Test Day 2 - Load vs Joint LVDT Measurement

No-Connection Detail with Poor Interface Roughening

Results from Cyclic Load Test

Based on the static tests carried out at 200,000 cycle intervals during the cyclic testing, no deterioration in performance of the specimen was observed. No visible cracks formed, and all instrumentation results were consistent. As with the welded connection test, the deflection measurements did not vary much during the periodic static load tests. The maximum deflection of approximately 0.018 in occurred at midspan. The LVDTs measured zero displacement at 30 kips for all of the intermittent static load tests, indicating no cracking or slipping of the interface during cycling. The measured strain on the reinforcing steel in the precast beam and the topping were small and consistent, with the largest value of 44 με being in the reinforcement in the cast-in-place concrete. The largest measured strain in the reinforcement for the precast beam was 24 με. These results were somewhat larger than the strains from the welded connection specimen, but still indicated that the steel was not experiencing high stresses and the concrete remained uncracked. The complete results of each piece of instrumentation can be found in Edwin (2017).

Results from Monotonic Test to Failure

During the monotonic test, first cracks were observed at a load of 40 kips and occurred at the interface between the two concrete components. These cracks began on the interface at the top of the flange of the south beam. Cracking at this load was small (less than 0.005 in), and no flexural cracks were observed in the beam concrete. At 50 kips, the interface crack propagated, and flexural cracks became noticeable in the precast beam. At this stage, there was still no flexural cracking in the cast-in-place concrete section in the joint region.

At 60 kips, the cracking at the interface of the two concretes, at the top of the flange near the joint, propagated along the top of the flange, increasing in length. Additionally, at this level of load, cracking began to occur at the interface between the two concretes along the inclined web in the sub-assemblages. Also, cracks in the topping concrete became observable near the region of the joint between flange tips. The cracking in the topping propagated upwards through approximately one half of the depth of the topping.

At an applied load of 63 kips, the specimen failed. The plane of failure was along the interface between the precast beam and topping concrete at the south beam location on both the east and western side. Crack openings were large. Rather than continuing along the interface plane, the crack at the top of the tapered web region turned up into the topping and went through over one half of the depth of the 7.5-in thick overlay. This failure can be seen in Figure 45.

Figure 45. No Connection Detail with Poor Roughening Specimen Cracking at Failure Load of 63 kips (crack at top of web left and crack at interface right)

Figure 46 shows the plot of load vs midspan displacement recorded by the north midspan string pot during monotonic testing to failure. For this figure, an average of the displacements at each support has been subtracted from the midspan deflection value. As can be seen, displacements increased approximately linearly with load until failure.

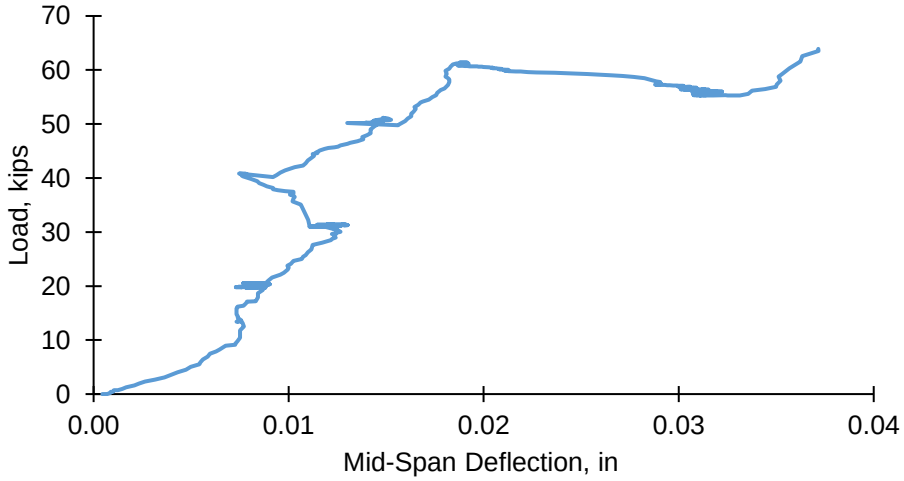

Figure 46. Load vs Deflection for No Connection Detail with Poor Roughening

Figure 47 shows the load vs strain in the reinforcement. At 60 kips, there was a significant increase in the strain and cracking in the topping was first observed. Although cracking did occur, the strains in the reinforcement at failure were less than the yield strain of 2070 με, indicating that the reinforcement had not yielded at failure.

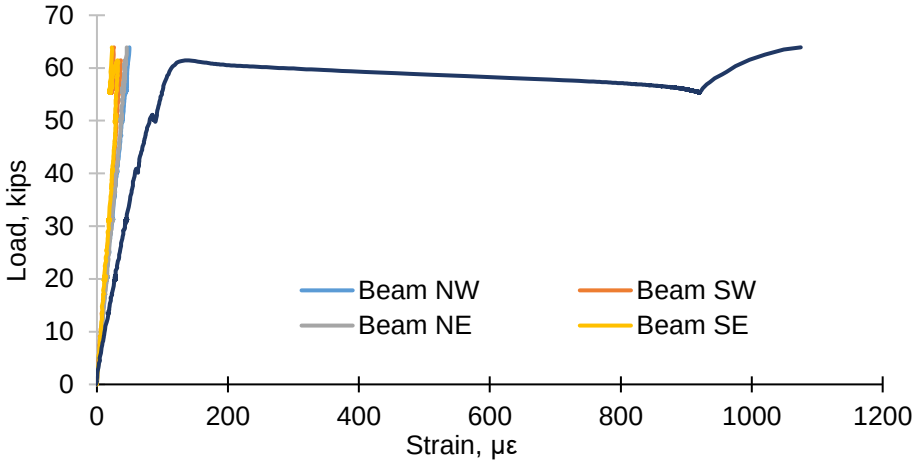

Figure 47. Load vs Reinforcing Strains for No Connection Detail with Poor Roughening

Figures 48 and 49 show the applied load plotted against corresponding LVDT measurements for the south tapered web, the midspan joint, and the north tapered web locations, respectively. Figures 27 and 28 show orientation of specimen and instrument labels.

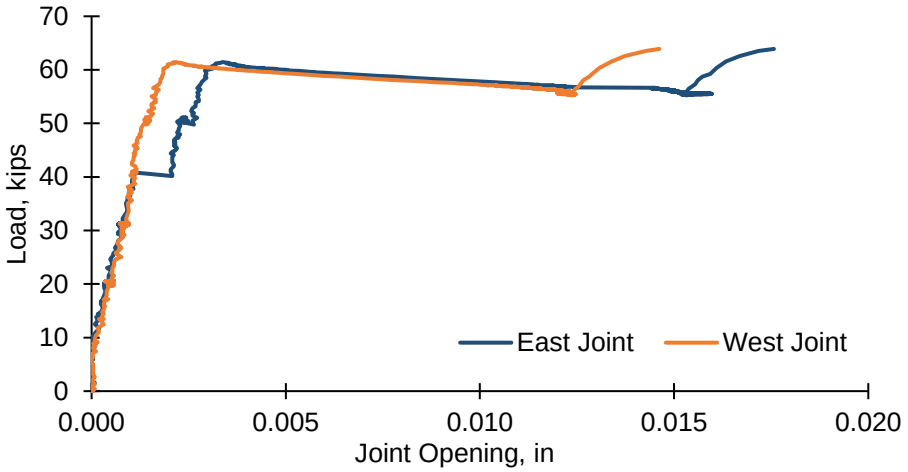

Figure 48. Load vs Joint Opening for No Connection Detail with Poor Roughening

Figure 48 shows that as the load on the specimen increased, the east and west joints showed similar behavior up to 40 kips, where first cracking occurred, and slippage at the surface interface was noted in the southwest beam-topping tapered web location. From zero load up to 40 kips, both joints behaved linearly. At 40 kips, there was approximately 0.001 in of additional opening in the east joint, while the west joint did not exhibit any significant additional deformation. With additional loading, the behavior was essentially linear up to 60 kips, where both joints began to open significantly until failure

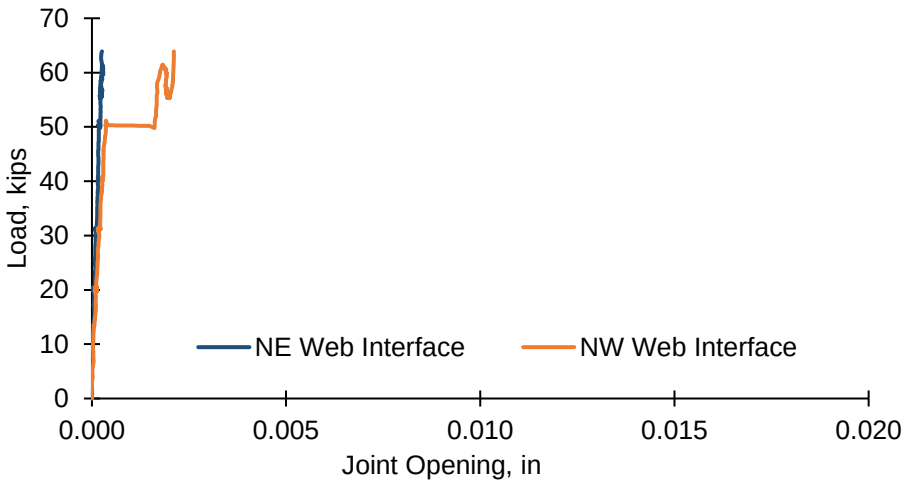

Figure 49. Load vs LVDT Slip Measured at the Precast Beam- Topping Interface North Side

Figure 49 shows that as applied load increased, the LVDT at the interface between the two concretes on the northeast side of the beam recorded a slow but steadily increasing interface slip. No significant jumps in slip were noted by this LVDT. On the northwest side of the beam, however, a large amount of slip occurred at a load of 50 kips. The slip at this surface then stabilized until 60 kips, when there was another slight increase in the slip. There was no measured interface opening on the south side web interface.

No-Connection Detail with Good Surface Roughening

Results from Cyclic Tests

The deflection and reinforcing strains in the precast concrete were essentially identical for all periodic static tests. The maximum midspan deflection did not exceed 0.025 in, and the maximum strain on the reinforcement in the precast concrete was 16 με. All throughout the cyclic tests, the LVDTs across the interfaces recorded zero opening, meaning that the interface remained fully bonded.

After the monotonic test at 3,300,000 cycles, hairline cracks were observed along the centerline on both sides of the specimen, extending from the precast sections' flange joint to close to the top of the topping slab. The applied load vs reinforcement strain in the topping concrete, reported by the east strain gauge, is shown in Figure 50. The data from the first four monotonic tests is very consistent, although each test showed a slight increase in the maximum strain in the reinforcement over the previous test on that specimen. However, it is apparent from the data that something changed within the specimen that increased the reinforcement strain in the topping slab and increased the joint opening towards the end of the test. It is possible that the hairline crack in the topping concrete was related to fatigue.

The applied load versus joint opening between the precast sections, reported by the east middle LVDT, is shown in Figure 51. This plot has the same trend as the applied load versus reinforcement strain plot, showing that the central joint between the precast beams began

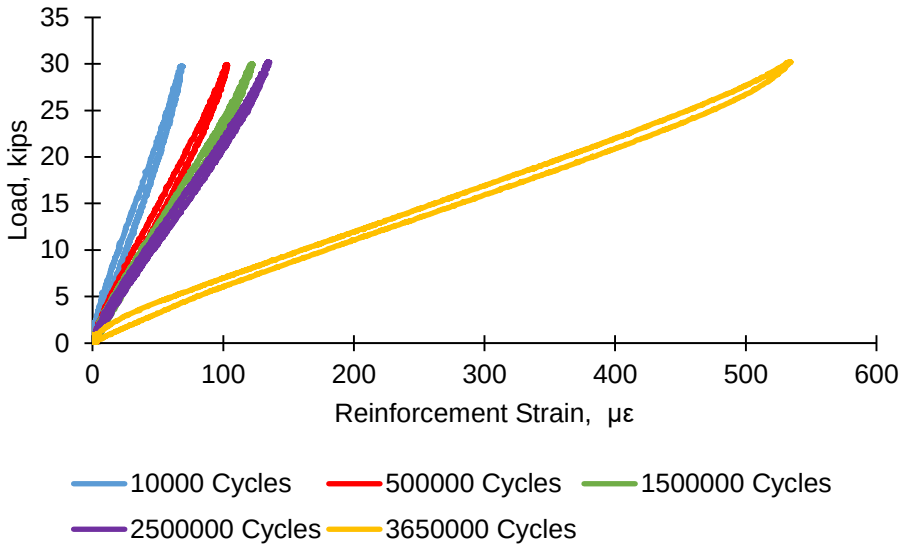

Figure 50. Load vs Reinforcement Strain in the Topping during Cyclic Tests for No Connection Specimen with Good Roughening

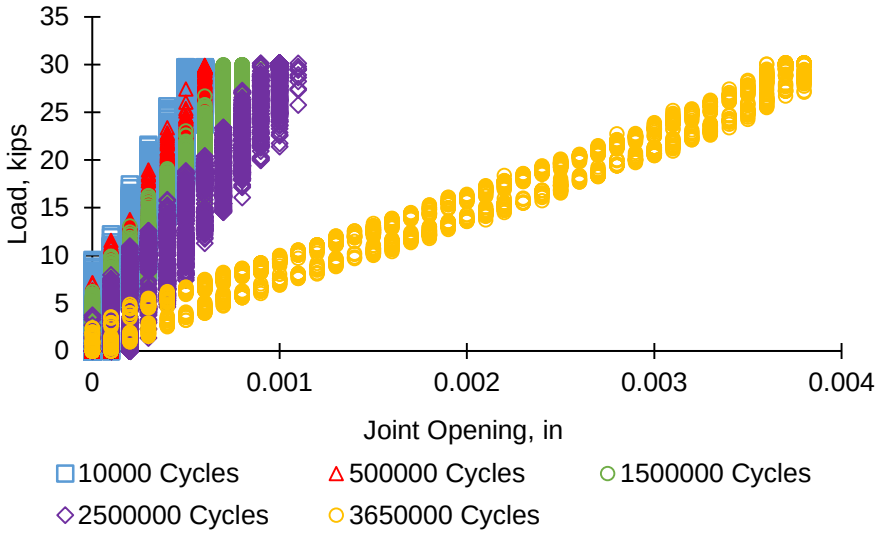

Figure 51. Load vs Joint Opening between Precast Sections during Cyclic Tests

opening approximately five times more than during the first four tests. The increase in the opening of the joint corresponds to the increase in reinforcement strain in the topping slab. Additional details about the data from these tests can be found in Gilbertson (2018).

Results from Monotonic Test to Failure

The interface between the precast and CIP sections on the south side of the specimen appeared to have cracks along the full surface (including the flange, sloped web, and level upper surface) at the 50-kip level. Similarly, the interface between the precast and cast-in-place section

on the north side of the specimen appeared to have cracks along the full surface at the 70-kip level. The ultimate load achieved by the specimen was 130 kips and the failure modes were flexural cracking in the cast-in-place slab above the precast joint and fracture of the center reinforcing bars in the topping slab. These failures were marked by an audible popping noise and a drop of the load to about 80-kips. Figure 52 shows the cracking on the east and west sides of the specimen after failure.

Figure 52. No Connection Specimen with Good Surface Roughening at Failure Load of 130 kips (East Side Left and West Side Right)

The load vs deflection plot for the specimen during the failure testing is shown in Figure 53. For the first 63-kips of the test, the plot was linear. At 63-kips, the deflection increased 0.1 in while the load remained steady. Then the load and deflection increased together again, but at a shallower slope. The trend remained linear until about 130 kips of load and 0.56 in of deflection, where the trend rounded out and began to decline. The specimen failed as soon as the load returned to 130-kips after the pause for inspection. Note that several of the wire pots along the bottom of the specimen had failures of their epoxy glue towards the end of the test such that there was no measurement of the deflection of the center of the specimen. Therefore, a manual recording was taken at 130-kips.

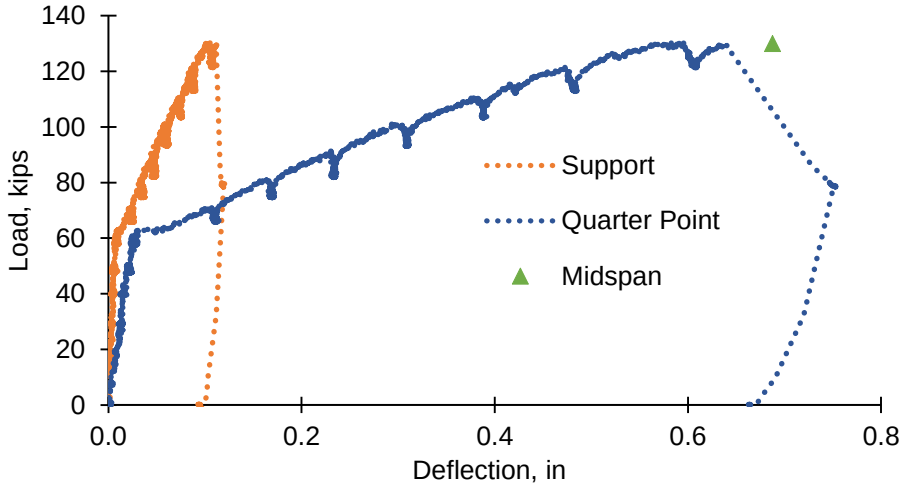

Figure 53. Load vs Midspan Deflection for No Connection Detail with Good Roughening

The measured opening of the joint between the precast sections, as reported by the east middle LVDT, is shown in Figure 54. The trend of this graph mirrors that of the load versus deflection graph, with an initial linear section until 50-kips, a slight decrease in slope until 63-kips, and a much less steep section until flattening out and failing at 130-kips.

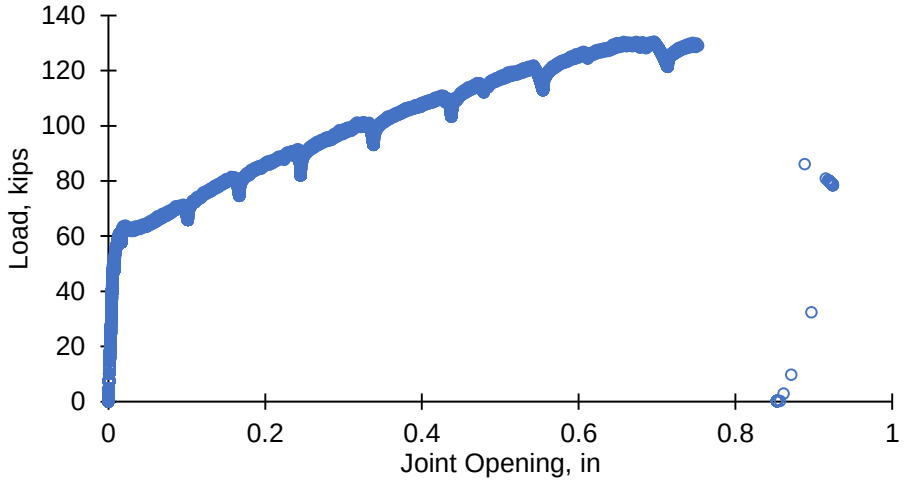

Figure 54. Load vs Joint Opening between Precast Sections

The reinforcement strain in the topping concrete, as reported by the east strain gauge, is shown in Figure 55. The plot shows that the strain increase was linear with respect to load until about 50 kips when yielding began. The trend plateaued at about 63-kips and the strain increased without a load increase until the strain gauges failed at approximately 18000 με.

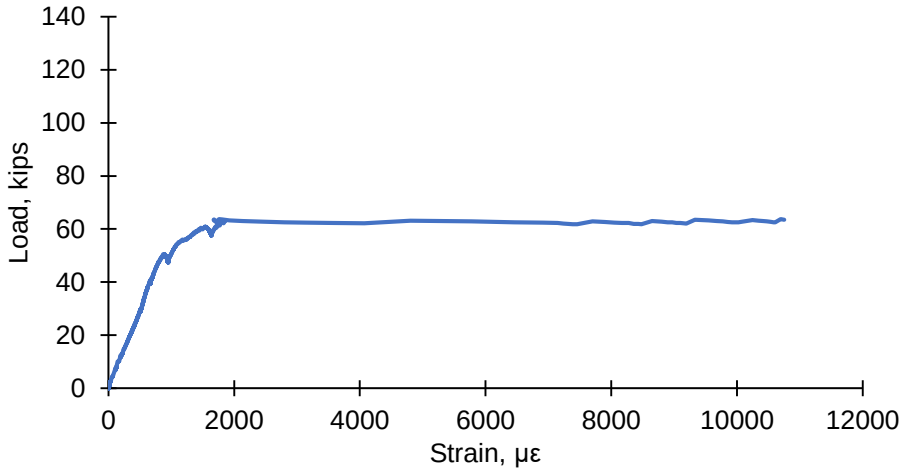

Figure 55. Load vs Reinforcement Strain in Topping Concrete

In the precast section, up to about 63 kips, the strain linearly increased to about 24 με. After 63 kips, the strain decreased to around 22 με, and then began to fall off at around 100 kips. This decrease occurred much sooner than the deflection or joint opening began to change, which showed that the load path within the specimen started to change earlier than the deflection would suggest.

Comparison to Previous No-Connection Detail Specimen Tests

Three no-connection detail sub-assemblage specimens with different reinforcing configurations were tested by Menkulasi (2014). Those specimens failed at loads that ranged from 90 to 240 kips, but the specimen most like those tested in this research was one that failed at 240 kips. Two of the specimens tested by Menkulasi and the specimen with good interface roughening of this research failed by way of a large crack in the CIP topping above the joint of the precast flange. Table 14 summarizes the results for all tests from the Menkulasi study and the current research.

Table 14. Comparison of Data from No-Connection Specimens

Specimen	Precast Flange Reinforcement	Cast-in-Place Reinforcement	Roughening	Loading	Ultimate Strength	Failure Mode
Menkulasi 1	No. 3 at 12 in	No. 6 at 12 in	1 in square	Monotonic	90 k	Flexure in Precast
Menkulasi 2	No. 6 at 12 in	No. 6 at 12 in	1 in square	Monotonic	240 k	Flexure in CIP
Menkulasi 3	No. 4 at 6 in.	No. 4 at 6 in.	1 in square	Monotonic	140 k	Flexure in CIP
Current Research 1	No. 6 at 12 in	No. 6 at 12 in	Cross hatch with plastic	Monotonic After Cyclic	63 k	Debonding between precast and CIP
Current Research 2	No. 6 at 12 in	No. 6 at 12 in	1 ½ in trapezoidal	Monotonic After Cyclic	130 k	Flexure in CIP

The failure of the specimen with poor roughening in the current study was due to a shear failure at the interface between the precast and cast-in-place sections. The 63-kip failure load was less than half of the strength achieved by the good roughening specimens. As the interface bond failed, the load found an alternate pathway, which resulted in a flexural failure and hinging of the topping concrete at the top of the inclined web. This is illustrated in Figure 56.

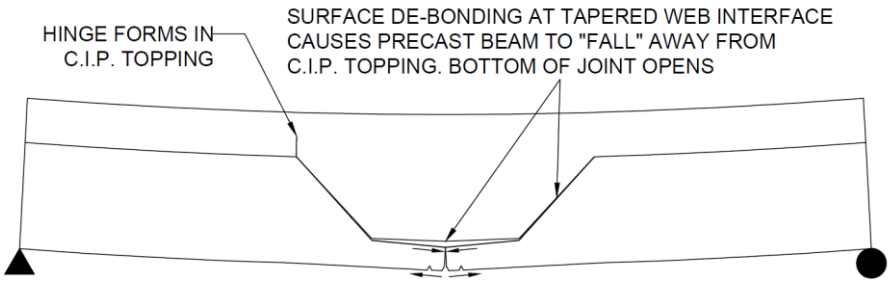

Figure 56. Tapered Web Interface Bond Failure Causing Joint Opening

A simple flexural strength calculation was performed for the cross-section above the joint, assuming the area of steel equal to 4 x 0.44 in^2 = 1.76 in^2, the section width equal to 48 in, and the depth to the reinforcing equal to 20 in. Using f'_c equal to 3800 psi, which was the strength of the no-connection detail with good roughening topping concrete, the flexural strength was 2080 in-kips. The mid-span self-weight moment was 231 in-kips, based on an 11-ft clear span length. The additional applied load to cause failure was calculated to be 124 kips, which was very similar to the applied load for the no-connection test with good roughening. If the steel could have reached its ultimate strength of 100 ksi, the calculated load to cause failure was 214

kips. Based on these calculations, the good surface roughening allowed the steel over the joint in the topping concrete to yield, but not strain harden.

It is also important to remember that the equivalent service load was 30 kips, so the good roughening specimen exhibited a factor of safety of 4.33, relative to the service load. Even the bad roughening specimen achieved a factor of safety of slightly over 2.0, relative to service load.

Comparison to Previous Welded Connection Specimen Tests

The embedded plate tapered web specimen tested by Mercer (2012) and Menkulasi (2014) did not fail under the same loading conditions as that of the current study. Their specimen was able to reach the frame capacity of 300 kips, without failing. During their test, they observed a large crack at the interface between the precast beam and topping concrete. In their test, they noted that the actuator load which caused first cracking was 110 kips. Although the first hairline cracks in the current welded specimen appeared at a load of 50 kips, a reduction in stiffness due to cracking did not occur until 110 kips (based on displacement, strain gauge, and LVDT results). Therefore, the early initial cracks were not detrimental to the performance of the specimen.

Though the welded connection specimen in this research failed at a load of 200 kips, it should be noted that after cycling the specimen for the equivalent of a 50-year design life, this strength was still over six times the service loading of 30 kips.

Results of Topping Concrete Optimization Study

Results Phase I

Fresh Concrete Properties

Tables 15 and 16 present the fresh concrete properties for mixes with NWCA and LWCA respectively in Phase I.

Table 15. Fresh Concrete Properties for NWCA Mixtures

Property/ Batch	NWCA+ SLAG	NWCA+ SLAG+ SLWF	NWCA+ FA	NWCA+ SLAG + SRA	Control mix NWCA
Slump, in	7	5.5	5	5	6
Air content, %	6	7	6.5	6.5	5.5
Unit weight, lb/yd^3	145	137	145	144	141

Table 16. Fresh Concrete Properties for LWCA Mixtures

Property/ Batch	LWCA+ SLAG	LWCA+ SLAG+ SLWF	LWCA+ FA	LWCA+ SLAG + SRA	Control mix LWCA
Slump, in	5	7.5	6	8	7.5
Air content, %	7.5	6	7.5	6.5	7
Unit weight, lb/yd^3	117	112	117	116	118

Compressive Strength

Table 17 presents the 28-day and 56-day strengths of all Phase I mixtures. Strengths at 7 and 14 days can be found in Pulumati (2018).

Table 17. Compressive Strength of Phase I Mixtures

Mixture	28-day strength, psi	56-day strength, psi
Control mix NWCA	6610	7010
NWCA+ SLAG	5890	6430
NWCA+ SLAG+ SLWF	5390	5840
6610NWCA+ FA	5120	5580
NWCA+ SLAG + SRA	5660	6010
Control mix LWCA	4730	5480
LWCA+ SLAG	4280	4770
LWCA+ SLAG+ SLWF	5880	6530
LWCA+ FA	4320	5450
LWCA+ SLAG + SRA	5070	5520

Splitting Tensile Strength

Table 18 shows the 28-day and 56-day splitting tensile strength of all Phase I mixtures. Strengths at 7 and 14 days can be found in Pulumati (2018).

Table 18. Splitting Tensile Strength of Phase I Mixtures

Mixture	28-day strength		56-day strength	
	psi	Strength/$\sqrt{f'_c}$	psi	Strength/$\sqrt{f'_c}$
Control mix NWCA	665	8.2	694	8.3
NWCA+ SLAG	475	6.2	513	6.4
NWCA+ SLAG+ SLWF	421	5.7	478	6.3
NWCA+ FA	475	6.6	513	6.9
NWCA+ SLAG + SRA	446	5.9	490	6.3
Control mix LWCA	465	6.8	475	6.4
LWCA+ SLAG	418	6.4	446	6.5
LWCA+ SLAG+ SLWF	437	5.7	484	6.0
LWCA+ FA	435	6.6	489	6.6
LWCA+ SLAG + SRA	454	6.4	498	6.7

Modulus of Elasticity

Table 19 presents the 28-day and 56-day moduli of elasticity of all Phase I mixtures. Moduli at 7 and 14 days can be found in Pulumati (2018).

Unrestrained Shrinkage

Tables 20 and 21 and Figures 57 and 58 show the unrestrained shrinkage of the Phase I mixtures. Figure 59 shows the comparison of the 28-day unrestrained shrinkage of NWCA and LWCA mixtures in Phase I.

Table 19. 28-day Modulus of Elasticity of Phase I Mixtures

Mixture	28-day Modulus, ksi	56-day Modulus, ksi
Control mix NWCA	4760	5140
NWCA+ SLAG	4780	5520
NWCA+ SLAG+ SLWF	3890	4440
NWCA+ FA	4320	4430
NWCA+ SLAG + SRA	4930	5190
Control mix LWCA	3490	3810
LWCA+ SLAG	3420	3870
LWCA+ SLAG+ SLWF	3310	3840
LWCA+ FA	4250	5260
LWCA+ SLAG + SRA	3530	4450

Table 20. Unrestrained Shrinkage of NWCA Mixtures

Age, days	Unrestrained Shrinkage of NWCA mixtures				
	NWCA+ SLAG	**NWCA+ SLAG+ SLWF**	**NWCA+ FA**	**NWCA+ SLAG + SRA**	**Control mix NWCA**
7	221	296	141	181	108
14	374	437	284	281	340
28	458	515	433	457	455
56	587	568	494	501	570

*All values are in -1 x micro strain.

Table 21. Unrestrained Shrinkage of LWCA Mixtures

Age, days	Unrestrained Shrinkage of LWCA mixtures				
	LWCA+ SLAG	**LWCA+ SLAG+ SLWF**	**LWCA+ FA**	**LWCA+ SLAG + SRA**	**Control mix LWCA**
7	136	303	50	105	143
14	375	542	275	225	292
28	470	718	387	332	442
56	561	750	462	469	547

*All values are in -1 x micro strain.

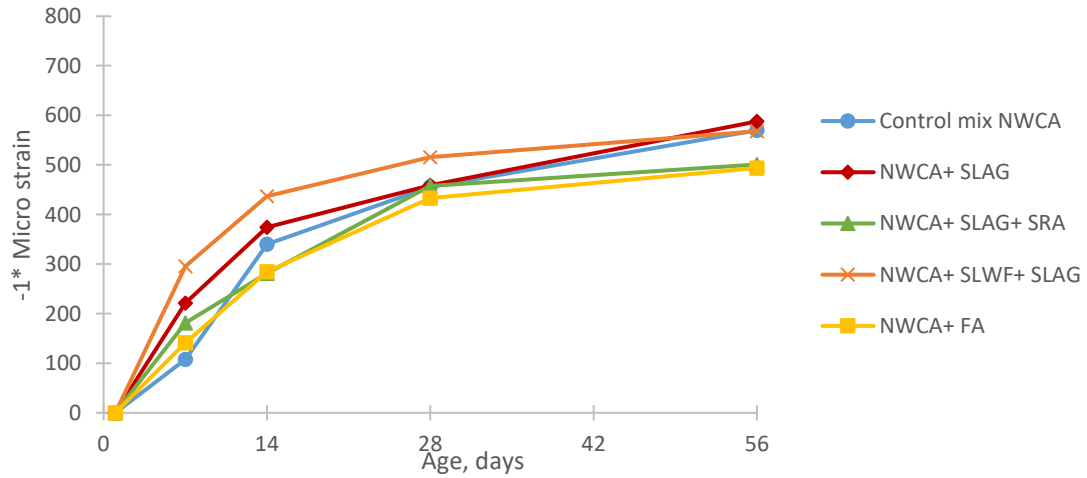

Figure 57. Unrestrained Shrinkage of NWCA Mixtures

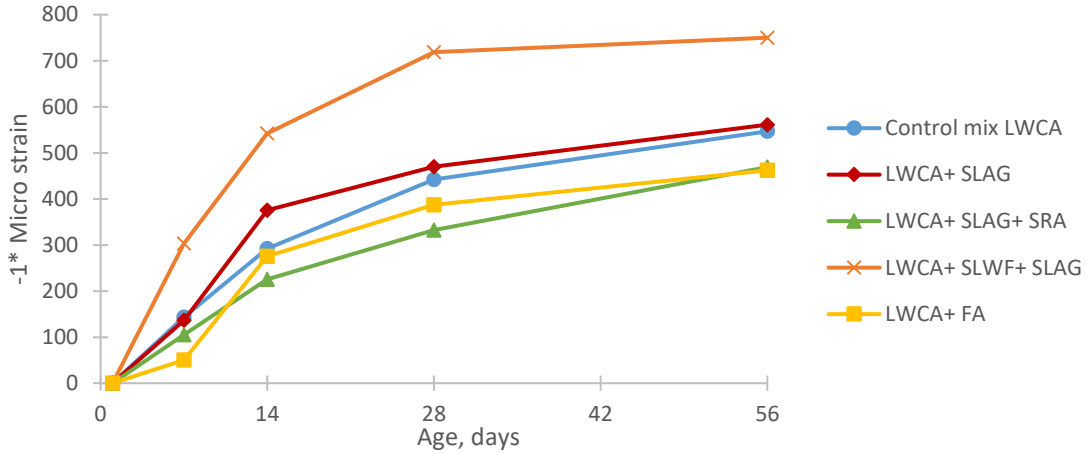

Figure 58. Unrestrained Shrinkage of LWCA Mixtures

Discussion of Phase I Tests

All mixtures showed adequate compressive strength, tensile strength and modulus, so the decision on which mixtures to test in Phase II was based on the unrestrained shrinkage tests. The decision was also to choose both a lightweight and normal weight concrete mixture for a given shrinkage-reducing strategy. Therefore, the two mixtures with fly ash and the two mixtures with slag and shrinkage reducing admixtures were selected for further testing in Phase II.

Results Phase II

Fresh Concrete Properties

Table 22 shows the fresh concrete properties observed for the mixtures in Phase II. The properties are slightly different from those in Table 16, due to minor mixture variations.

Compressive Strength, Tensile Strength and Modulus

Table 23 shows the 28-day compressive strength, tensile strength, and modulus of elasticity for mixes in Phase II

Table 22. Fresh Concrete Properties of Phase II Mixtures

Property	LWCA+ SLAG+ SRA	NWCA+ SLAG+ SRA	LWCA+ FA	NWCA+ FA
Slump, in	6.5	6.5	7.5	5.5
Air content-%	7	5.5	7.5	7
Unit weight, lb/yd^3	116	143	117	142

Table 23. Properties of Phase II Mixtures

Property	LWCA+ SLAG+ SRA	NWCA+ SLAG+ SRA	LWCA+ FA	NWCA+ FA
Compressive Strength, psi	5540	6830	4690	5310
Tensile Strength, psi	418	446	427	484
Modulus, ksi	3190	5020	3080	5540

Overall, all the mixtures exhibited 28-day compressive strengths higher than the required strength of 4000 psi at 28 days. All properties in this phase were consistent with the results from Phase I (Pulumati, 2018). The LWCA mixtures had lower moduli than the NWCA mixtures, as would be expected with lightweight aggregate concretes.

Unrestrained Shrinkage

Figure 60 shows the unrestrained shrinkage of the specimens in Phase II. The four mixtures exhibited very similar shrinkage strains and were similar to the Phase I batches at 56 days.

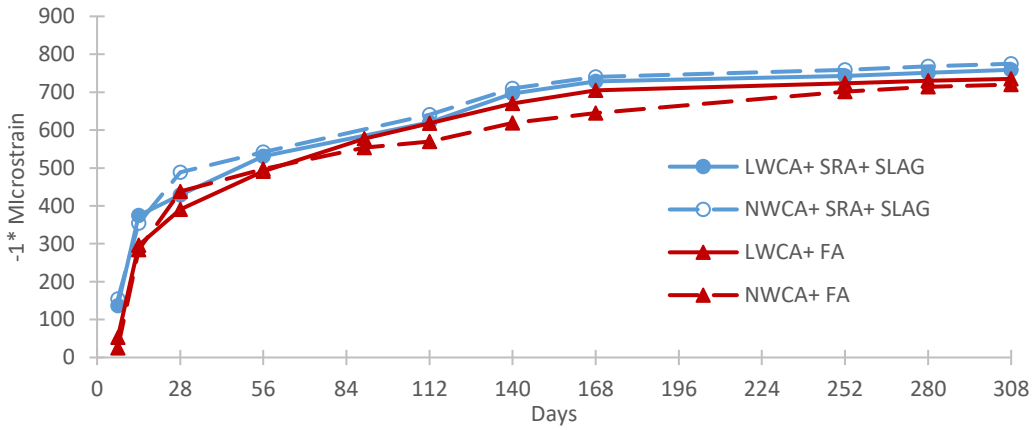

Figure 60. Unrestrained Shrinkage of Mixtures in Phase II. Note that the NWCA Mixes are Shown in Dashed Lines, While the LWCA Mixes Are Shown in Solid Lines

Compressive Creep

Figure 61 shows the creep coefficient calculated using the data obtained from the compressive creep tests. As mentioned previously, the creep coefficient is the creep strain divided by the initial elastic strain. Generally speaking, mixtures with fly ash exhibited more creep compared to mixtures with slag as the supplemental cementitious material. Also, the NWCA mixtures exhibited more creep than the mixtures with LWCA. Thus, the mixture with NWCA and fly ash exhibited the highest creep out of the four mixtures tested, while the mixture with LWCA and slag and SRA exhibited the lowest creep.

Table 24 presents the 28-day shrinkage and 90-day creep coefficients for the four Phase II mixtures. All mixtures had shrinkage strains less than 500με at 28 days, and three of the four mixtures had creep coefficients greater than 1.8 at 90 days. It is unknown why the LWCA+SRA+SLAG mixture had such a low creep coefficient.

Comparison of Time Dependent Behavior to Models

Figure 62 and Figure 63 present the measured creep and shrinkage data for the four Phase II mixtures compared to the three considered models: ACI 209, CEB MC90-99 and AASHTO LRFD. Table 25 presents the evaluation of which model provided the best prediction for each mixture. Early age is considered to be the first 28 days, and later is beyond 28 days. Overall, the

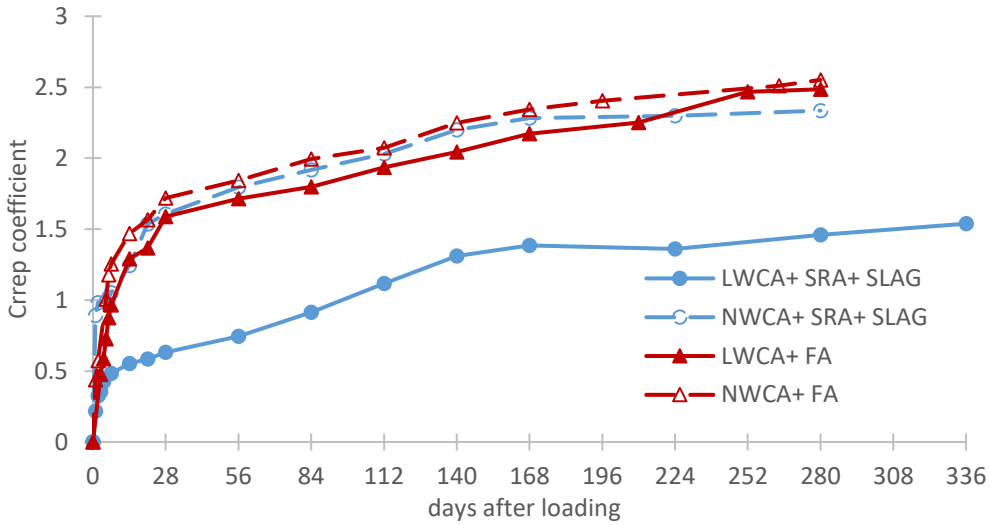

Figure 61. Creep Coefficient for Mixtures in Phase II. Note that the NWCA Mixes are Shown in Dashed Lines, While the LWCA Mixes Are Shown in Solid Lines

Table 24. 28-day Shrinkage and 90- day Creep Coefficient

	28-day shrinkage Phase I*	28-day Shrinkage Phase II*	Creep Coefficient
LWCA+SRA+SLAG	332	429	0.91
NWCA+SRA+SLAG	457	489	1.92
LWCA+ FA	387	391	1.80
NWCA+ FA	433	438	1.99

Shrinkage values in -1 microstrain.

ACI 209 model was selected as the best model to predict the shrinkage and creep of the mixtures, and was used in the study of the effect of differential shrinkage on tensile stress and reflective cracking of the topping mixture. Additional details on the comparisons can be found in Pulumati (2018).

Age-Adjusted Effective Modulus Method

Baseline Analysis

Table 26 shows the stresses in the composite section for all the mixtures in Phase II. Note that tension was considered positive and compression was considered as negative. Figure 64 shows the variation of stresses through the depth of the cross section for mixtures in Phase II due to the differential shrinkage of the topping concrete relative to the precast beam. The figure shows that the maximum tensile stress occurred in the topping concrete at the interface between the topping and the precast concrete. If this stress exceeded the tensile strength of the concrete, the crack had a likelihood of propagating to the top of the deck. This tensile stress was probably the cause of the reflective cracking seen in the Minnesota inverted T-beam bridges. Figure 65 compares the stress at the bottom of the deck to that of the tensile strength of concrete given by Equation 10, where f`$_c$ was the specified compressive strength of 4000 psi at 28 days.

$$f_r = 7.5 * \sqrt{f`c} \qquad \text{Equation 10}$$

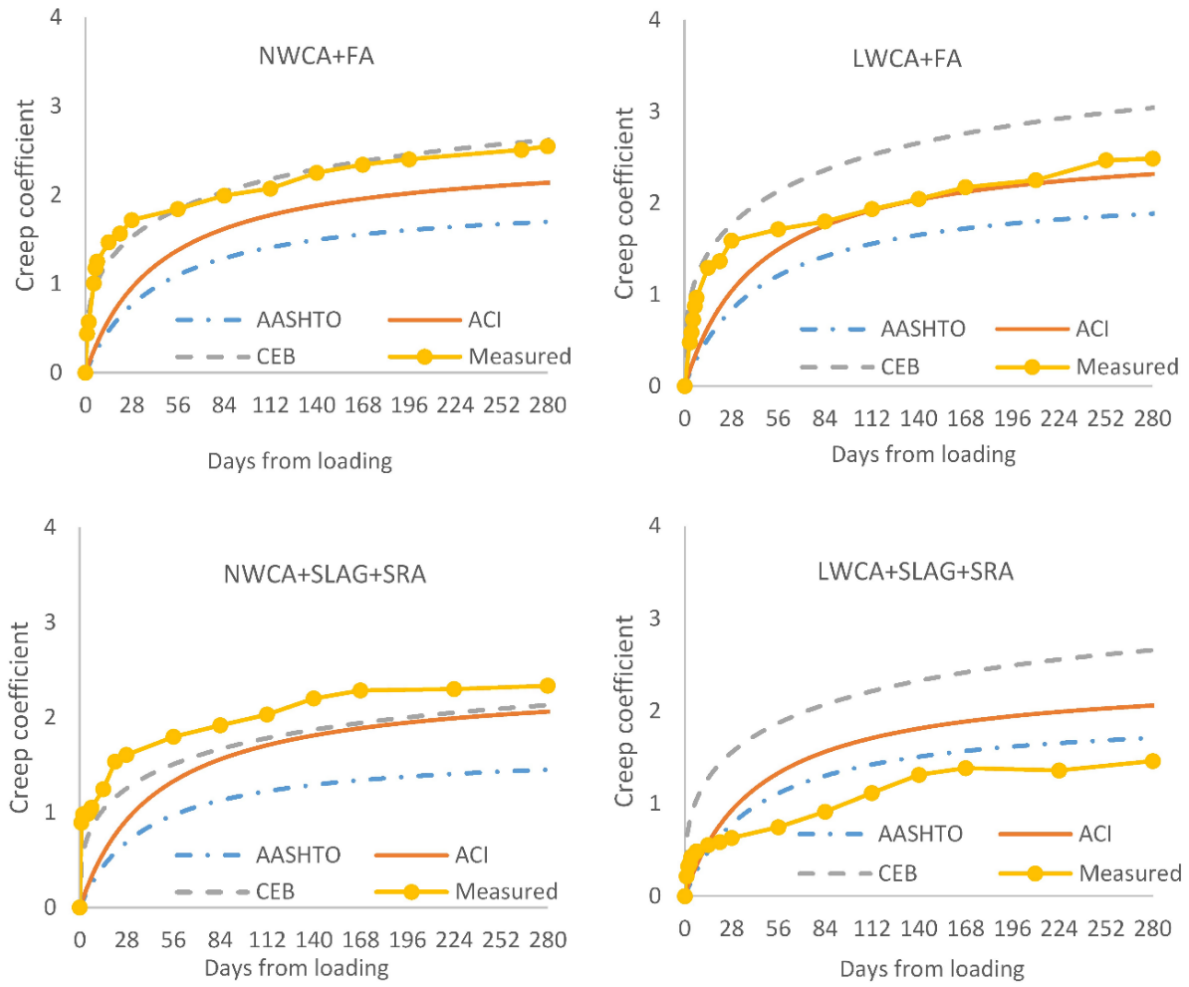

Figure 62. Comparison of Creep Data to Prediction Models

Based on Equation 10, all of the mixtures tested in Phase II developed stresses that were smaller than the cracking strength of 4000 psi concrete, or 474 psi. The mix with LWCA and fly ash had the highest stress at the bottom of the deck, while the mix with NWCA plus slag plus SRA developed the smallest stress. Although Figure 65 compares the maximum tensile stresses to the design modulus of rupture of 474 psi, the calculated tensile stresses were also less than the measured 28-day tensile strengths of the mixtures presented in Table 18 and Table 23. Some of the concrete mixtures had tensile strengths less than that calculated with Equation 10.

Parametric Study of the Influence of Volume-to-Surface Ratio

Table 27 shows the calculated stress in the topping at the interface for each topping mixture and the three investigated volume-to-surface (V/S) ratios for the topping. Although the variation in V/S ratio of the precast beam was investigated, that variable had no effect on the stresses in the section.

Figure 66 compares the magnitude of the stresses in the bottom of the deck with varying volume-to-surface ratio of the deck for each mixture. It is clear that larger V/S ratios reduce the

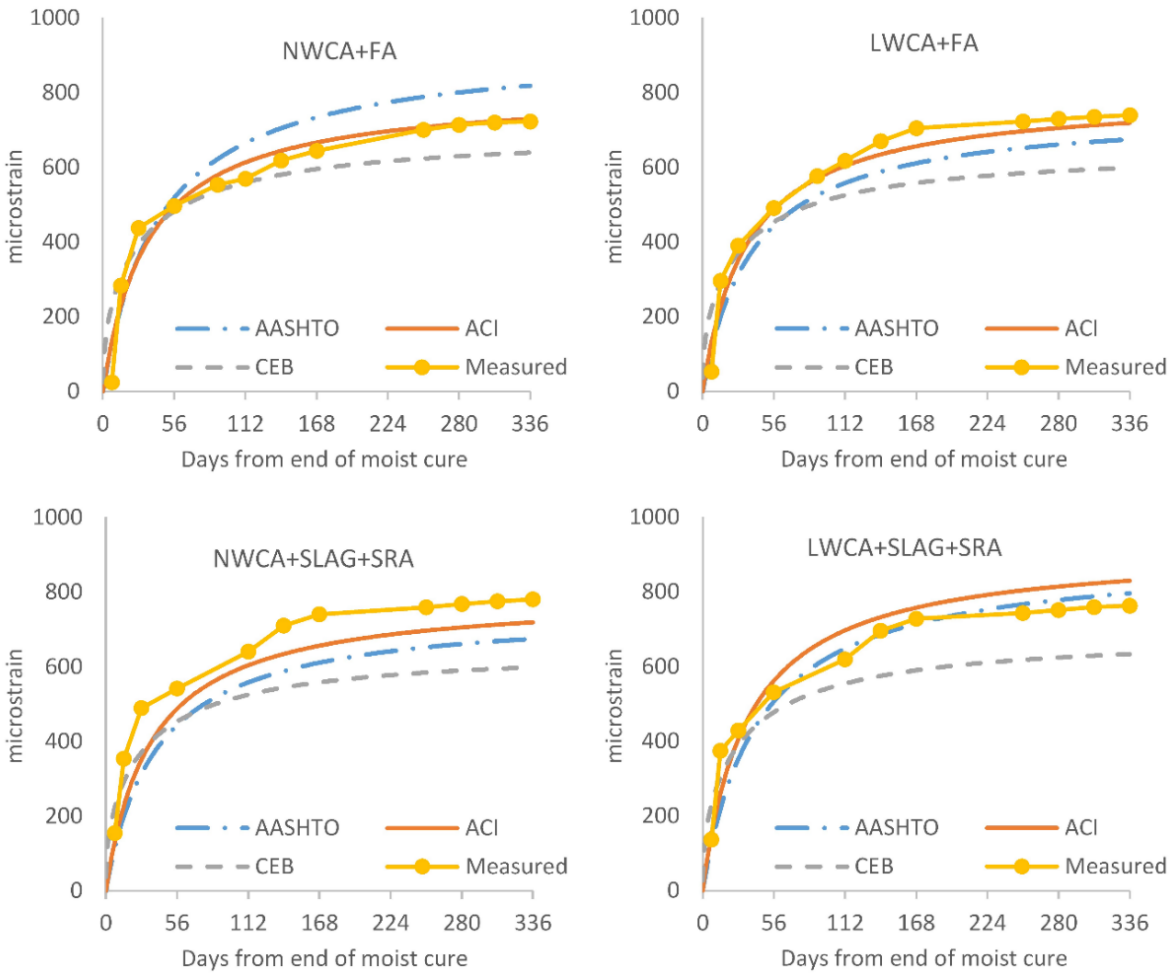

Figure 63. Comparison of Shrinkage Data to Prediction Models

Table 25. Comparison of Best Prediction Models for Phase II Mixtures

Mix	Shrinkage Prediction			Creep Coefficient Prediction		
	Early age	Later age	Overall	Early age	Later age	Overall
LWCA+ SLAG+SRA	ACI	AASHTO/ ACI	ACI	ACI	AASHTO	ACI
NWCA+ SLAG+SRA	ACI	ACI	ACI	CEB	CEB/ACI	ACI
LWCA+ FA	ACI	ACI	ACI	CEB	ACI	ACI
NWCA+ FA	ACI	ACI	ACI	CEB	CEB	CEB

Table 26. Stresses in Composite Section for Mixtures in Phase II – Baseline Analysis

Depth from bottom		LWCA+SLAG+ SRA	NWCA+SLAG+ SRA	LWCA+ FA	NWCA+ FA
Stress at top of deck	25	0.241	0.205	0.249	0.217
Stress at center of deck	21.5	0.309	0.263	0.316	0.277
Stress at bottom of deck	18	0.377	0.322	0.384	0.338
Stress at top of beam	18	-0.481	-0.404	-0.493	-0.428
Stress at center of beam	9	-0.090	-0.075	-0.093	-0.080
Stress at bottom of beam	0	0.300	0.254	0.308	0.268

All stresses are in ksi, depth in inches

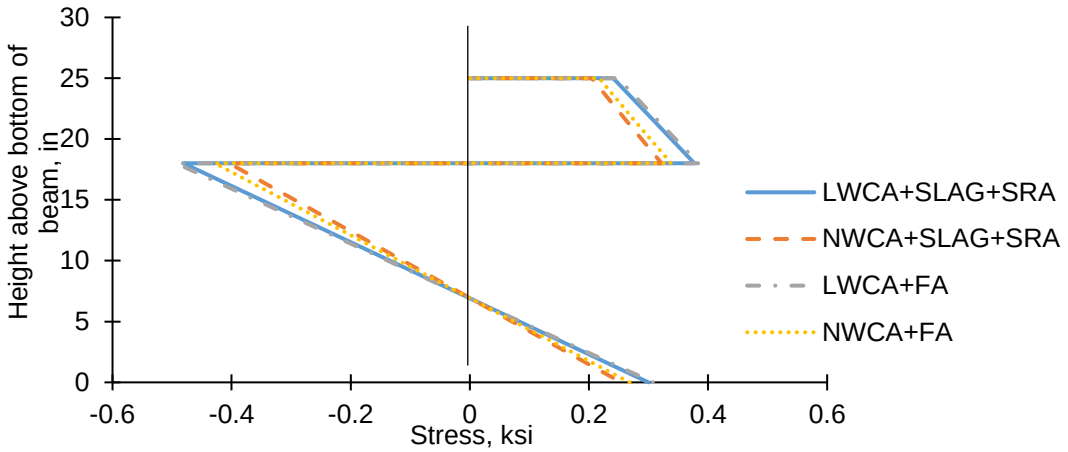

Figure 64. Stresses in the Composite Section for Mixtures in Phase II

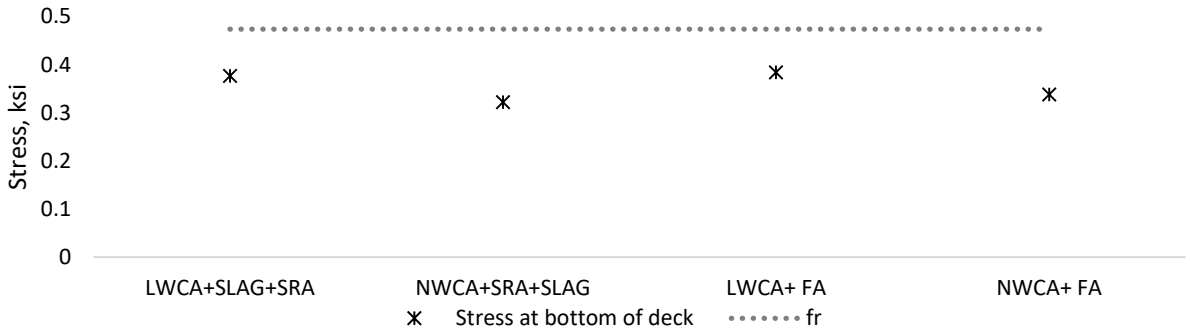

Figure 65. Stresses at Bottom of the Topping for Mixtures in Phase II

Table 27. Stress in Topping Concrete at the Precast Interface for Varying V/S Ratio of Deck, in ksi units

Topping Mixture Design	V/S Deck = 2 in	V/S Deck = 3.5 in	V/S Deck = 7 in
LWCA+SLAG+ SRA	0.383	0.326	0.188
NLWCA+SLAG+ SRA	0.322	0.272	0.152
LWCA+ FA	0.413	0.352	0.205
NWCA+ FA	0.338	0.287	0.163

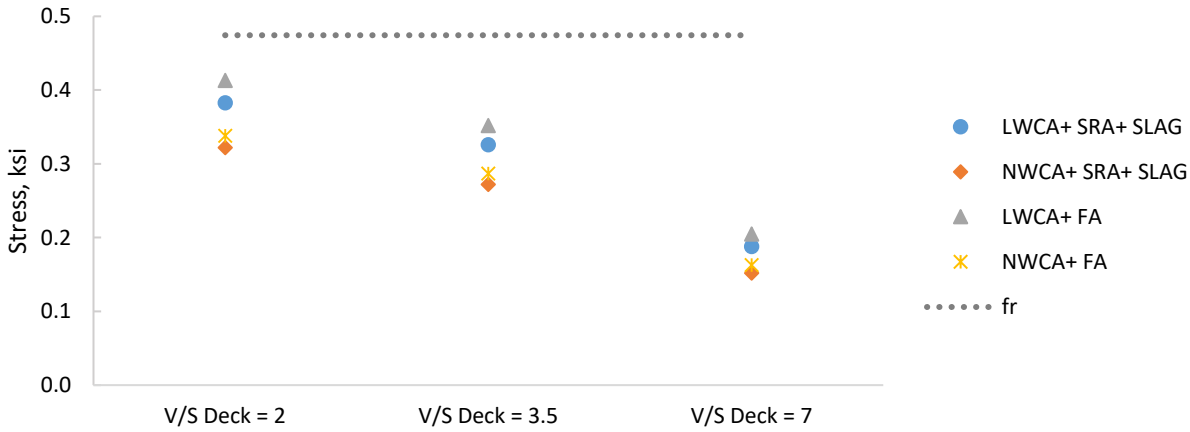

Figure 66. Comparison of Stresses at the Bottom of the Deck with Varying Volume-to-Surface Ratios

magnitude of the shrinkage and therefore reduce the stresses in the topping due to restrained shrinkage. So, by ensuring the precast concrete is saturated prior to casting the topping, the distance free water has to migrate to evaporate will increase, which decreases the magnitude of shrinkage. This, in turn, will reduce the restrained shrinkage tensile stresses, and reduce the likelihood of cracking.

Parametric Study of Effect of Slump

Table 28 shows the stresses in the topping concrete at the interface between the topping and the deck, given varying slumps and a constant V/S ratio of 3.5 and 9 in for the deck and girder, respectively. Figure 67 compares the magnitudes of the stress at the bottom of the deck for each mixture and slump. It can be seen that the effect of slump is very small.

Table 28. Stresses in the Section for Varying Slump, in ksi

Topping Mixture Design	Slump = 3 in	Slump = 4.5 in	Slump = 6 in	Slump = 7.5 in
LWCA+SLAG+ SRA	0.317	0.33	0.342	0.354
NWCA+SLAG+ SRA	0.264	0.276	0.287	0.297
LWCA+ FA	0.321	0.333	0.344	0.355
NWCA+ FA	0.279	0.291	0.301	0.312

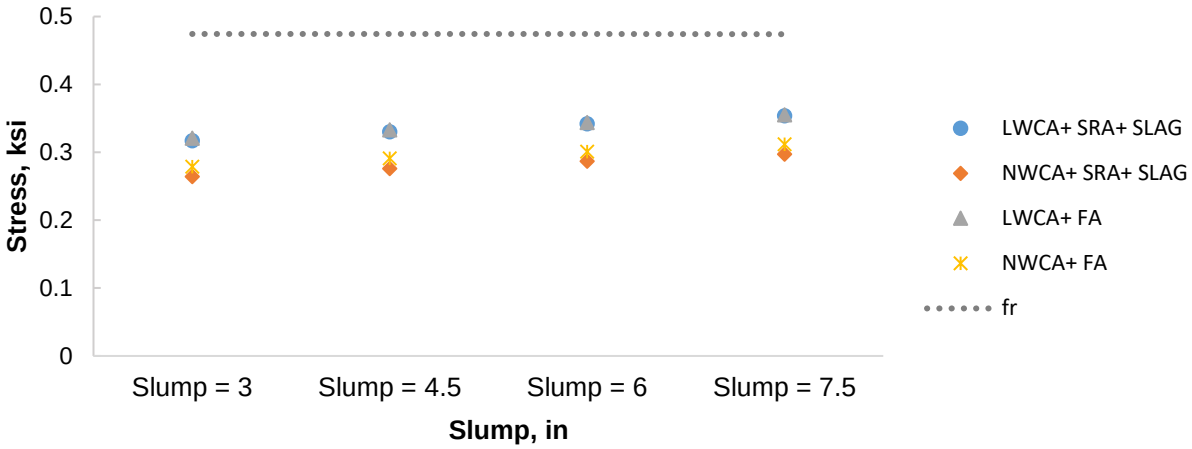

Figure 67. Comparisons of Stresses at the Bottom of the Deck with Varying Slump

Discussion of Age-Adjusted Effective Modulus Study

For all four of the mixtures examined in this age-adjusted modulus study, the tensile stresses that developed in the cross-section due to differential shrinkage remained below the expected tensile strength of the concrete. The analysis shows that a large volume-to-surface ratio in the topping reduces the tensile stresses. A large V/S ratio can effectively be achieved for the topping by thoroughly saturating the surface of the precast beam prior to the topping concrete placement. Saturating the beam surface will result in little moisture loss into the precast beam, forcing excess moisture to travel a greater distance to reach the surface and evaporate. The study also indicated that lower slump concrete will produce smaller tensile stresses, but the effect is small.

Reinforcement in the Topping Concrete for Skew Bridges

The finite element analysis indicated that the maximum transverse tensile stresses in the inverted T-beam system decreased as the skew increased, based on average stresses above the joint between adjacent flanges. The worst case loading was for the center of the wheel patches located directly over the joints. Table 29 presents the results for 0 and 30 degree skew.

Table 29. Stress in Concrete and Steel Reinforcement Due to Skew and Wheel Locations, in psi Units

Skew Angle	Wheels over Webs		Wheels over Joints	
	Concrete	Reinforcing	Concrete	Reinforcing
0	164	700	190	800
30	99	340	126	460

The study indicated that under typical traffic loading, the stresses in the concrete and in the reinforcing steel were very low. Therefore, the orientation of the reinforcing steel across the joint was not critical. Intuitively, for the best performance of the no-connection detail, the reinforcing steel in the topping should be oriented in the same direction as the reinforcing in the flanges of the precast beam. This orientation would result in the most efficient non-contact lap splice. However, when the skew is less than about 15 degrees, aligning the topping reinforcing parallel to the skew is not anticipated to be detrimental to the performance of the system, even if there is slight cracking in the topping concrete.

CONCLUSIONS

Preliminary Design Tables

- *The maximum span length for the medium-size Virginia inverted T-beam section is 50 ft for all combinations of normal weight and lightweight concrete when no special construction method is employed.* Strand debonding will be required to achieve this maximum span length. Altering the concrete unit weight reduces the number of prestressing strands needed, but does not increase span length. Reaching spans up to 70 ft is possible with the medium size section studied, but requires time-consuming construction methods such as staged deck placement, temporary mid-span shoring, and/or cutting top strands in the beam prior to deck placement.

Horizontal Shear Push-off Specimens

- *For applications where horizontal shear strength is desired in two perpendicular directions, a cross hatch type texture is the most effective.* The top of the bottom flange is subjected to horizontal shear in two directions from longitudinal and transverse bending. Other characteristics of the surface textures that produced higher horizontal shear strengths are sharp edges and equal amounts of surface area allotted to the high and low points of the texture. When using plywood forms, the application of debonding agents such as TuffCoat® spray is effective in creating the desired sharp edges in the textures.

- *Textures at a 0.25-in amplitude are adequate to develop full composite action for transverse bending, if the spacing is specified to be 1 in.* The horizontal shear strength is dependent upon the spacing of the grooves; the closer they are, the higher the strength.

Sub-Assemblage Testing

- *When an adequate surface treatment is used on the interface between the precast and cast-in-place sections, the Virginia inverted T-beam bridge system, with either connection, has the 50-year design life to warrant its use for high daily traffic bridges.* The designs have substantial factors of safety against cracking and failure. While careful attention must be paid to the weld geometry and quality, the welded connection has adequate ductility. In order to avoid a transverse flexure-type failure in the no-connection design, the system will have to have adequate horizontal shear resistance.

- *Inverted T-beam bridges constructed with either the no-connection detail or the welded connection detail can exceed a 50-year fatigue life.* The sub-assemblage specimens in this study exhibited no degradation of stiffness over time under 3.65 million cycles of service load, which equates to 50 years, assuming an average daily truck traffic (ADTT) of 200.

- *The surface roughening used in the no-connection detail must be adequate in order to avoid an unanticipated failure mode.* The surface of the inverted T-beam must promote good mechanical interlock and bond with the cast-in-place concrete topping. Examples of texture patterns and techniques that will yield this type of surface can be found in this report.

- *The geometry of the welded connection detail can lead to large localized stresses, which can be exacerbated by poor weld quality at the root pass.*

Optimization of Topping Mixture Study

- *The ACI 209 model is the best at predicting the creep and shrinkage of the cast-in-place concrete topping for the Virginia inverted T-beam bridge system.*

- *Maximizing the volume-to-surface ratio of the cast-in-place concrete topping is an effective method to reduce shrinkage in the topping and decrease tensile stresses due to differential shrinkage between the topping and the precast beam.* A larger volume-to-surface ratio can be achieved by ensuring the surfaces of the precast inverted T-beams are in a saturated-surface-dry condition prior to placement of the topping concrete. This reduces the amount of moisture absorbed by the precast concrete.

Reinforcement in the Topping Concrete for Skew Bridges

- *The orientation of the transverse reinforcement in the concrete topping and across the connection between adjacent Virginia inverted T-beams is not critical for structures with*

skews up to 30°. The stresses in the transverse reinforcement are lower for skew bridges than straight bridges.

RECOMMENDATIONS

1. *VDOT's Structure and Bridge Division should allow the use of the no-connection detail for bridges on high traffic corridors.* The no-connection detail specimen showed no degradation of response for the equivalent of 200 ADTT.

2. *VDOT's Structure and Bridge Division should continue specifying the following roughening requirements for the Virginia inverted T-beam system with the no-connection detail:*

    - For surfaces cast against formwork, such as sloped webs and the tops of the flanges, grooves should be spaced between 1 in and 3 in, and the sides of the grooves should be angled between 0° and 45°.

    - For the surfaces exposed during casting, such as the tops of the beams, grooves should be rolled or deformed at a spacing of 1 in to 3 in. Raking the surface is not an acceptable method for roughening.

    - All roughening should have a ¼-in amplitude.

3. *VDOT's Structure and Bridge Division should specify VDOT's A4 low-shrinkage concrete for the cast-in-place topping.*

4. *VDOT's Structure and Bridge Division should specify that the top surfaces of the inverted T-beams be in saturated surface dry condition prior to placement of the topping concrete, and the topping concrete should be moist cured for a minimum of 7 days.*

5. *VDOT should allow the maximum span length of the inverted T-beam to be 50 ft and should limit the maximum skew to 30°.*

IMPLEMENTATION AND BENEFITS

Implementation

VDOT's Structure and Bridge Division will consider expanding the use of the no-connection detail from *Recommendation 1* as a design alternative for bridges with a maximum ADTT of 200 in the *Manual of the Structure and Bridge Division, Part 2: Design Aids and Typical Details, Chapter 12 – Prestressed and Post-Tensioned Concrete*. Final consideration for this inclusion will be made by August 30, 2020.

Regarding *Recommendations 2 through 5, the* Structure and Bridge Division will insert the requisite language into the *Manual of the Structure and Bridge Division, Part 2: Design Aids and Typical Details, Chapter 12 – Prestressed and Post-Tensioned Concrete*. These edits will be completed by August 30, 2020.

Benefits

The inverted T-beam system is a viable alternative to precast concrete adjacent voided slabs for spans up to 50 ft. The work done in this project shows that the no-connection detail with adequately roughened web and bottom flange surfaces can be used on bridges with high traffic volume. Based on the fact that there was no change in behavior throughout the cyclic testing, this study suggests that the inverted T-beam system should have an infinite service life. Compared to adjacent prestressed voided slabs with the newly adopted longitudinal shear key and splice details, the Virginia inverted T-beam bridge system could last 30 or 35 years longer (based on the results from the Halbe et al. study [2017]). This new design could last at least 50 years longer than the average 37-year life adjacent members with the conventional shear key design. Furthermore, using the recommended properties or mixture proportions for the topping, and ensuring that the beams are in the saturated surface dry condition prior to placement of the topping, should result in a low likelihood of restrained shrinkage cracking in the deck surface. By avoiding cracking in the topping, chloride-laden surface water will take longer to reach the reinforcement in the system, thus ensuring longer durability and lower life cycle costs.

ACKNOWLEDGMENTS

The authors gratefully acknowledge the guidance and assistance of Bernie Kassner of the Virginia Transportation Research Council and Andy Zickler of VDOT's Structure and Bridge Division. The contributions of Brett Farmer, Dennis Huffman and Dr. David Mokarem at the Murray Structural Engineering Laboratory are also acknowledged. Performance of the topping concrete optimization study was partially supported by the University Transportation Center at CAIT/Rutgers, which is gratefully acknowledged as well. The opinions in this report are those of the authors and not necessarily those of the sponsors.

REFERENCES

AASHTO (2014). "AASHTO LRFD Bridge Design Specifications."Washington D.C.

ACI-209. (2008). *Guide for Modeling and Calculating Shrinkage and Creep in Hardened Concrete.* Farmington Hills, MI: American Concrete Institute.

CEB. (1999). "Structural Concrete – Textbook on the Behavior, Design and Performance. Updated Knowledge of the CEB/FIP Model Code 1990," *fib Bulletin 2,* V.@, Federation International du Beton, Lausanne, Switzerland, pp. 37-52.

Edwin, E. B. A. (2017). "Refinement of the Inverted T-Beam Bridge System for Virginia," Virginia Polytechnic Institute and State University, MS Thesis, Blacksburg, VA, 2017.

Gilbertson, R. (2018). "Recommendations for Surface Treatment for Virginia Inverted T-Beam Bridge System", MS Thesis, Virginia Polytechnic Institute and State University, Blacksburg, VA, 2018.

Hagen, K., Ellis, S., Fishbein, J., Molnau, K., Wolhowe, E., and Dorgan, D. (2005). "Development and Construction of a Precast Inverted T System for Expediting Minnesota Slab Span Bridge Projects." *Proceedings of the 2005 Concrete Bridge Conference,* Palm Springs, CA, October 16-19, 2005.

Halbe, K., Joyce, P., Roberts-Wollmann, C. L., and Cousins, T.E. *Development of Improved Connection Details for Adjacent Prestressed Member Bridges*. VTRC 17-R27. Virginia Transportation Research Council, Charlottesville, VA, 2017.

Henkensiefken, R.D. (2009). "Volume Change and Cracking in Internally Cured Mixtures Made with Saturated Lightweight Aggregate under Sealed and Unsealed Conditions." *Cement and Concrete Composites,* 427-437."

Menkulasi, F. (2014). "The Development of a Composite Concrete Bridge System for Short-to-Medium-Span Bridges." PhD Dissertation, Virginia Polytechnic Institute and State University, Blacksburg, VA, 2014.

Mercer, M. S. (2012). "Transverse Sub-Assemblage Testing of the Inverted-T Bridge System." MS Thesis, Virginia Polytechnic Institute and State University, Blacksburg, VA, 2014.

Mokarem, D. S. (2008). *Measurement of Early Age Shrinkage of Virginia Concrete Mixtures - VTRC 08-R9.* Charlottesville, Virginia: Virginia Transportation Research Council.

Pulumati, V. (2018). "Investigation of Concrete Mixtures to Reduce Differential Shrinkage Cracking in Inverted T-Beam System", MS Thesis, Virginia Polytechnic Institute and State University, Blacksburg, VA, 2018.

Ralls, M. L., Tang, B., Bhidé, S., Brecto, B., Calvert, E., Capers, H., Dorgan, D., Matsumoto, E., Napier, C., Nickas, W., and Russell, H. (2005). "Prefabricated Bridge Elements and Systems in Japan and Europe." Federal Highway Administration,

Roberts-Wollmann, C. L., Zickler, A. M., and Brown, M. C. (2016). "Virginia's Development of an Inverted-tee Beam Bridge Superstructure System." *ASPIRE - The Concrete Bridge Magazine,* Precast Concrete Institute (PCI).